MCDONNELL DOUGLAS

STUDY AND DESIGN OF A CRYOGENIC PROPELLANT ACQUISITION SYSTEM

FOURTH QUARTERLY REPORT
1 APRIL 1972 THROUGH 30 JUNE 1972

15 JULY 1972

MDC G3695

PREPARED BY:

G. W. BURGE
PROGRAM MANAGER, NAS8-27685
PROPULSION DEPARTMENT

J. B. BLACKMON
DEPUTY PROGRAM MANAGER
PROPULSION DEPARTMENT

APPROVED BY:

P. L. KLEVATT
CHIEF TECHNOLOGY ENGINEER–PROPULSION
RESEARCH AND DEVELOPMENT
ADVANCE SYSTEMS AND TECHNOLOGY

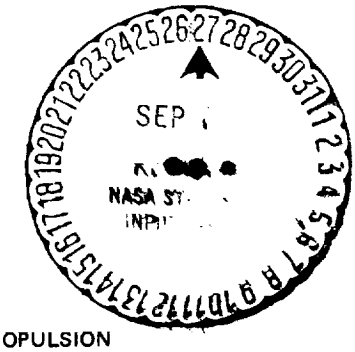

PREPARED FOR
NATIONAL AERONAUTICS AND SPACE ADMINISTRATION
MARSHALL SPACE FLIGHT CENTER
HUNTSVILLE, ALABAMA
CONTRACT NAS8-27685

MCDONNELL DOUGLAS ASTRONAUTICS COMPANY-WEST
5301 Bolsa Avenue, Huntington Beach, CA 92647

PREFACE

This is the fourth quarterly progress report on the program, "Study and Design of a Cryogenic Propellant Acquisition System." The period covered is 1 April to 30 June 1972. This work is being carried out by McDonnell Douglas Astronautics Company (MDAC) for the National Aeronautics and Space Administration, Marshall Space Flight Center, Huntsville, Alabama, under Contract NAS8-27685. Mr. G. M. Young serves as the principal NASA contracting officer representative. The MDAC technical effort is being conducted under the direction of G. W. Burge, Program Manager, and Dr. J. B. Blackmon, Deputy Program Manager. Major contributions to this report were made by J. N. Castle, B. R. Heckman, D. W. Kendle, and Dr. R. A. Madsen.

CONTENTS

Section 1	INTRODUCTION		1
	1.1	Objectives	1
	1.2	Program Summary	1
Section 2	SUMMARY		5
Section 3	TECHNICAL DISCUSSION		9
	3.1	Phase II, Task A–Preliminary Design/Comparison	9
	3.2	Phase II, Task B–Bench Testing	100
	REFERENCES		145
Appendix	POTENTIAL SCREEN RETENTION BREAKDOWN PROBLEMS INDUCED BY INTERACTION BETWEEN SCREEN DEVICE AND AUTOGENOUS PRESSURIZATION GAS		147
	REFERENCES FOR APPENDIX		159

FIGURES

1	Proposed Progress Schedule	6
2	Channel Segment Sizes (LH_2 Tank)	15
3	Detail of Representative Joint Section Clamps	17
4	Candidate Acquisition Duct Design Cross Sections (LH_2 Tank)	19
5	Influence of Straight Duct Segments on Proximity to Wall	22
6	Distributed Channel Acquisition System Configuration	24
7	Channel Duct Details	25
8	Candidate Channel Support Concepts	27
9	Comparison of Autogenous and Cold Helium LH_2 Tank Pressurization	31
10	LH_2 Tank Pressurization System Weights	32
11	Cold GH_2 Conditioning Concepts	35
12	LO_2 Tank Pressurization Requirements—200°R Helium	38
13	Cold Helium Pressurization System Schematic (Distributed Channel Acquisition System)	40
14	Cold GH_2 Pressurization System Schematic (Distributed Channel Acquisition System)	41
15	Vacuum Vent/Refill Start Tank Concept	51
16	Main Tank Propellant Acquisition for Start Tank Vacuum Refill	52
17	Orientations of Intersecting Channels	57
18	Square Cross Section All-Screen Contoured Channel	60

19	Circular Cross Section All-Screen Straight Channel	60
20	Retention Safety Factor for LH_2 Channels in 2.8 M^3 (100 ft^3) Start Tank	62
21	Retention Safety Factor for LH_2 Channels in 1.4 M^3 (50 ft^3) Start Tank	63
22	Solid Duct Channel with Auxiliary Screen Liner	67
23	All-Screen Channel with Inner Liner Auxiliary Screen	67
24	Square Cross Section All-Screen Channel with Auxiliary Corner Channels	69
25	Circular Cross Section All-Screen Channel with Auxiliary Tube Channels	70
26	Manhole Cover Flange Design	78
27	Schematic Diagram of LH_2 Start Tank System	80
28	Start Tank Concept Pressurization System Weights	84
29	Start Tank Boiloff Penalty	85
30	Influence of Start Tank Size and Boiloff Penalty	86
31	Square Cross Section All-Screen Channel Wall	88
32	Bubble Point Verification Procedure	98
33	Section View of Screen Sample Plate (Full Scale)	103
34	Forced Heat Transfer Coefficient at Screen	105
35	Bubble Point Data for 250 X 1370 Mesh in LH_2	106
36	Comparison of Bench and Subsystem Screen Heat Transfer Experiments	108
37	Fabricated Screen Elements	109
38	Screen Elements—Rear View	111
39	LH_2 Bubble Point Test	112
40	Bubble Point Pressure of Selected Fine Mesh Screens	114

41	LH_2 Bubble Point with GHe Present	115
42	Vibration Test Apparatus	118
43	Vibration Test Apparatus	119
44	Vibration Test Apparatus Disassembled	120
45	Vertical Sinusoidal Vibration–Shallow	121
46	Vertical Sinusoidal Vibration–Shallow	122
47	Horizontal Sinusoidal Vibration	124
48	Horizontal Sinusoidal Vibration	125
49	Vertical Sinusoidal Vibration–200 X 600 Dutch Twill	126
50	Vertical Sinusoidal Acceleration–200 X 1400 Dutch Twill	127
51	Vertical Sinusoidal Vibration–250 X 1370 Dutch Twill	128
52	Bubble Point Performance of Pleated Screens	131
53	Pleated Screen Sample	132
54	Pleated Screen Flow Loss Measurements	134
55	Fabricated Solid Duct	137
56	Attachment Evaluation Test Apparatus	139
57	Film Bubble Point Evaluation Test Apparatus	142
A-1	Temperature Profile for Condensation	149
A-2	Temperature Profile for Evaporation	149
A-3	Condensate Film Thickness Time Dependence–Small Temperature Difference Approximation	150
A-4	Temperature Response During Pressure Decay of One-Component System	152

TABLES

1	Influence of Screen Mesh on Main Tank Channel Retention Performance	11
2	Final Computed Main Tank Channel Retention Performance	13
3	Main Tank Distributed Channel Design Comparisons	20
4	Distributed Acquisition System Weight Estimates (LH_2 Tank)	29
5	Distributed Acquisition System Weight Estimates LO_2 Tank–B2' Duct Design	30
6	Distributed Channel Basic Pressurization System Weight (LH_2 Tank)	37
7	Cold Helium Pressurization System Weights LO_2 Tankage	39
8	LH_2 System Component Weights (Cold Helium Pressurization)	42
9	LH_2 System Component Weights (Cold GH_2 Pressurization)	43
10	LO_2 System Component Weights (Cold Helium Pressurization)	44
11	Tankage Thermal Protection System Weight Estimates	45
12	Distributed Channel Acquisition System Weight Summary	47
13	Effect of Channel Orientation on Channel LH_2 Acquisition Performance	59
14	Channel Acquisition Device Performance–Liquid Hydrogen Start-Tank Application 200 x 600 Mesh Screen–Bubble Point Pressure = 181.9 N/m^2 (3.8 lb/ft^2)	64

15	Channel Acquisition Device Performance—Liquid Hydrogen Start-Tank Application 200 x 600 Mesh Screen—Bubble Point Pressure = 1,250 N/m^2 (26.1 lb/ft^2)	65
16	Auxiliary Channel Performance in Liquid Hydrogen Start Tank	72
17	Auxiliary Channel Performance in Liquid Oxygen Start Tank	73
18	Annular Screen Performance in Liquid Hydrogen Start Tank	74
19	Annular Screen Performance in Liquid Oxygen Start Tank	75
20	LH_2 Start Tank System Component Weights Vacuum Vent/Refill Design*	81
21	LO_2 Start Tank System Component Weights Vacuum Vent/Refill Design*	82
22	Acquisition Device Weights for 2.8 M^3 (100 Ft^3) LH_2 Start Tank	90
23	Start Tank Acquisition System Weights (Liquid Hydrogen)	91
24	Start Tank Acquisition System Weights (Liquid Oxygen)	92
25	Liquid Hydrogen Start Tank System Weight Summary	93
26	Liquid Oxygen Start Tank System Weight Summary	94
27	Total Start Tank System Weight Summary	95
28	Bench Testing Status	101
29	Influence of Pleating on Retention Capability	135
A-1	Parameters for Shuttle Tank Pressure Decay	157

Section 1
INTRODUCTION

1.1 OBJECTIVES

The objectives of this project are to investigate, define, and demonstrate, through ground testing, an acquisition system for supplying subcooled LH_2 and LO_2 under in-orbit conditions to satisfy integrated cryogenic feed system requirements for advanced space systems such as a Space Shuttle cryogenic auxiliary propulsion system (APS) and spacecraft main propulsion. This effort will concentrate on concepts that utilize the favorable surface tension characteristics of fine-mesh screens and will significantly advance cryogenic acquisition technology in general. The anticipated analytical and experimental results will provide a sound technology base for the subsequent design of cryogen supply subsystems for future space vehicles. These objectives will be achieved by a four-phase program covering 20 months.

1.2 PROGRAM SUMMARY

1.2.1 Phase I—Analysis

The objectives of this phase are to: (1) evolve conceptual designs for candidate acquisition systems, (2) formulate the analytical models needed to anayze these systems, and (3) generate parametric data on overall candidate system performance, characteristics, and operational features in sufficient depth to establish critical design problems and criteria to support a sound system design and evaluation.

1.2.1.1 Task A—Design Studies

Candidate surface-tension-type acquisition systems will be conceptually defined relative to anticipated requirements for candidate applications and studied in detail. This will include not only the acquisition subsystem but also all other subsystems that interact with the acquisition device, such as the

propellant storage, pressurization, and vent subsystem. This will be approached by establishing a workable design for a baseline system using the distributed channel acquisition concept; analyzing this system in detail with respect to failure modes, performance, design criteria, and areas of potential and significant improvement; and perturbing or evolving the baseline design in areas where these potential improvements exist and can technically be accomplished. This procedure may thus result in establishing several variations in a system design or several different system designs with individual or specialized characteristics that will ultimately be compared. Analysis and design models and/or procedures will be modified or developed as necessary to support this investigation. The study will include a failure mode analysis for the promising candidates.

1.2.1.2 Parametric Studies

Critical parametric data will be generated for each promising candidate to identify and define critical design factors and criteria for each concept. Design limits and performance parameters such as head retention capability and weight will be evaluated over a range of conditions so that the impact of variation in system design requirements can be assessed for each promising candidate concept.

1.2.2 Phase II—Design

The objective of this phase will be to use the theoretical models and parametric results generated in Phase I to arrive at (1) a selected acquisition concept and resulting preliminary design for a Shuttle-class APS and other advanced space cryogen feed systems, (2) a test prototype design for a representative acquisition subsystem that will permit meaningful ground testing to verify the design concepts, and (3) a test plan to control the prototype testing to produce maximum usable results.

1.2.2.1 Task A—Preliminary Design/Comparison

Feed system preliminary designs will be produced based on the candidate acquisition concepts and the general results from Phase I. These designs will be in sufficient detail to permit a valid performance comparison of the potential candidates. This task will be completed with the final selection of the

recommended feed system design for a Shuttle-class APS and a spacecraft main propulsion system. Selection criteria will stress the ability to satisfy flexible vehicle mission and duty cycle requirements and compatibility with a minimum-cost, high "probability of success" development program.

1.2.2.2 Task B—Bench Testing

Bench testing will be conducted relative to critical problems that must be resolved in order to realistically complete the preliminary designs. These tests will be conducted in parallel with the design activity.

1.2.2.3 Task C—Prototype Design

The objective of this task is to prepare a detailed design for a large-scale prototype acquisition system test apparatus, suitable to support a ground test program, that is compatible with the systems selected in Task A of Phase II. The prototype will be designed and instrumented to demonstrate the critical operational aspects of the systems and show that practical fabrication is possible. The current plan is to incorporate the acquisition hardware into the MSFC H_2/O_2 APS breadboard.

A test plan defining the installation and the tests to be conducted will be prepared as part of the design activity.

1.2.2.4 Task D—Reporting

Monthly and quarterly reports, and a final and an interim report will be submitted as defined by the program schedule. This effort will also include oral reviews and status reports.

1.2.3 Phase III—Fabrication

During this phase, the prototype design generated under Task C of Phase II will be fabricated and/or assembled.

1.2.4 Phase IV—Testing

The objective of this task is to coordinate test operations at MSFC to verify the performance of the prototype system and to analyze and evaluate the test results.

1.2.4.1 Task A—Checkout and Ship

A leak test will be conducted on the fabricated hardware. After final assembly, the completed test prototype device(s) will be sent to MSFC.

1.2.4.2 Task B—Test Operation

Engineering support will be provided at MSFC to direct and coordinate installation and performance evaluation testing of the prototype system as outlined in the developed test plan.

1.2.4.3 Task C—Analysis and Reporting

The test results will be analyzed to assess the demonstrated performance and characteristics of the prototype feed system and to compare them with anticipated behavior. These results will be documented in the final report, thus concluding the program.

Section 2
SUMMARY

During the fourth quarter of this program, effort concentrated on Phase II-Design, in accordance with the program plan shown in Figure 1. Both Task A, Preliminary Design/Comparison, and Task B, Bench Testing, were conducted in parallel with free interchange of information between the two activities. Effort during the preliminary design task was divided between the distributed channel and the pressure isolated start tank acquisition design concepts.

According to the original program plan, Phase II was to have been completed by the end of the fourth quarter. However, during early June technical redirection was mutually agreed upon which would extend the duration of Phase II and provide time to investigate the acquisition subsystem design for a representative cryogen space propulsion system. This would be in addition to the Shuttle class cryogenic APS application currently being investigated. To accomplish this at no cost increase or significant schedule slip, planned hardware design/fabrication efforts will be changed to delete the modifications to the recently insulated NASA 105-inch LH_2 test tank. Instead, the acquisition device will be installed on the O_2/H_2 APS breadboard LH_2 tank by MDAC at MSFC with all necessary tank modifications being performed by NASA. Detailed milestones have not been firmly fixed at this point; therefore, the approximate durations of the Phase II tasks are shown by dashed lines in Figure 1.

During the quarter, the preliminary designs for the Shuttle class cryogenic APS feed system have been nearly completed, although there are minor details to be finally resolved such as final channel joint/coupling seal design. Preliminary design sketches have been made and system weights for each system have been tabulated.

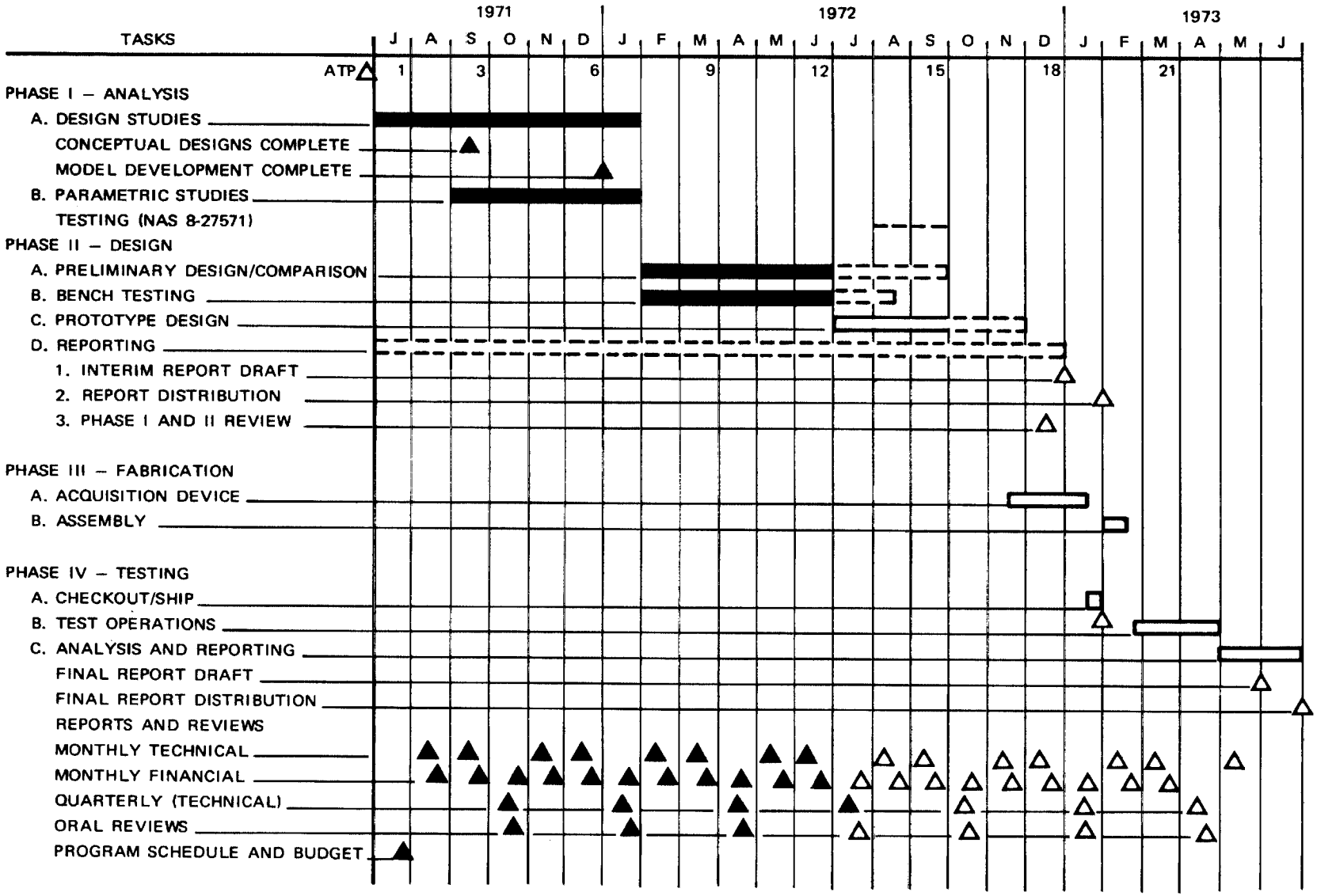

Figure 1. Proposed Progress Schedule

Efforts to accumulate a set of general requirements for the advanced cryogenic space propulsion systems have also been initiated but have not been reported in this document because of incompleteness at this point.

All of the essential planned bench testing was completed during the quarter. This work proved of great value in support of the preliminary design task and in fact had a major impact in not only design refinements but in effecting significant changes in the design approach. For example, bench tests showed that warm hydrogen vapor in direct contact with a screen caused severe loss in retention capability and that riveting could not be used to achieve a sufficiently leak-tight joint. On the positive side, other bench tests showed that screen assemblies could be practically welded and pleated without significant bubble point loss and that a technique for in-place bubble point checkout of an all-screen channel is feasible. A bench test series also resulted in evolving a simple design fix, e.g., a coarse mesh intermediate screen was found to eliminate the high flow loss originally encountered with a fine mesh screen directly supported by a perforated backup plate.

Past work and the added interest in the spacecraft main propulsion application has led to the requirement for some additional bench tests that will be conducted during the next six weeks.

Details of this work are contained in Section 3.

Section 3
TECHNICAL DISCUSSION

During the fourth quarter of this program, work essentially proceeded according to the program plan on Phase II, Design. This phase had been initiated during the third quarter as reported in Reference 1. Work continued in parallel on Task A, Preliminary Design, and Task B, Bench Testing. Both of these activities are continuing into the next quarter.

3.1 PHASE II, TASK A - PRELIMINARY DESIGN/COMPARISON

The objective of this task is to evolve preliminary designs for the acquisition concepts identified in Phase I and integrate these into total feed systems compatible with advanced H_2/O_2 system requirements. A final design will then be selected for prototype evaluation in subsequent program phases. The baseline acquisition concepts were evolved during Phase I and for reference purposes are shown in Figure 2 of Reference 1.

The preliminary design discussion is broken down to cover the two basic types of acquisition systems under study: (1) the distributed channel, and (2) the pressure isolated start tank.

3.1.1 Preliminary Design - Main Tank Distributed Channel Concept

As discussed in the preceding progress reports, the preliminary baseline distributed channel acquisition system is based on the concept of a fine mesh screen surface tension device configured in the form of a series of rings positioned around the walls of the tank. The rings are positioned so as to always contact liquid at some point throughout the mission duration. The size of the rings and the screen mesh size are selected to provide fluid retention

safety factors (RSF) of at least 2* under most adverse loads, but with a minimum weight penalty. The device must be practical to fabricate and install, and within the limits of demonstrated technology. Considerable effort has been expended during Task B, reported in Section 3.2, to demonstrate that critical potential design problems can be solved or avoided by the final preliminary designs.

3.1.1.1 Overall Design Criteria

Calculations for evaluating the influence of channel cross section and screen mesh on retention performance were performed using the MDAC screen acquisition device sizing code. Previous calculations of this type were made and reported in Tables 3 and 4 of Reference 2. However, before running the final computations, all applicable results from the Task B bench tests were incorporated into the codes, including new screen flow-through pressure drop data, bubble points, etc. The results are shown in Table 1 in terms of RSF for a range of screens and one specific channel rectangular cross section for LH_2 and LO_2. A range of limiting design conditions were calculated and in each case calculations were made assuming that screen was used only on one long face of the channel (solid channel) or on all four faces (screen channel). Several conclusions can be drawn from these results.

A. The positive axial 0.46 m/sec^2 (1.5 ft/sec^2) acceleration with low screen coverage represents the most severe design condition.

B. Over the range investigated, the finest mesh screen resulted in highest retention performance.

C. The all-screen channel produces higher retention performance than the solid channel (for the same flow cross section).

D. Use of a finer mesh on the top channel than on the bottom channel results in performance improvements.

---

*$\text{RSF} = \frac{\text{Screen Bubble Point Pressure}}{\text{Maximum Computed Device } \Delta P}$

Use of a RSF of 2 assumes that the computations are made with the best available data and flow analysis.

Table 1

INFLUENCE OF SCREEN MESH ON MAIN TANK CHANNEL RETENTION PERFORMANCE

Propellant	Channel Size (m x m)	Flowrate (kg/sec)	Acceleration (m/sec^2)	Fraction Covered	Safety Factor							
					Mesh Size							
					250 x 1370		325 x 1900		325 x 2300		Top Bottom 325 x 2300 250 x 1370	
					Solid Channel	Screen Channel	Solid Channel	Screen Channel	Solid Channel	Screen Channel	Solid Channel	Screen Channel
LH_2	Top	2.04	0.292	0.50	3.11	4.17	3.42	4.74	3.84	5.16		
			0.124	0.25	2.02	3.17	2.19	3.55	2.59	3.92		
			0.124	0.50	2.86	3.73	3.16	4.26	3.53	4.61		
	Bottom		0.292	0.50	3.38	4.57	3.71	5.19	4.17	5.65		
		2.70	0.457	0.25	1.12	1.49	1.25	1.70	1.41	1.84	1.38	1.83
		2.70	0.457	0.50	1.40	1.64	1.59	1.89	1.73	2.03		
LO_2	Top	6.85	0.183	0.50	4.39	6.70	4.71	7.48	5.41	8.28		
			0.124	0.25	2.60	4.82	2.76	5.26	3.35	5.94		
			0.124	0.50	4.13	6.13	4.46	6.87	5.10	7.57		
	Bottom		0.183	0.50	4.26	7.00	4.52	7.73	5.25	8.64		
		13.50	0.457	0.25	0.87	1.53	0.95	1.70	1.17	1.88	1.07	1.89
		13.50	0.457	0.50	1.36	1.81	1.49	2.06	1.68	2.24		

90% Effective open area

Corrected flow properties

LH_2 tank has two primary rings and LO_2 and has three primary rings

Since it is desirable to use coarse mesh screen whenever possible from a clogging standpoint, use of two screen meshes is desirable and was adopted (325 x 2300 on top and 250 x 1370 on bottom). However, the 25.4 x 10.2 cm channel, in all cases, did not satisfy the RSF ≥ 2 requirement. Therefore, calculations were repeated to find the channel size that would meet RSF = 2. It was found that a 28 x 11.2 cm and 19.1 x 3.6 cm channel for LH_2 and LO_2 respectively was needed. Resulting safety factors are shown in Table 2.

Supplementary calculations were run and it was found that the specific geometry of the duct was not controlling in terms of safety factor. The actual criteria for the specific screen selection are as follows:

A. Duct flow area must be at least 0.0313 m^2 (48.5 $in.^2$) and 0.0145 m^2 (22.5 $in.^2$) for LH_2 and LO_2 respectively.

B. Screen actual width measured around the cross-sectional perimeter must be at least 0.787m (31 in.) and 0.533m (21 in.)

Thus, variations in the duct cross-sectional shape within these constraints are permissible.

In addition to these fluid mechanics criteria, certain fabrication, installation, and structural criteria must be satisfied, most of which were evolved through the Task B Bench Testing or as a result of MDAC experience in building and testing fine mesh screen acquisition devices. These criteria include the following:

A. 0.057 cm (.020 in.) sheet material in either steel or aluminum when used for basic duct structure provides a sufficiently rigid structure (see Section 3.2.8).

B. Riveting of duct sections should not be used when zero leakage sealing against bubble point pressure is required (see Section 3.2.8).

C. The composite fine mesh screen, perforated backup plate, and the edge frame can be welded together using either fusion or roll-spot welding, but the picture frame structure is essential (see Section 3.2.2).

D. In order to eliminate high flow-through pressure losses, a very coarse mesh aluminum screen must be used between the fine mesh and the perforated backup plate (see Section 3.2.4).

Table 2

FINAL COMPUTED MAIN TANK CHANNEL RETENTION PERFORMANCE

SCREENS — TOP CHANNEL 325 x 2300; BOTTOM CHANNEL 250 x 1370

90% OPEN AREA ON ALL SIDES

Propellant	Channel Size (m x m)	Wetted Channel	Flowrate (kg/sec)	Acceleration (m/sec^2)	Fraction Covered	RSF
LH_2	0.279 x 0.112	Top	2.04	0.292	0.50	4.91
				0.124	0.25	3.73
					0.50	4.46
		Bottom		0.292		6.78
			2.70	0.457	0.25	2.05
					0.50	2.25
LO_2	0.190 x 0.076	Top	6.85	0.183	0.50	7.57
				0.124	0.25	5.24
					0.50	6.74
		Bottom		0.183		8.64
			13.50	0.457	0.25	2.11
					0.50	2.53

E. The fine mesh screen element should not be contacted by warm gas pressurant (see Section 3.2.1).

F. Compound curvature of fine mesh screen should be avoided to prevent local folding and stress points which could possibly degrade screen performance.

G. Pleated screens can be used to achieve an effective increase of a factor of three in screen area including the effects of small changes in bubble point and flow loss (see Section 3.2.7).

H. In attaching screen elements to the channel duct, screws can be used with spacing as great as 2.5 cm, if the elements are attached to a rigid duct lip and an indium-tin seal is used (see Section 3.2.8).

Details of a channel design are influenced by the size of the individual channel segments; Figure 2 shows the individual channel package size as related to the number of segments.

To be practical, the design must be such that two men working within the tank can accomplish the installation with access through a conventional manhole. On this basis, an installation unit package greater than 2 by 0.5m would appear unrealistic. Thus, at least six segments per ring would be necessary. This would yield an installation unit package of 1.83 by 0.46m. The original channel installation would occur prior to tank installation within the vehicle, but screen maintenance and repair should be possible without tank removal from the vehicle. Thus, screen installation unit package sizes would be more restrictive. If complete channel segments must be withdrawn to remove the defective screen (screen element removal is the other alternative), at least eight segments should be used, resulting in an installation unit package of 1.45 by 0.38m.

In order to increase the reliability of the acquisition system, a technique for checking the bubble point performance of the system in an as-installed condition immediately after installation and at periodic times throughout the life of the vehicle appears highly desirable. This ideally should be accomplished without requiring access into the tank. If the test indicates a loss in bubble point,

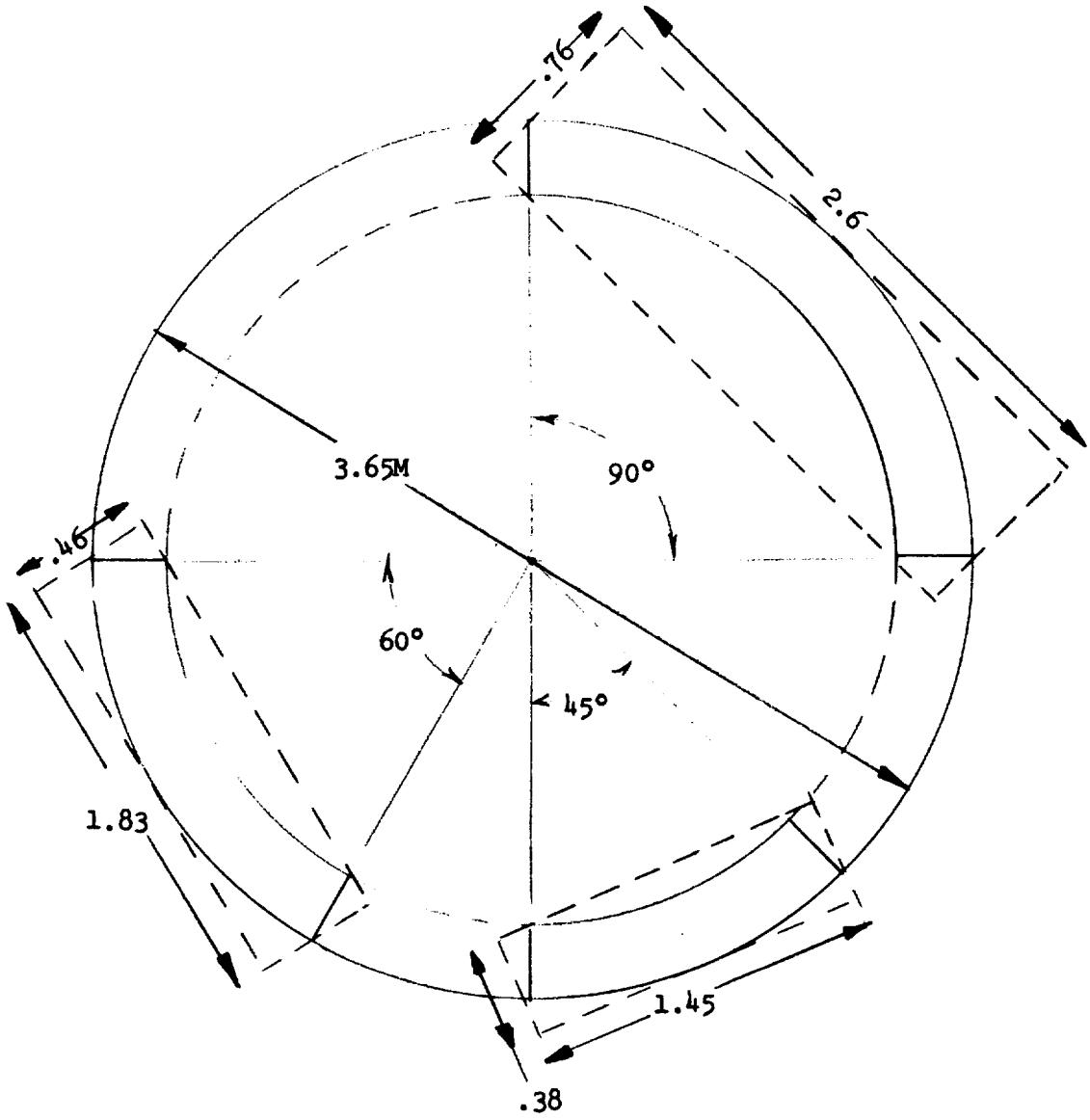

Segments	Package Dimensions (M)
4	2.6 x .76
6	1.83 x .46
8	1.45 x .38

Figure 2. Channel Segment Sizes (LH_2 Tank)

the tank can then be opened, the system inspected and the suspected screen sections removed and repaired or replaced. As discussed in previous reports, direct immersion bubble point testing is possible with a solid duct channel which can hold fluid with pressure being applied across the single plain screen. The immersion technique is not directly applicable with an all-screen channel. However, as discussed under Task B, Section 3.2.9, a liquid film technique has been demonstrated, at least in terms of overall feasibility, that could be used to verify the bubble point performance of an all-screen channel. Specific test procedures are outlined in Section 3.1.3.

Joining of the duct sections can be a critical problem. The joint must reliably provide a seal better than that provided by the fine mesh screen, it must be easy to install within the tank, and should not result in excessive weight penalty. Conventional bolted flanges were deemed to be too heavy and would involve complex manual operations within the tank. During the bench testing, simple riveting was checked out but did not generally prove to be adequate. After considering various alternatives, it was concluded that the best potential solution was to use a Marman V-Band type joint. This is available in a wide variety of sizes and flange details and provides a simple one or two bolt attachment per joint. This design requires a circular duct section at the joint which demands either a circular duct or local transition sections from the normal duct cross section to a circular shape at the joint. This constraint does not present a problem as long as the joint is selected so that the flow area through the circular section does not drop below that required by the flow criteria. For the baseline distributed channel, a minimum diameter of 19.8 cm (7.8 in.) and 13.7 cm (5.4 in.) for LH_2 and LO_2 respectively is required. Marman joints of several types are available in these and larger sizes. Figure 3 pictures the details of such a joint and presents a weight breakdown for an 0.204 m (8 in.) and 0.254 m (10 in.) diameter coupling assembly. Flanges are available in aluminum and stainless steel. The data shown is for a 4584 type design. Variations on this design are still being investigated.

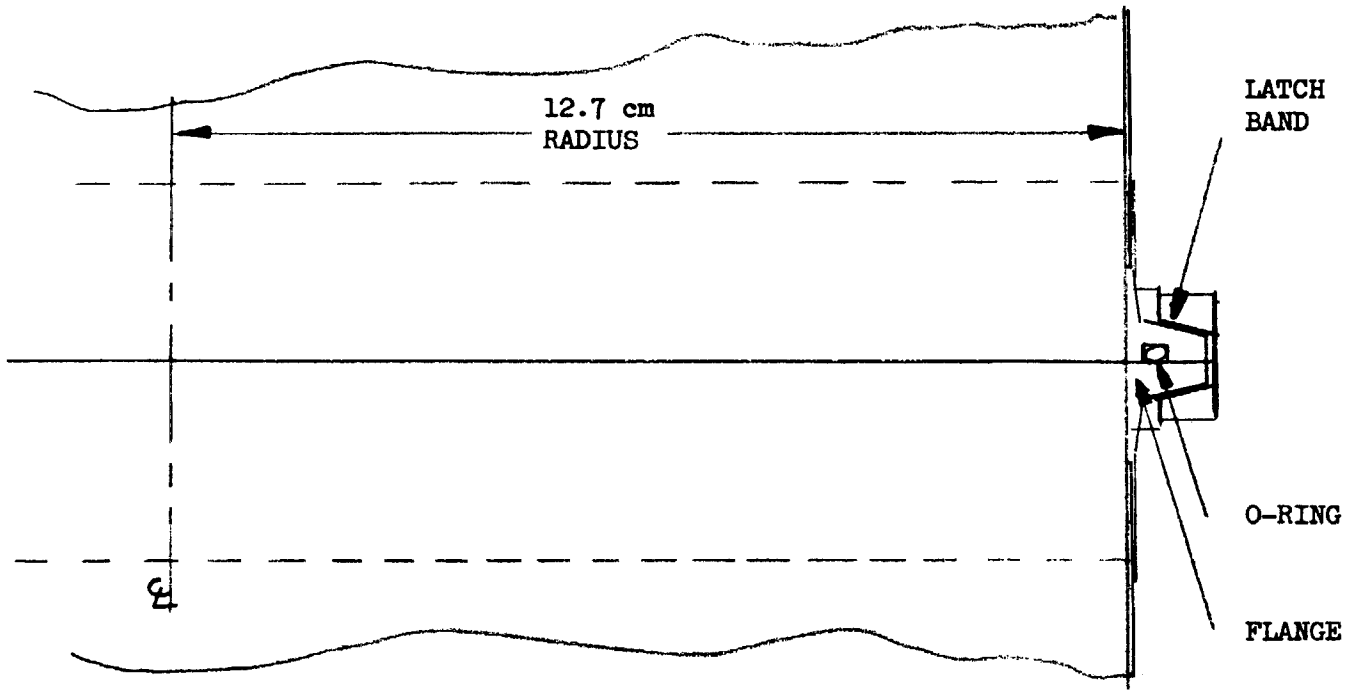

DUCT SIZE	0.254 m DIAMETER (10 in)		.203 m DIAMETER (8 in)	
MATERIAL	STEEL	ALUMINUM	STEEL	ALUMINUM
WEIGHTS (Kg)				
Coupling	.573	.573	.427	.427
Female Flange	.424	.144	.349	.115
O-Ring Flange	.555	.168	.397	.134
Total	1.552 Kg	.885 Kg	1.173 Kg	.676 Kg
NOTES	2 BOLT LATCH		1 BOLT LATCH	

Figure 3. Detail of Representative Joint Section Clamps

3.1.1.2 Channel Design/Comparison Study

The most desirable configuration for the acquistion device is a ring-shaped duct positioned as close to the tank wall as practical. During the conceptual design phase, the principal design concept considered consisted of a solid duct with the fine mesh screen on only the top surface as documented in References 1 and 2. This design facilitates simple immersion bubble point testing, is easy to fabricate, and is adaptable to screen element removal. However, to satisfy the screen area requirement, a 0.79 m (31 in.) channel width is required which is totally impractical. This problem can be avoided by using a pleated screen element which was found, during the Task B bench tests, to offer a good increase in effective screen flow area (3.5 to 4.0 times the projected area) with only minor degradation in bubble point or flow loss characteristics. With a pleated screen element a width equal to 0.262 m (10.3 in.) would satisfy the retention criteria. The screen could be pleated in either direction, but would provide fewer difficulties with the pleats running in a radial direction relative to the tank. The cross section for this design is shown in Figure 4 along with the other possible candidates. To provide adequate sealing of the screen elements, the top of the channel is formed from a 2.5 by 2.5 by 0.25 cm aluminum L-section. The remainder of the duct including transition sections from the near hemisphere to the circular cross section at the joint is made of 0.051-cm aluminum sheet. The screen elements which are sized for 3 to a duct section or 18 per ring are about 0.31 by 0.64 m (12 by 25 in.) and consist of the fine mesh screen in its pleated form, a very coarse mesh aluminum screen, a perforated (50 percent open area) 0.051-cm steel backup plate and a 0.051 by 2 cm steel frame. This sandwich is welded together. Each element is attached to the duct by 60 screws and a simple indium-tin seal is used within this joint to provide a leak path less than that of the fine mesh screen itself. Characteristics of this and the other candidate designs considered are summarized in Table 3.

The weight of a 3.67 m diameter ring is 43.3 kg composed of ducts, 18.5 kg, screen elements, 20.7 kg, and joint/couplings, 4.1 kg.

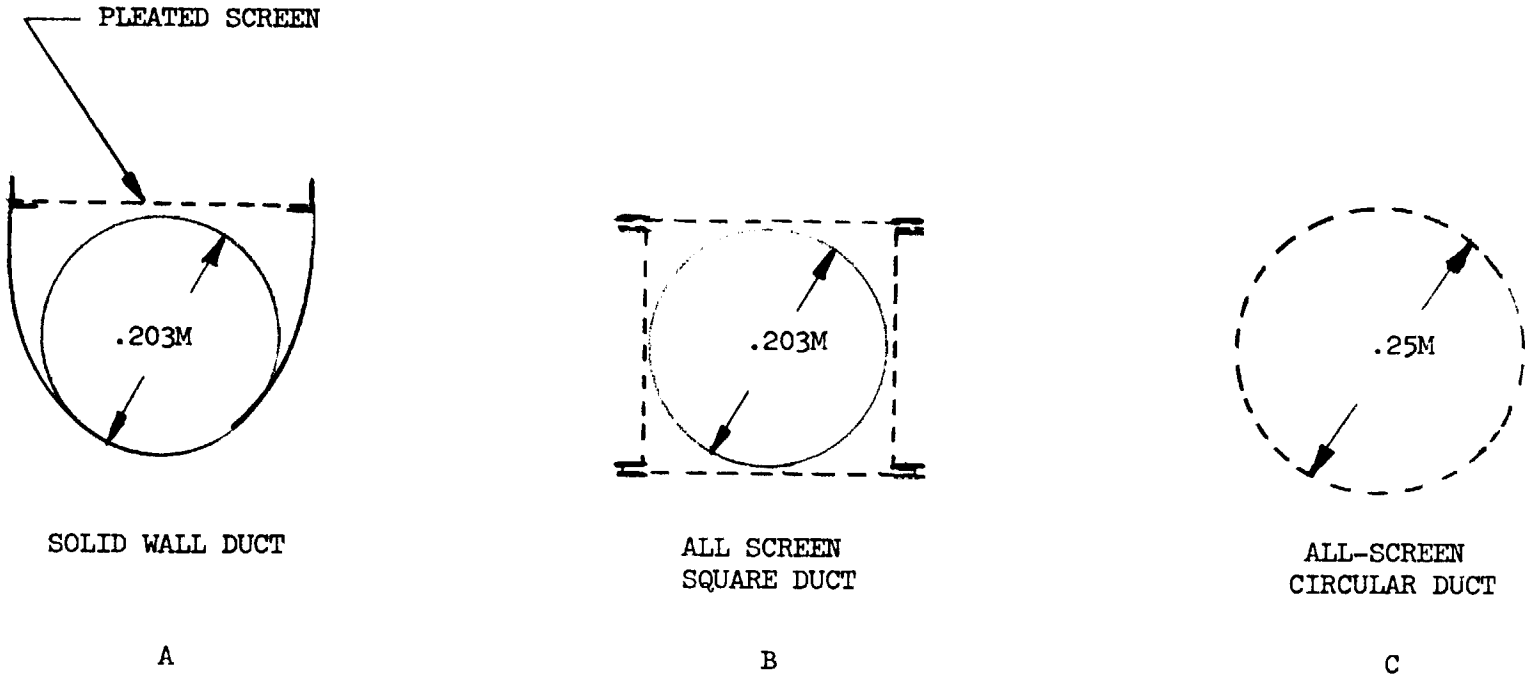

Figure 4. Candidate Acquisition Duct Design Cross Sections (LH_2 Tank)

Table 3

MAIN TANK DISTRIBUTED CHANNEL DESIGN COMPARISONS

Type	Type Cross Section	Segments Per Ring	Weight for 3.6m Diameter Ring (kg)	Screen Replacement Approach	Bubble Point Test Technique	Fabrication Problems	Notes
A1	See A, Figure 4	6	39.5	Remove element	Immersion	Welding of pleated screen	Pleated screen must be used
A2	(Same as A1)	8	66.5	Remove duct section	Immersion	Welding of pleated screen	Pleating essential; all steel construction
A2'	(Same as A2)	8	53.7	Remove duct section	Immersion	Welding of pleated screen; bimetallic joint	Same as A2 except that bimetallic joint allows use of aluminum for most of duct
B1	See B, Figure 4	8	42.5	Remove duct section	Liquid film	Extensive welding along four seams	All screen channel; all steel
B2	See C, Figure 4	8	40.4	Remove duct sections	Liquid film		Simple construction; duct is formed in 16 straight sections to avoid compound curvature; all steel construction
B2'	(Same as B2)	8	29.0	Remove duct sections	Liquid film	Possible overheating of aluminum during screen welding	Use aluminum backup material to save weight

Two variations to the above concept were considered, as noted in Table 3. In the A2 design, rather than remove the screen elements, the duct sections are removed and the screen elements are permanently welded into the duct. (Number of duct sections is increased to 8.) This alternative primarily eliminates the tedious screw attachment operation within the tank. However, this requires an all steel channel which results in a relatively heavy weight. To reduce this weight penalty, the A2' design was evolved which uses a bimetallic joint just below the screen element and employs aluminum for the lower portion of the duct. This design, however, is still relatively heavy.

The other three designs shown in Table 3 and Figure 4 depart from the solid wall concept and use a nearly all screen configuration. This design requires that bubble point testing within the tank be performed using the liquid film technique and that screen removal be accomplished by removing duct sections. In the B1 design, a square duct is used so that the individual screens can be attached to each of the four faces without compound curvature. This results in essentially an all steel structure with an extensive degree of welding. The edges were specifically configured to facilitate the welding (see Figure 4). This design has a competitive weight, 42.5 kg composed of duct/screens, 33.1 kg, and joint/couplings, 9.4 kg.

Design B2 uses a circular duct cross section, but has the ring built up of straight sections to avoid compound curvature. To satisfy the fluid dynamics criteria, the duct must be at least 0.249 m (9.8 in.) in diameter. The maximum distance that the duct will be set off from the wall is a function of the number of straight sections used to form the ring (see Figure 5). To minimize this offset, at least 16 straight sections should be used. Two adjacent sections would be permanently welded and the V-Band joint/couplings would be used at 8 points. Although the B2 design is all steel, it has a relatively low weight, 40.4 kg composed of ducts/screens, 28 kg and joint/couplings, 12.4 kg. Note that the joint/coupling weight is a relatively high percentage (31 percent) of the total because of the large diameter and steel joint flanges.

NUMBER OF STRAIGHT SEGMENTS	d MAXIMUM DISTANCE FROM TANK WALL (M)
4	.53
6	.24
8	.14
16	.038

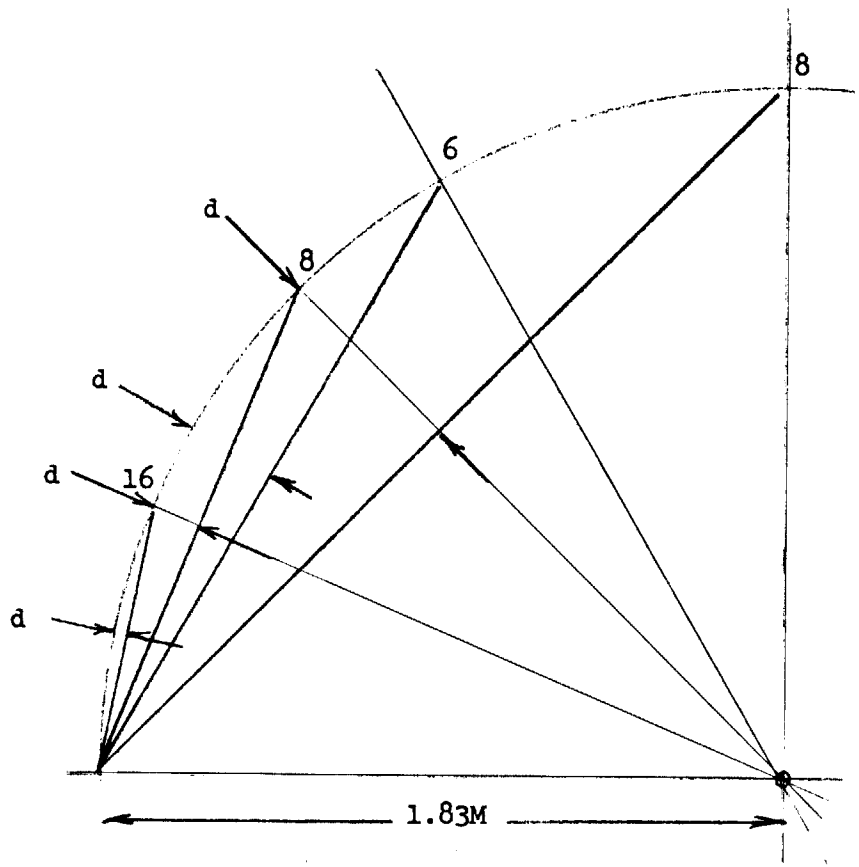

Figure 5. Influence of Straight Duct Segments on Proximity to Wall

A major weight savings can be affected in the B1 design by using an aluminum perforated tube which is attached via riveting to the steel end pieces. This reduces the weight by almost 10 kg/ring but complicates the fabrication. Weight could also be saved if aluminum joint flanges could be used, but this would require bimetallic joints which would further complicate the fabrication and involve additional weight which would offset much of the savings. This idea was therefore dropped from further consideration. The fabrication problem with the B2' design appears to be potential damage of the aluminum from the heat generated during welding. This is currently being studied by MDAC welding specialists.

Designs A1 and B2/B2' appear to be the most desirable designs. B2' is the lowest weight and is relatively straightforward to fabricate. A and B designs differ in the servicing philosophy and in the bubble point test approach. On balance however, the B2/B2' design was tentatively selected as the main tank distributed channel preliminary design.

3.1.1.3 Final System Preliminary Design

The preliminary design of the feed system was continued based on the selection of the B2/B2' ring design.

Acquisition Subsystem

Figures 6 and 7 show layouts of the 3.66m (12 ft) diameter ring assembly. Note that shallow angle elbow sections are used to keep the V-Band joints at a circular cross section. The overall duct system orientation is shown in Figure 6. Two primary acquisition rings are used. A third ring, which provides acquisition during the early portion of the reentry period and general redundancy, is positioned within the propellant trap region. The trap baffle is positioned so that the trap can contain 2.83 m^3 (100 ft^3) of LH_2. This provides propellant for all functions during reentry. An allowance was made for the helium bottle which was sized for cold helium pressurization requirements.

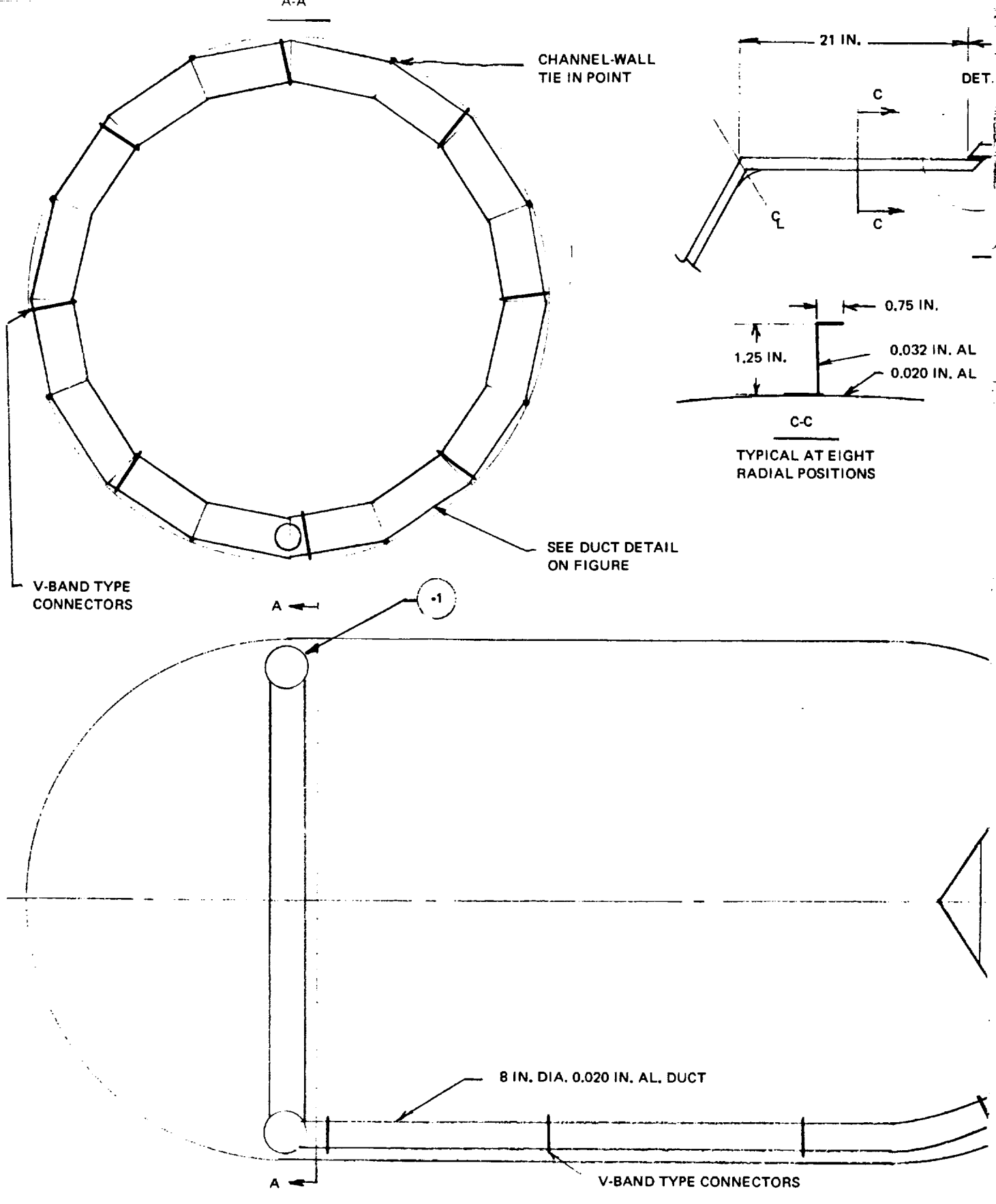

Figure 6. Distributed Channel Acquisition System Configuration

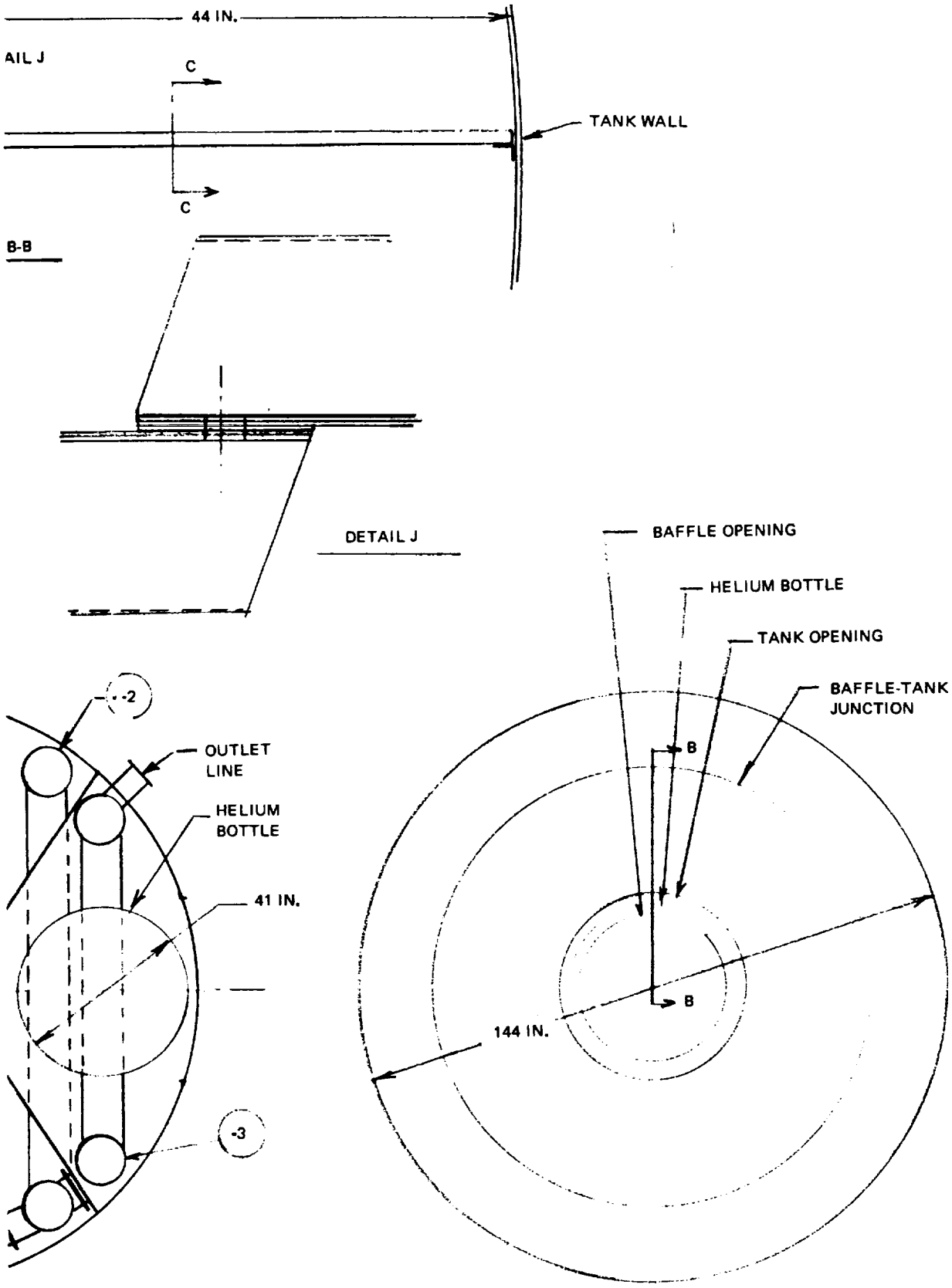
44 IN.
AIL J
C
C
TANK WALL
B-B
DETAIL J
BAFFLE OPENING
HELIUM BOTTLE
TANK OPENING
BAFFLE-TANK JUNCTION
-2
OUTLET LINE
HELIUM BOTTLE
41 IN.
-3
B
B
144 IN.

CHANNEL LOC	A	B
TOP	27.6 IN.	25.8 IN.
BOTTOM	22.8 IN.	21.0 IN.
BAFFLE	18.0 IN.	16.2 IN

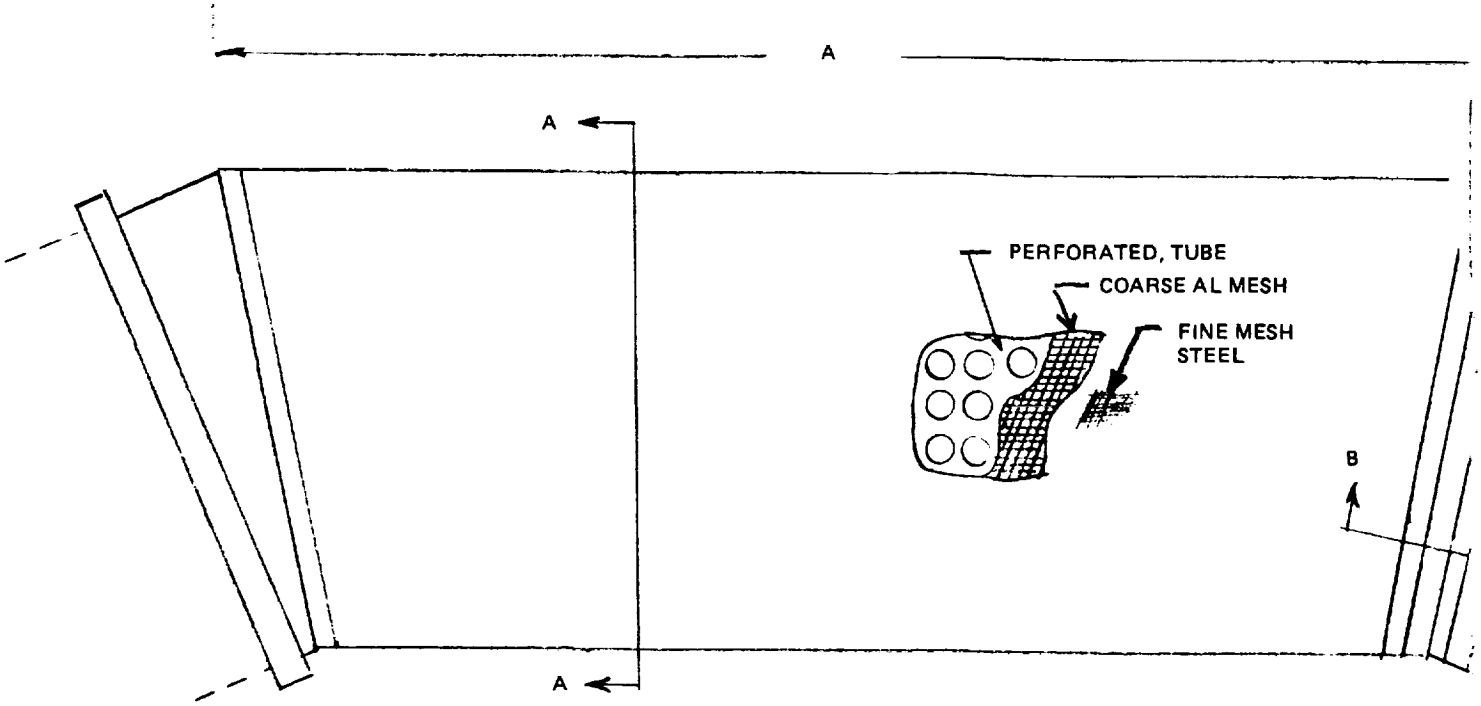

1/4 SCALE

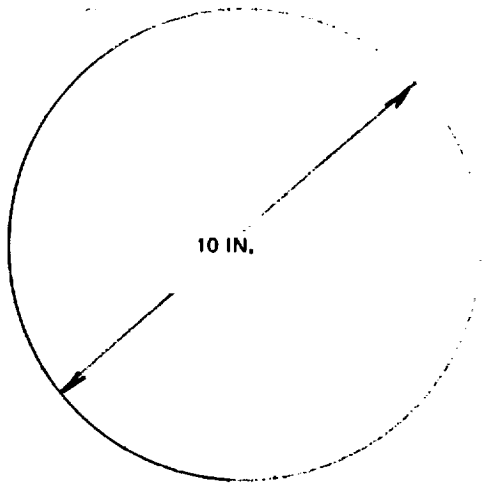

A-A

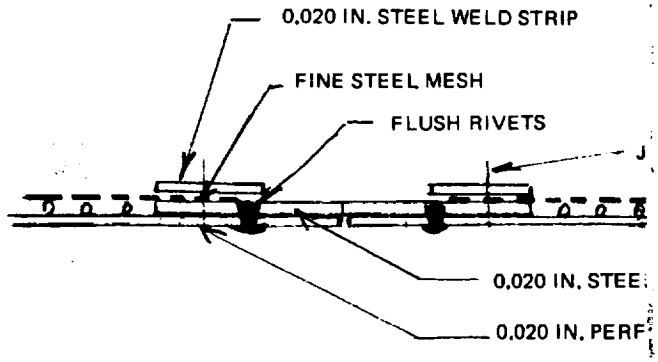

B-B (1/1)

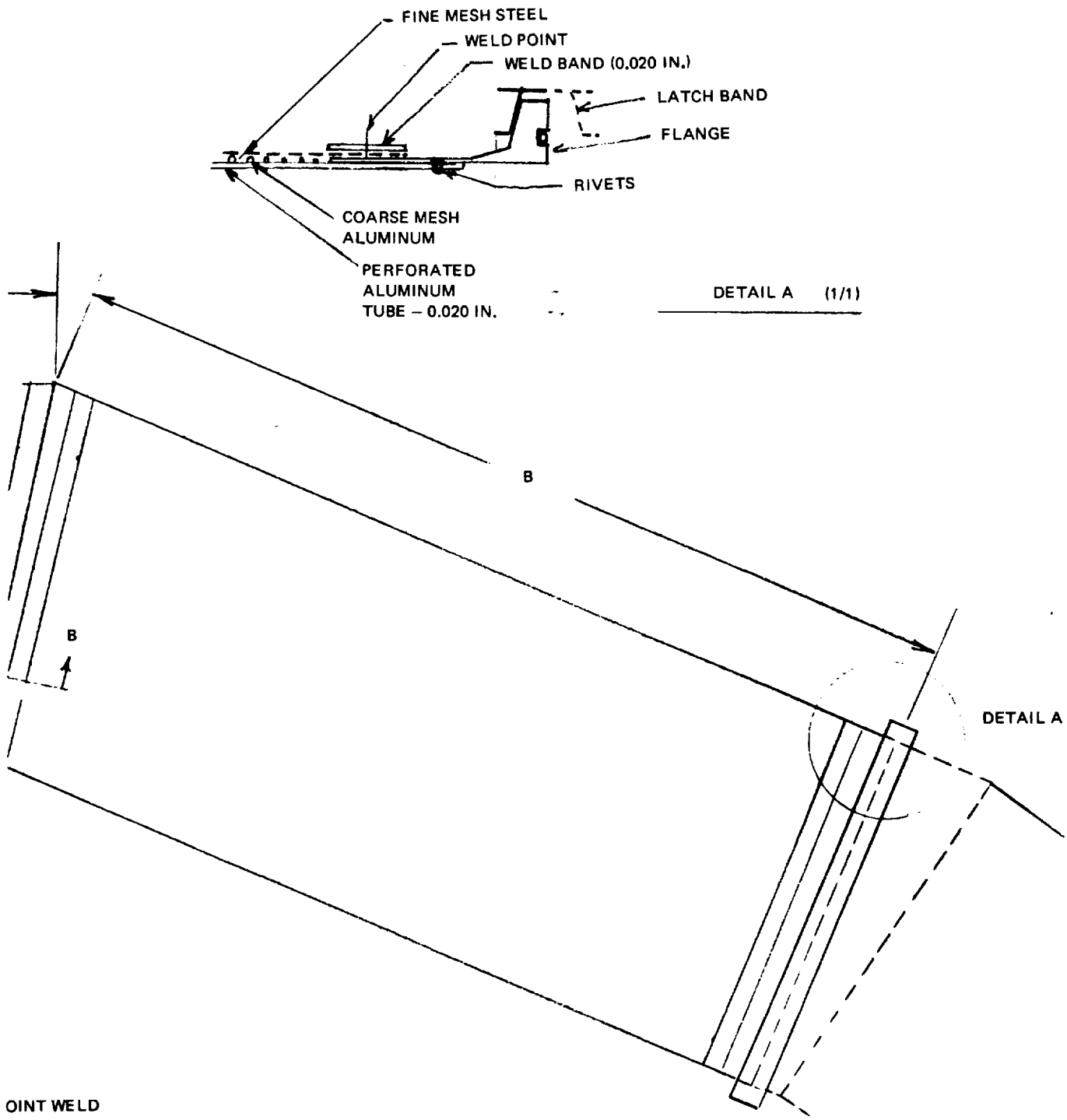

Figure 7. Channel Duct Details

The details shown in Figures 6 and 7 are for the B2' design which uses an aluminum perforated tube. The channel is first formed by rolling the perforated aluminum into two 25.4 cm (10 in.) diameter cylinders. The two cylinders are riveted to the short steel center elbow and the steel end flanges are riveted to the aluminum tube ends to accommodate the V-Band couplings. The flush rivets structurally hold the various elements together but do not provide any form of seal. The coarse mesh aluminum screen (used to reduce pressure loss) is next put into place over the perforated cylinder (no physical attachment) and the fine mesh steel screen is cut and layed in place. Thin (1.27 cm) bands are then clamped along the screen edges and the bands, screen, and steel end pieces are welded together to complete the duct section assembly.

The rings are connected to the sump baffle through 20.3 cm (8 in.) diameter aluminum collector ducts. Similar V-Band joint/couplings are used to join the collector duct sections and to join the collector duct to the rings and the sump baffle.

Details of the thin aluminum baffle are shown in Figure 6. It is made up of 0.051 cm (0.020 in.) aluminum reinforced by eight radially running Z-sections made of 0.081-cm aluminum. The center portion of the baffle cone is removable to provide about a 1m access diameter into the main portion of the tank. The tank itself provides a manhold sufficiently large to accommodate the helium bottle. Fabrication details are presently being reviewed to be sure that additional design compromises will not be necessary to facilitate fabrication.

Each ring is attached to the tank at eight locations as noted in Figure 6. Two techniques have been evolved for attaching the rings to tank wall: a hinge arrangement as presented in Reference 2, and a cable/turnbuckle concept. These are illustrated in Figure 8. Details of the attachment support structure are still under investigation but the weight would be about 0.25 kg for each of the eight ring sections.

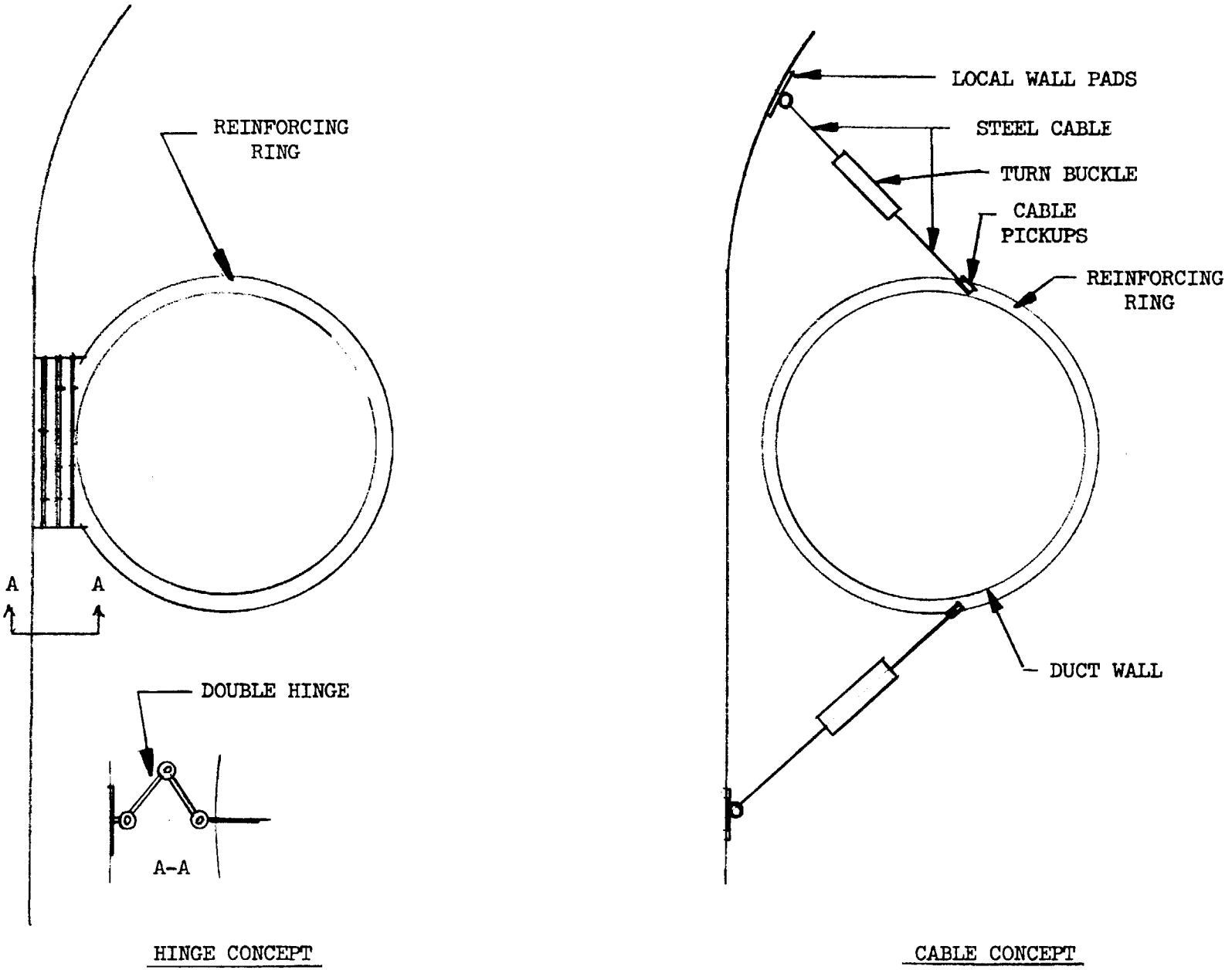

Figure 8. Candidate Channel Support Concepts

Based on the preliminary design as developed to this point, a weight estimate of the acquisition system was made. The breakdown is illustrated in Table 4. In addition to the B2' design, the weight is also shown for the all stainless steel B2 design. Weights are slightly higher than estimated for the comparison study (large B2' channel weight is 29.5 kg instead of 29.1 kg). The acquisition system for the LO_2 tank is similar to that for the LH_2 tank except that three rings are used in the main tank. The duct cross-sectional diameter is only 17.8 cm (7 in.) since this will satisfy all flow requirements. The required baffle volume is also only about 0.623 m^3 (22 ft^3) which means the baffle weight is much smaller. The weight summary for the LO_2 tank acquisition system is shown in Table 5 assuming the B2' duct design.

Pressurization

Extensive pressurization analyses were reported in previous quarterly reports. These studies generally addressed the comparison of cold helium and autogenous pressurization for the LH_2 tank. The results are summarized in Figure 9, which shows that the basic weight of a cold helium system is about 327 kg and about 165 kg for an optimum autogenous system based on maintaining $34.6.10^3$ N/m^2 (5 psi) NPSP. However, the bench tests conducted for screen heating from a warm GH_2 ullage (see Section 3.2.1) showed that retention or at least a severe loss in bubble point performance can result when using a warm gas pressurant. Thus the 200°R inlet temperatures, which are optimum for autogenous pressurization system, should be avoided. The weight penalty involved in using a cold helium system is relatively high and thus an alternate approach using cold GH_2 was investigated. Figure 10 shows the basic pressurization weights for the alternate systems for both 18 and 6 expulsion step duty-cycles. (18 steps are more representative of a Shuttle class vehicle and 6 burns are more in line with advanced cryogenic spacecraft requirement.) Various liquid usage distributions were also considered:

A. 18 identical expulsion steps evenly distributed over the 7-day mission 5 percent initial ullage.

B. 18 identical expulsion steps evenly distributed over the 7-day mission 30 percent initial ullage.

Table 4

DISTRIBUTED ACQUISITION SYSTEM WEIGHT ESTIMATES (LH_2 TANK)

	B2' Duct Design		B2 Duct Design	
- 1 Duct	29.5 kg	(64.9 lb)	40.8 kg	(90.0 lb)
- 2 Duct	25.9	(57.1 lb)	36.2	(79.7 lb)
- 3 Duct	23.6	(52.1 lb)	31.1	(68.4 lb)
Collection duct	8.8	(19.3 lb)	8.8	(19.3 lb)
Baffle	23.6	(52.1 lb)	23.6	(52.1 lb)
Subtotal	111.4	(245.5 lb)	140.5	(309.5 lb)
Support/attachments	6.2	(13.5)	6.2	(13.5)
Total	117.6 kg	(259.0 lb)	146.7 kg	(323.0 lb)

Table 5

DISTRIBUTED ACQUISITION SYSTEM WEIGHT ESTIMATES
LO_2 TANK - B2' DUCT DESIGN

- 1 Duct	16.3 kg	(35.8 lb)
- 2 Duct	18.9	(41.7)
- 3 Duct	15.4	(34.0)
- 4 Duct	15.0	(33.0)
Collector duct	3.7	(8.1)
Baffle	5.7	(12.5)
Subtotal	75.0 kg	(165.1 lb)
Support/attachments	8.3	(18.3)
Total	83.3 kg	(183.4 lb)

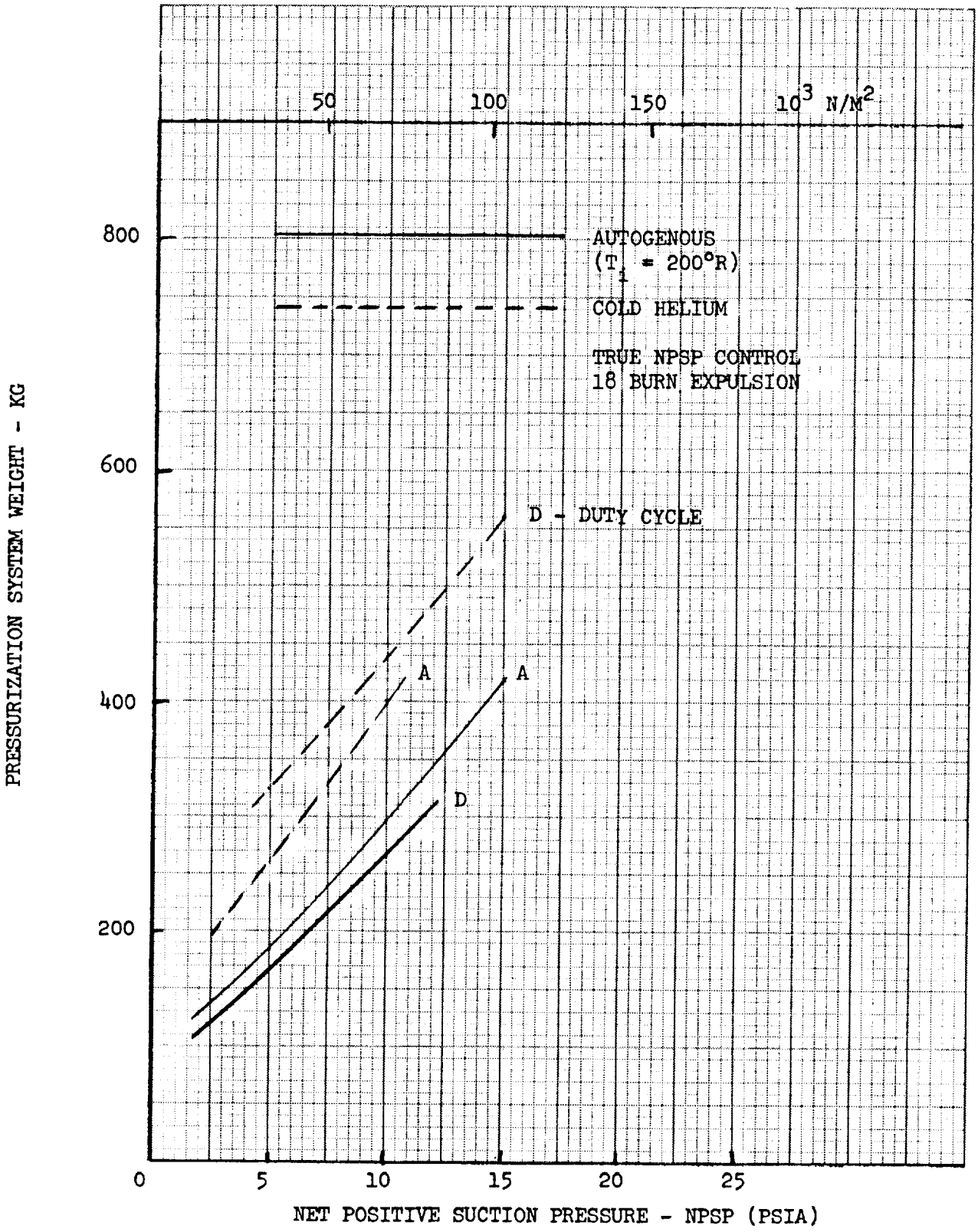

Figure 9. Comparison of Autogenous and Cold Helium LH_2 Tank Pressurization

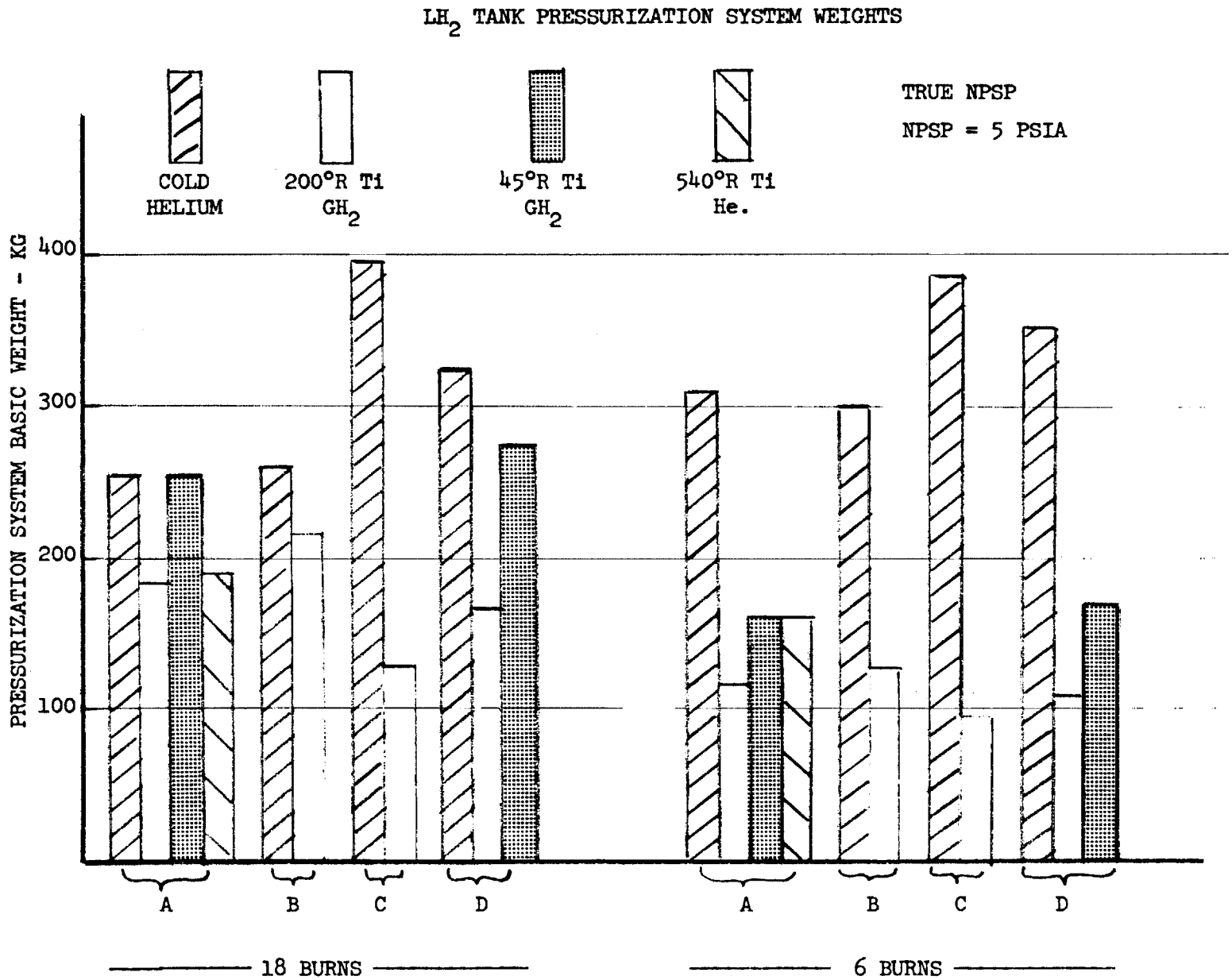

Figure 10. LH_2 Tank Pressurization System Weights

C. First expulsion step occurs at very beginning of mission consuming 40 percent of LH_2. The next 16 expulsion steps are identical and evenly spaced over 7 days with a total consumption of 20 percent of the loaded LH_2. Last burn occurs at end of mission consuming 40 percent of loaded LH_2; 5 percent initial ullage volume.

D. Same expulsion cycle as C but with 30 percent initial ullage volume.

The D condition most nearly approximates Shuttle AFP type operations and is the selected design condition.

Figure 10 shows that cold GH_2 can reduce the basic pressurization system weight relative to cold helium by about 55 kg or 17 percent. The performance of cold GH_2 should also be noted for the 6 burn case. Here the corresponding weight savings is about 180 kg or 51 percent. Also, the weight savings in going to 200°R GH_2 is only about another 60 kg. Thus, for an advanced cryogenic vehicle, a cold GH_2 system is a most viable candidate.

The autogenous, hot and cold, pressurization concept involves certain fundamental thermodynamic and mechanical problems when used with an open screen acquisition device. For example, interaction between autogenous pressurant gases and screen devices causes vapor condensation and ingestion into the screen device which can result in retention breakdown. This ingested fluid is warmer than that retained in the device and pressure decay induced vaporization of hydrogen within the screen device can result in subsequent screen retention breakdown. Also, the condensed liquid at the screen surface, being at a somewhat higher temperature than the bulk, will require increasing of the tank pressure to meet NPSP requirements. This will thus result in system weight increases. These various problems are discussed in detail in the Appendix. Before the cold GH_2 system can be adopted, an experimental investigation into the severity and characterization of these problems must be conducted. A bench test is being evolved to answer some of the critical questions (see Section 3.2.10).

From a mechanical standpoint, some means must be provided for supplying low-temperature hydrogen gas. The APS accumulators provide a high-pressure gas source, but this gas is at too high a temperature (110 to 170°K) and it must be cooled. Using the accumulator as the high-pressure GH_2 source at least 135×10^3 watt (128 Btu/sec) must be removed from the GH_2 before entering the tank at close to LH_2 temperatures. If a heat exchanger were submerged in the LH_2 tank utilizing free convection, 560 m^2 (6,000 ft^2) of heat transfer area would be needed, which is impractical. A more reasonable approach is to use a compact heat exchanger which uses pumped LH_2 taken from the acquisition device to cool down the GH_2 being supplied from the accumulator. In the process the liquid flow will vaporize. Of course, a booster type pump must be used to feed the LH_2 from the acquisition device into the heat exchanger. Furthermore, to conserve fluid, both flows are mixed upon leaving the heat exchanger to form the actual pressurant stream entering the tank. For a specific accumulator gas temperature, the ratio of the LH_2 flow through the heat exchanger to the gas flow has a certain theoretical value as shown below

$T_{accumulator}$	$\frac{\dot{W}_{liquid}}{\dot{W}_{gas}} = \frac{C_p \Delta T_G}{H_v}$
111°K (200°R)	2.53
139°K (250°R)	3.31
117°K (300°R)	4.11

For the 111°K case, 37×10^3 watt (36 Btu/sec) must be removed from the GH_2 thus requiring about 7.17m^2 (72 ft^2) which is more reasonable but would still be heavy (about 18 to 20 kg). A simpler and potentially more efficient approach is to intimately mix the LH_2 and warm GH_2 in a vaporizer/cooler. This vaporizer/cooler should weigh only about 3 to 5 kg. Schematics for the two GH_2 conditioning concepts are shown in Figure 11.

The pump must be capable of providing about 0.086 kg/sec with a pressure rise of 173×10^3 N/m^2 (25 psi) which is essentially governed by injector differential pressure. Assuming a pump efficiency of 65 percent, this requires a 324-watt pump and about a 540-watt motor.

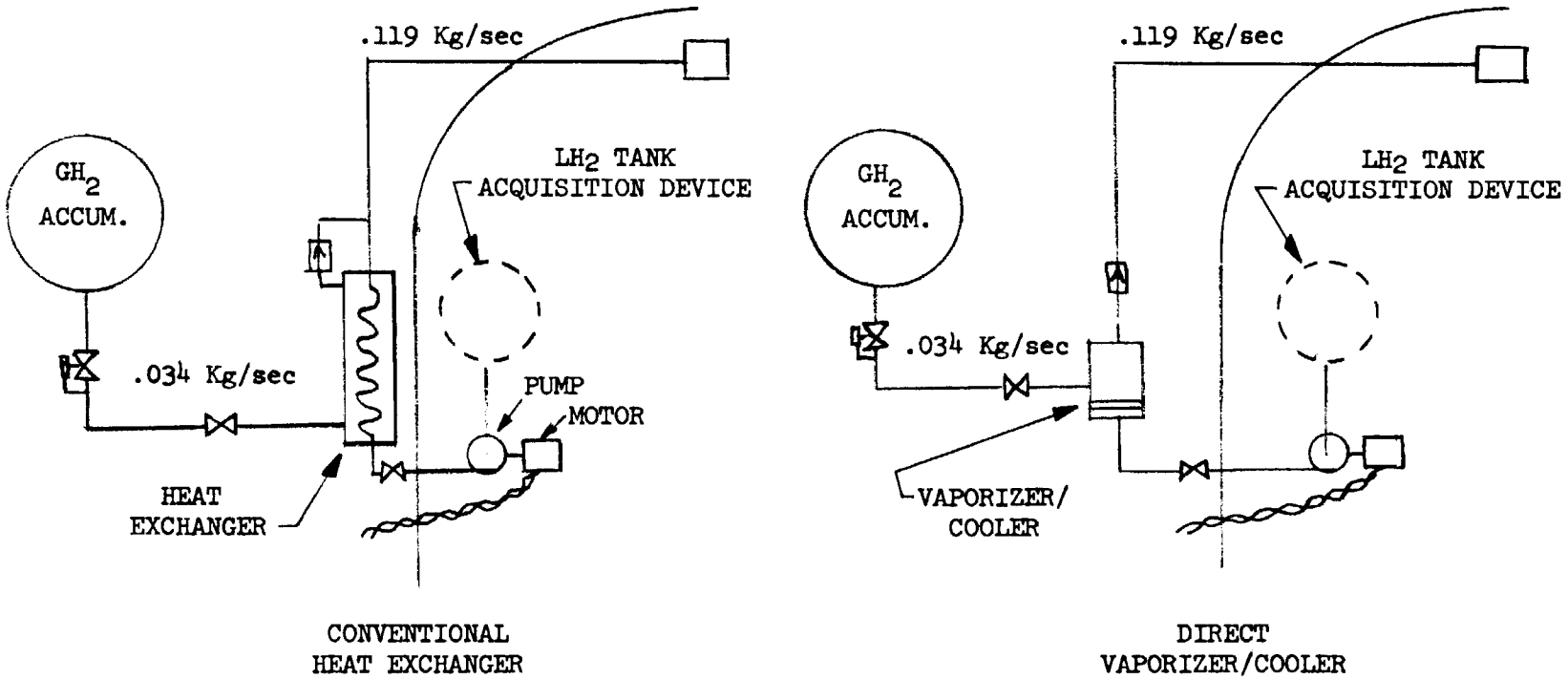

Figure 11. Cold GH_2 Conditioning Concepts

Based on very preliminary numbers, the vaporizer/cooler GH_2 conditioning device should have the following weights.

Pump	2.0 kg
Motor	2.0
Vaporizer/Cooler	4.0
Supports, etc.	0.8
	8.8 kg

This compares favorably with the 55-kg savings afforded by the cold GH_2 system relative to the cold helium.

A pressurization system weight summary has been prepared for each pressurization system in Table 6.

As reported in Reference 2, an LO_2 tank helium pressurization system with an inlet temperature close to that of the liquid was selected. Pressurization requirements for a Class D, 18 burn expulsion cycle was made (see Figure 12) and the LO_2 pressurization system weights were estimated as summarized in Table 7.

Integration

Previous sections have defined the basic acquistion and pressurization system components and weights. Figures 13 and 14 present the schematics for the candidate distributed acquisition systems for both cold helium and cold GH_2. These define the essential control components and the line sections. No provisions for redundancy are included at this time. The systems are generally straightforward. It will be noted that in both cases true NPSP control is provided. The corresponding line and control component weights are shown in Tables 8, 9, and 10.

The insulation system weights for the LH_2 and LO_2 tanks are summarized in Table 11. The weights are for the optimum insulation system defined in Reference 1, and the weights are as shown in Figure 8 of Reference 1, except for the updating of the purge bag weight and MLI layers per the values reported in Reference 3.

Table 6

DISTRIBUTED CHANNEL BASIC PRESSURIZATION SYSTEM WEIGHT (LH_2 TANK)

	Pressurization Concept	
	Cold Helium	Cold GH_2
Helium	102 kg	--- kg
GH_2 Vapor	60	239
Helium Bottle	147	---
Bottle Supports	14	---
ΔWT (Bottle)	7	---
ΔWT (Vapor)	7	26
ΔWT Insulation	4	7
	341 kg	272 kg

True NPSP

ΔP = 5

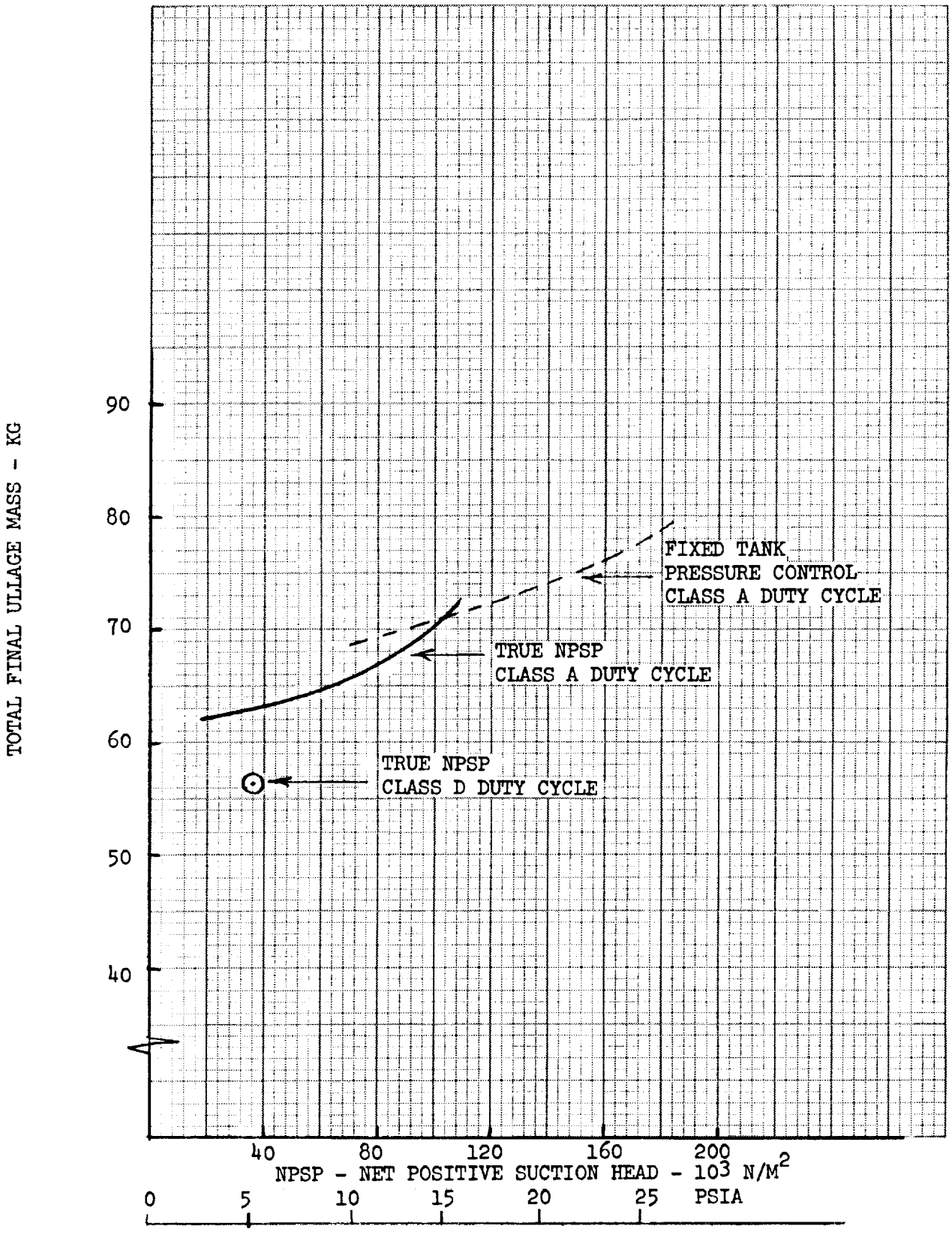

Figure 12. LO_2 Tank Pressurization Requirements -- 200°R Helium

Table 7

COLD HELIUM PRESSURIZATION SYSTEM WEIGHTS LO_2 TANKAGE

Helium	5.5 kg	(12 lb)
Gaseous Oxygen	51.0	(113 lb)
Helium Bottle	7.9	(17 lb)
Bottle Supports	0.8	(1.8 lb)
Vapor Tank Weight Penalty	2.7	(6.0 lb)
Bottle Tank Weight Penalty	0.4	(0.8 lb)
	68.3 kg	(150.6 lb)

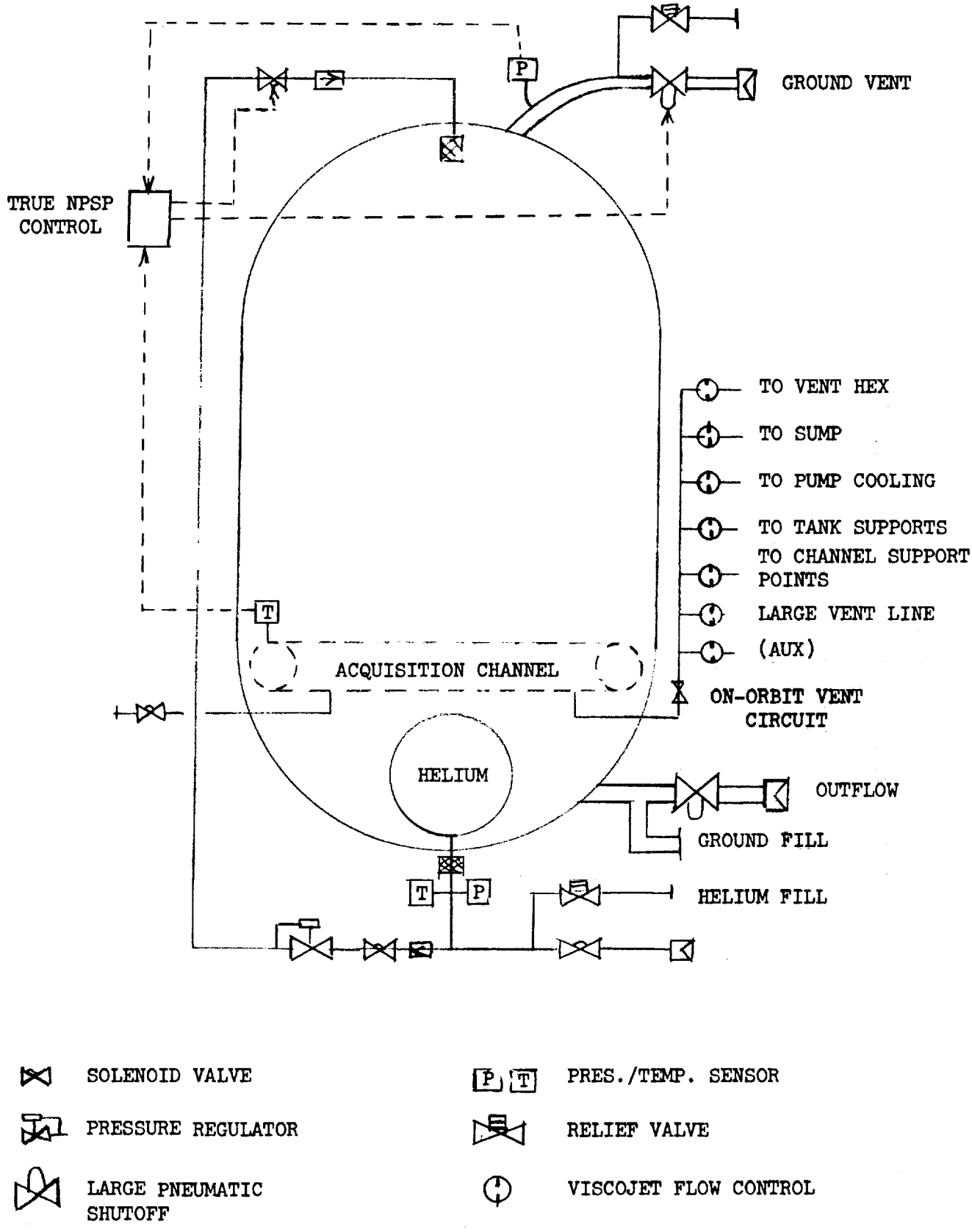

Figure 13. Cold Helium Pressurization System Schematic (Distributed Channel Acquisition System)

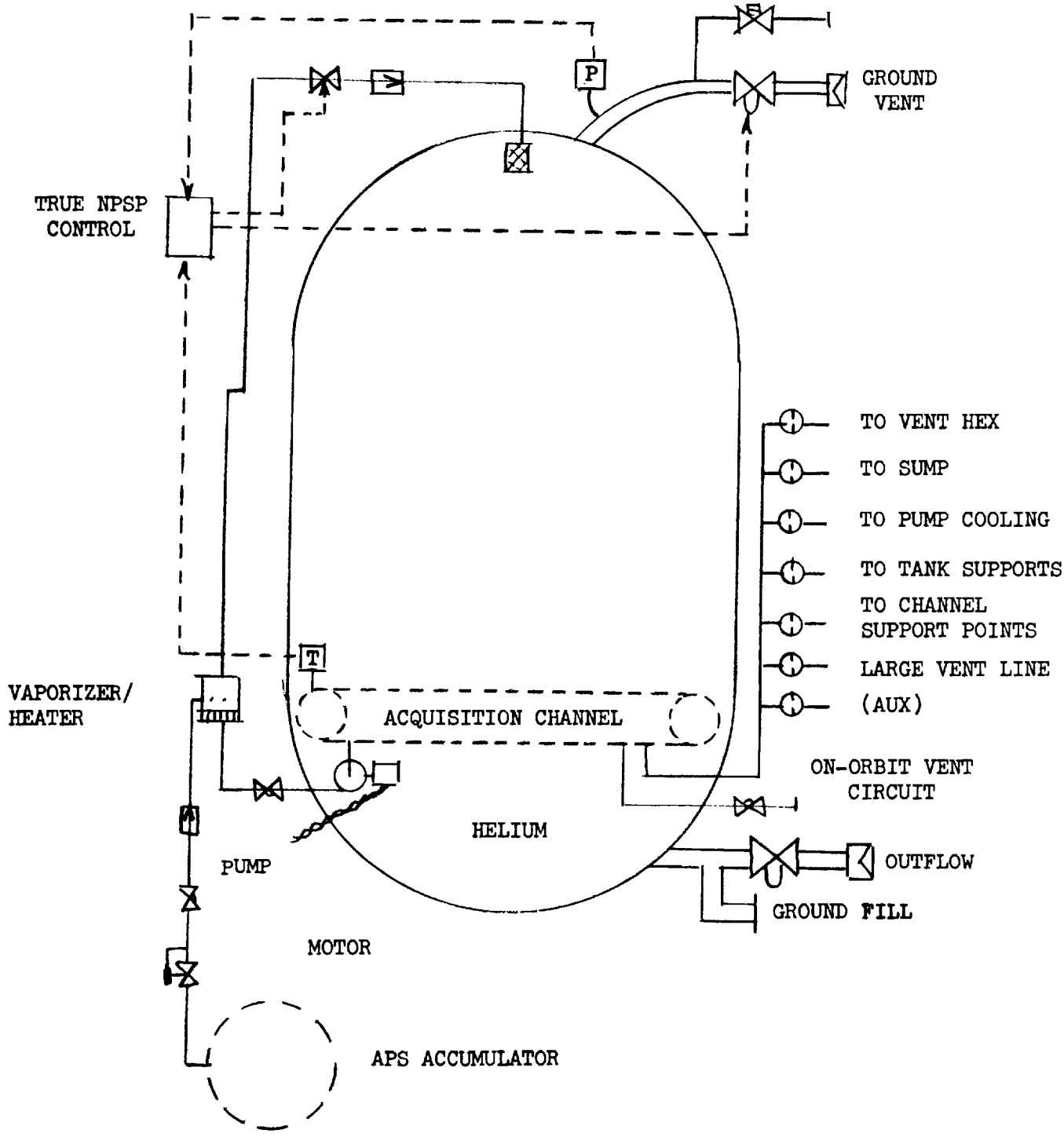

Figure 14. Cold GH_2 Pressurization System Schematic (Distributed Channel Acquisition System)

Table 8

LH_2 SYSTEM COMPONENT WEIGHTS (COLD HELIUM PRESSURIZATION)

Quantity	Item	Weights	
1	Outlet shutoff valve (2-inch ball)	6.35 kg	(14 lb)
1	2-inch quick-disconnect	2.27	(5 lb)
1	4-inch vent valve	9.10	(20 lb)
1	4-inch gas quick disconnect	2.72	(6 lb)
2	Pressure sensors	0.68	(1.5 lb)
1	Pressurization diffuser	0.45	(1.0 lb)
2	Check valves (1 inch)	1.36	(3 lb)
2	Solenoid valves (1 inch)	1.82	(4 lb)
1	Pressure controller (split with LO_2 tank)	3.18	(7 lb)
2	Solenoid valves (1/2 inch)	0.73	(1.6 lb)
2	Temperature sensors	0.45	(1.0 lb)
1	Filter	1.36	(3.0 lb)
7	Viscojets	0.32	(0.7 lb)
1	High-pressure relief (1 inch	2.72	(6.0 lb)
1	High-pressure solenoid (1 inch)	1.82	(4.0 lb)
1	1-inch quick-disconnect	0.91	(2.0 lb)
1	High-pressure regulator	2.27	(5.0 lb)
	Component support hardware	4.54	(10.0 lb)
		52.15 kg	(113.8 lb)
	Feed lines (2 inch)	0.91	(2.0 lb)
	Vent lines (4 inch)	5.90	(13.0 lb)
	Pressurization lines (1 inch)	10.45	(23.0 lb)
	Miscellaneous lines	3.18	(7.0 lb)
	Fittings	2.27	(5.0 lb)
	Supports and miscellaneous hardware	2.27	(5.0 lb)
		24.98 kg	(55.0 lb)

Table 9

LH_2 SYSTEM COMPONENT WEIGHTS (COLD GH_2 PRESSURIZATION)

Quantity	Item	Weights	
1	Outlet shutoff valve (2-inch ball)	6.35 kg	(14 lb)
1	2-inch quick-disconnect	2.7	(5 lb)
1	4-inch vent valve	9.10	(20 lb)
1	4-inch relief vlave	9.10	(20 lb)
1	4-inch gas quick-disconnect	2.72	(6 lb)
2	Pressure sensors	0.68	(1.5 lb)
1	LH_2 boost pump	2.00	(4.4 lb)
1	Electric motor	2.00	(4.4 lb)
1	Vaporizor/cooler	4.00	(8.8 lb)
1	Pressurization diffuser	0.45	(1.0 lb)
2	Check valves (1 inch)	1.36	(3.0 lb)
1	Solenoid valves (1 inch	0.91	(2.0 lb)
1	Pressure controller (slit with LO_2 tank)	3.18	(7.0 lb)
2	Solenoids (1/2 inch)	0.73	(1.6 lb)
2	Temperature sensors	0.45	(1.0 lb)
7	Viscojets	0.32	(1.1 lb)
1	High-pressure solenoid (1 inch)	1.82	(4.0 lb)
1	High-pressure regulator	2.27	(5.0 lb)
	Component support hardware	4.60	(10.0 lb)
		54.31 kg	(119.8 lb)
	Feed lines (2 inch)	0.91	(2.0 lb)
	Vent lines (4 inch)	5.90	(13.0 lb)
	Pressurization lines (1 inch)	10.45	(23.0 lb)
	Miscellaneous lines	3.18	(7.0 lb)
	Fitting	2.27	(5.0 lb)
	Support and miscellaneous hardware	2.27	(5.0 lb)
		24.98 kg	(55.0 lb)

Table 10

LO_2 SYSTEM COMPONENT WEIGHTS (COLD HELIUM PRESSURIZATION)

Quantity	Item	Weights	
1	Outlet shutoff valve (2 inch ball)	6.35 kg	(14 lb)
1	2-inch quick-disconnect	2.27	(5 lb)
1	3-inch vent valve	5.45	(12 lb)
1	3-inch gas quick-disconnect	2.72	(6 lb)
1	Pressure sensor	0.36	(0.8 lb)
1	Pressurization diffuser	0.45	(1.0 lb)
1	Check valve (1 inch)	0.68	(1.5 lb)
2	Solenoid valves (1 inch)	1.82	(4 lb)
1	Pressure controller (split with LO_2 tank)	3.18	(7 lb)
2	Solenoid valves (1/2 inch)	0.73	(1.6 lb)
1	Temperature sensor	0.23	(0.5 lb)
7	Viscojets	0.32	(0.7 lb)
1	High-pressure solenoid (1 inch)	1.82	(4.0 lb)
	Component support hardware	3.63	(8.0 lb)
		29.92 kg	(66.1 lb)
	Feed lines (2 inch)	0.91	(2.0 lb)
	Vent lines (3 inch)	4.50	(10.0 lb)
	Pressurization lines (1 inch)	10.45	(23.0 lb)
	Miscellaneous lines	3.18	(7.0 lb)
	Fittings	2.27	(5.0 lb)
	Supports and miscellaneous hardware	2.27	(5.0 lb)
		23.58 kg	(52.0 lb)

Table 11

TANKAGE THERMAL PROTECTION SYSTEM WEIGHT ESTIMATES

	LH_2 Tank	LO_2 Tank
Purge bag	36.3 kg	16.8 kg
MLI face sheets	35.2	15.0
MLI	63.5	12.4
Attachments	1.1	.6
Tape and thread	2.6	1.5
Foam	58.0	0
	196.7 kg (437 lb)*	46.3 kg (102 lb)*

*Does not include insulation penalties attributed to pressurization

The various subsystems were next combined together to yield a total feed system weight for the distributed channel acquisition system for both the cold helium and cold GH_2 pressurization options on the LH_2 side (see Table 12). Weights have been extracted from preceding tables except for the boiloff loss, coolant loss, pump startup and shutdown loss, and the vent system weights which are identified by the footnotes.

3.1.2 Preliminary Design – Start Tank Concept

During Phase I, start tank acquisition concept design studies were conducted relative to the Shuttle APS class requirement, as reported in Reference 2. Two overall conclusions were reached as a result of this work: (1) based on a conservative cryogen usage, a large start tank size of 22 m^3 (778 ft^3) is required when utilizing only available high acceleration flight periods for start tank refill, and (2) the use of programmed or dedicated periods for acceleration or dynamic refill resulted in reducing the start tank size but also necessitated an unacceptably large weight penalty in expended propellant used to produce the settling acceleration.

Two approaches are now being explored that will evolve more favorable start tank design alternatives. These include (1) extablishing a more realistic cryogen usage requirement and (2) the incorporation of a zero-g start tank refill concept. The revision to the cryogen usage requirement is still being investigated, but the study into a low-g refill concept termed "vacuum vent/refill" has essentially been completed and is outlined below including a comparison with an updated 22-m^3 start tank using available high acceleration flight periods for dynamic refill.

Following are some of the conclusions reached in this particular start tank study:

A. All-screen channels significantly minimize channel weight and the feasibility of an appropriate bubble point test technique for an all-screen design has been demonstrated.

B. The vacuum vent/refill concept is feasible and allows the LH_2 start tank size and weight to be minimized. The start tank size is then dictated by the propellant expulsion requirements necessary for the reentry and landing phase. However, the maximum size dynamic refill LO_2 start tank is the minimum weight system.

Table 12

DISTRIBUTED CHANNEL ACQUISITION SYSTEM WEIGHT SUMMARY

Pressurization Concept	LH_2 Tank		LO_2 Tank
	Cold Helium	Cold GH_2	Cold Helium
Acquisition System	117.6 kg	117.6 kg	83.3 kg
Pressurization System	341.0	272.0	68.3
Feed System Components	77.2	79.3	54.0
Insulation System	196.7	196.7	46.3
Thermal Induced Boiloff	112.0	112.0	0
Basic Tankage [1]	678.0	678.0	265.0
Low-g Tank Pressure Control [2]	41.8	41.8	20.9
Cryogen Loss for Cooling - LH_2	60.2	60.2	0
	1624.5 kg	1557.6 kg	537.8 kg
Pump Bypass Loss [3]	260	260	490

[1] Does not include penalties incurred by other-systems - these are included with the subsystem of concern

[2] Assumed vapor cooled shroud TVS

[3] Assumes direct overboard dumping of 100% bypass for 50 startup/shutdown cycles

C. The vacuum vent/refill start tank is highly flexible in terms of meeting a wide range of propellant requirements during the orbital maneuvers.

D. The vacuum vent/refill start tank, being a relatively small, localized screen device, is capable of meeting relatively higher acceleration loads with coarser mesh screens than larger screen devices.

E. The vacuum vent/refill operation provides a unique acceleration-level independent capability for reestablishing retention and acquisition in the screen devices. Thus, an inadvertent, unexpected screen breakdown can be corrected and the mission continued rather than initiating emergency reentry and landing procedures.

F. Nearly all of the pump bypass propellants (startup and shutdown losses) can be added back into the main tanks as a part of the pressurization system without incurring penalties on the pressure isolated screen devices in the start tank; a significant weight reduction results since this propellant would normally be dumped overboard.

G. Weight reductions are achievable by use of bimetallic (aluminum and steel) channels; all aluminum channels with aluminum screen, and start tanks with part of the pressure shell common to the main tank wall. The start tank size is also reduced by expelling the cooling hydrogen from the main tank channel used during start tank vacuum refill. These additional weight reductions will be considered as refinements to the designs developed to this point during the next reporting period.

H. Access to the start tank for replacement of the acquisition system components is accomplished through removable manhole covers in the start tank or, in the case of the small LO_2 start tanks, removal of the start tank through the main tank manhole cover.

I. Marman clamps are used for removal of channel sections.

The operation, design, and performance of the start tank including vacuum vent/refill are discussed in the following paragraphs.

3.1.2.1 Vacuum Vent/Refill Start Tank Concept and Operation

Rather than employ a start tank which is sized for refill only during the

relatively high-g vehicle maneuvers, a smaller start tank is considered with the additional capability of zero-g or low-g refill. Dynamic refill is still used during the positive acceleration engine burns, which settles the main tank propellant, but the propellant flow demands required during the long-term coast periods are met by periodically refilling a relatively small start tank. For example, with the Shuttle APS, a liquid hydrogen start tank of 22 m^3 (778 ft^3) is required if dynamic refill alone is used, whereas a 1.4 to 2.8 m^3 (50 to 100 ft^3) (or smaller) liquid hydrogen start tank may be used if vacuum vent/refill is used. Experiments performed to date with liquid hydrogen show that the concept is practical. MDAC IRAD tests performed with a 10-gallon liquid hydrogen start tank demonstrated complete refill in periods of the order of 15 seconds. The vacuum vent/refill procedure is acceleration level independent and can be completely developed without the need for in-orbit testing. The LH_2 start tank size and system weight is greatly reduced; in the case of a Shuttle requiring propellant storage through reentry and landing, the size is determined by the propellant volumes required for these operations. The addition of this capability to the start tank renders it essentially mission independent, if time periods of the order of 5 to 15 minutes are available for the vent and refill operation. With high-pressure accumulators providing flow of gaseous propellant, the normal time to empty the accumulator is greater than practical start tank vacuum refill times, and therefore propellant flow demands for intermittent ACS maneuvers, life support, and fuel cells can be met while the start tank is refilled.

In view of the need for thoroughly verifying the vacuum refill concept, a series of additional tests have been scheduled during the checkout of the Interface Demonstration Unit (IDU) being fabricated under a parallel contract, NAS 8-27571. These tests will determine the refill time and pressure response for a range of initial pressures. A major objective of these tests is to prove that the screen device is completely refilled with liquid.

The basic vacuum vent/refill operations and design concepts associated with both the start tank and main tank propellant control are discussed below.

Vacuum Vent/Refill-Start Tank Operation

The configuration of the start tank with vacuum vent/refill capability is

shown in Figure 15. The start tank size is less than the maximum required if no separate refills are performed, but large enough to contain the propellant required for control during the reentry maneuvers and landing. Assume that the start tank has been partially emptied by various low-g propellant demands and that it is necessary to initiate refill in preparation for a low-g propellant expulsion, such as accumulator refill of the ACPS. (If engine restart were required, refill could be accomplished during the engine burn, which is the normal start tank refill mode.) If necessary, the start tank pressure is first increased 1 to 2 psi above the main tank pressure. In the simplest design, a small bypass valve between the start tank channels and the main tank is then opened. Propellant flows out of the start tank into the main tank until surface tension breakdown occurs in the screen device, assumed to be one of the channels. The total residual liquid remaining in the start tank at this point is the liquid in the channels and the liquid on the walls of the start tank. This liquid, as well as the helium pressurant and hydrogen vapor, is then vented overboard. The start tank vent valve is then closed. The refill valve, which is connected to a redundant screen device (e.g., a ring channel contained in the trap region), is then opened and liquid propellant flows into the start tank. This process involves essentially reversible evaporation and condensation and has been shown (References 4 and 5) to result in refill. It should be noted that in a low-g environment the principal problem with refill of a start tank or any localized screen device (e.g., start basket) is the difficulty in venting pure vapor, not liquid, overboard as the device is filled. The vacuum vent/refill procedure discussed below is used in lieu of such techniques as liquid/vapor separators (centrifugal, electrophoretic, dielectrophoretic, etc.) and vehicle acceleration.

As a refinement of the basic concept described above, auxiliary screen devices in the channel and on the inside start tank wall (shown in Figure 15) are used to transfer nearly all of the propellant back into the main tank before the vacuum vent operation. Details of the auxiliary screen device design are given in following sections.

Vacuum Vent/Refill-Main Tank Operation

Liquid propellant is supplied to the start tank during the vacuum refill operation by a separate main tank channel, submerged in a main tank screen "trap" region. One concept to accomplish this refill is illustrated in Figure 16. The

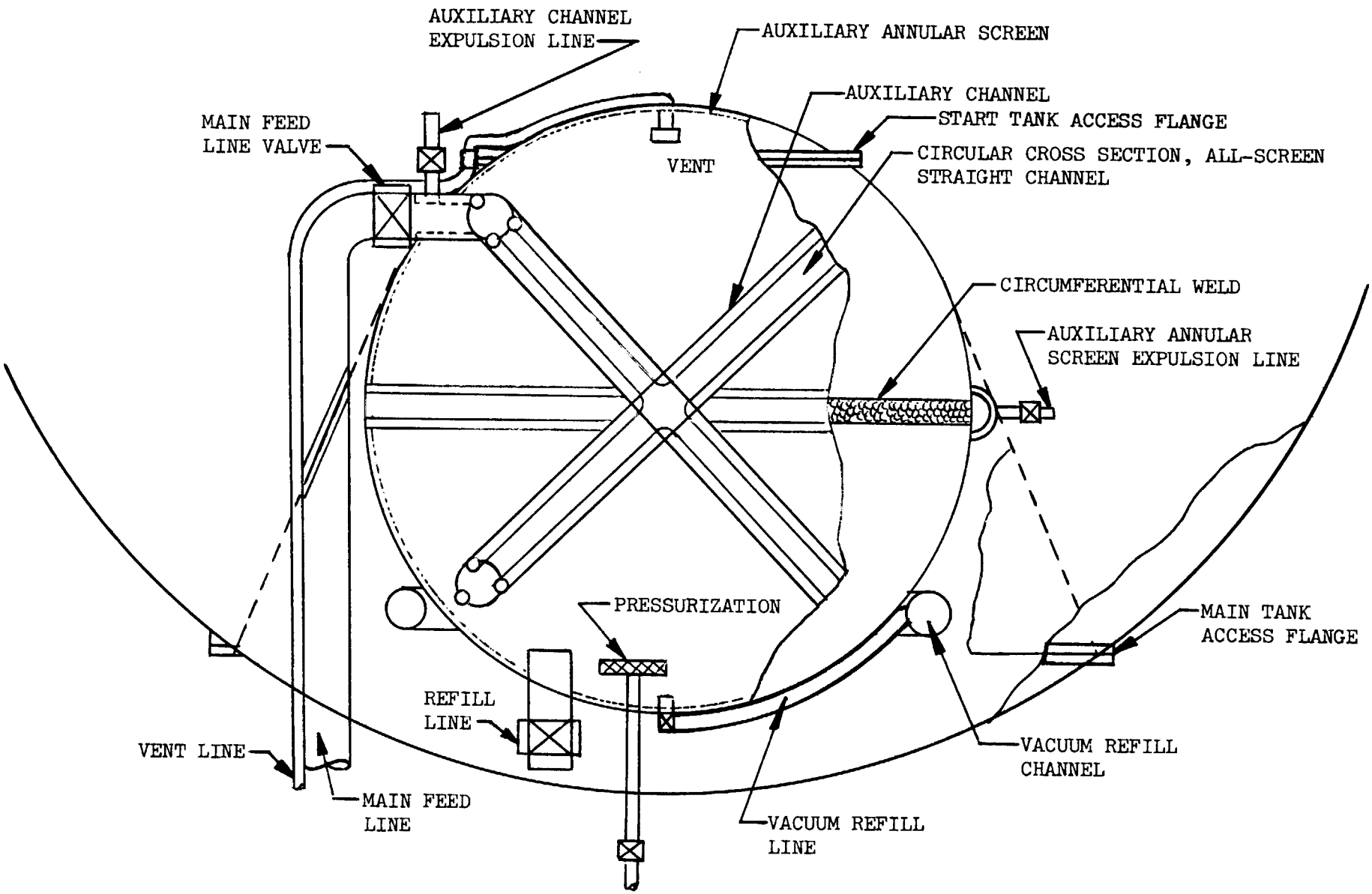

Figure 15. Vacuum Vent/Refill Start Tank Concept

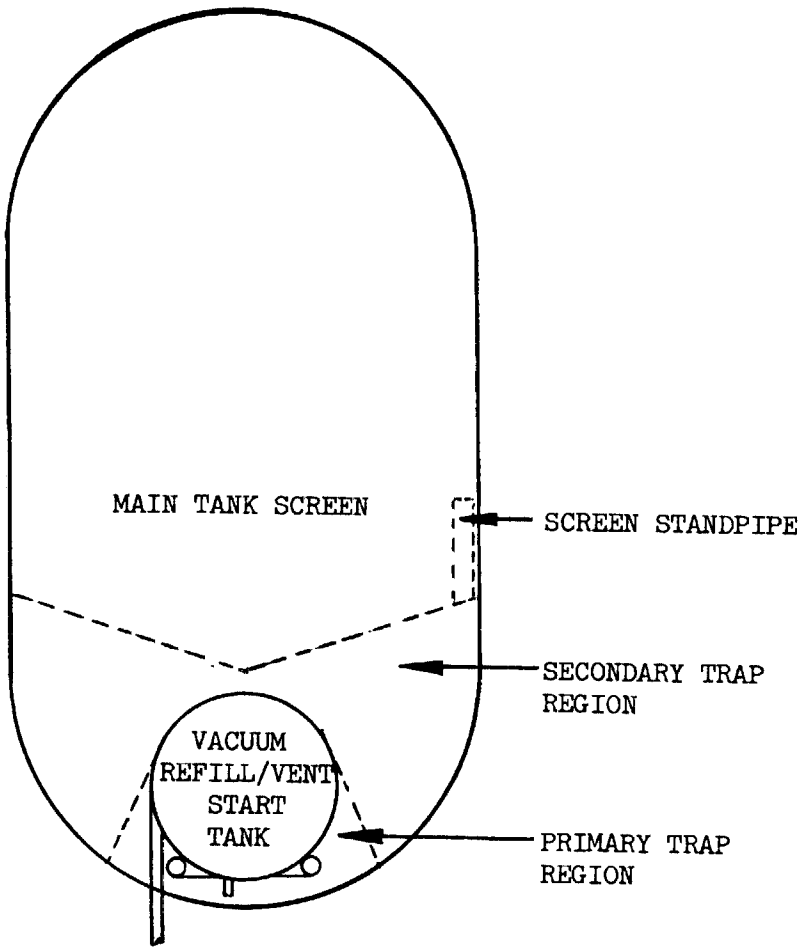

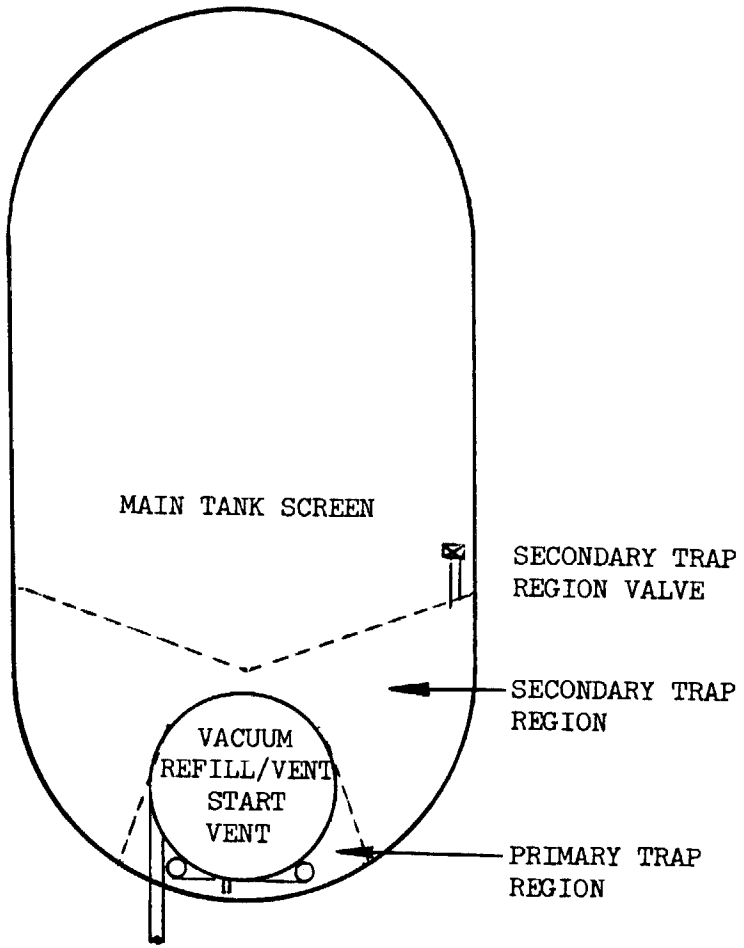

Figure 16. Main Tank Propellant Acquisition for Start Tank Vacuum Refill

primary trap region is maintained full of liquid until the final deorbit engine burn. The screen mesh is sized so that breakdown does not occur for any of the acceleration magnitudes imposed on the vehicle during orbital coast. The secondary trap region serves two purposes; primary trap propellant replacement and propellant refill during vehicle positive accelerations.

During start tank vacuum refill, propellant flowing from the primary trap region is replaced by propellant from the secondary trap region, which is filled by propellant in the main tank contacting the screen. If no main tank propellant contacts the upper screen of the secondary trap region, breakdown will occur. Although liquid could then flow out of the secondary region into the main tank, the g-levels would be so low that the outflow rate would be negligible, relative to that replacing liquid in the primary region. For this worst case operation, it is necessary that the propellant volume contained in the secondary region exceed the volume required for the maximum on-orbit propellant requirements between dynamic refills. For the baseline Shuttle APS application, shown in Figure 16, this requirement is met with the maximum liquid hydrogen volume required being of the order of 19.7 m^3 (700 ft^3). The total volume of liquid hydrogen required for the on-orbit coast was conservatively determined to be 22 m^3 (778 ft^3) for the mission assumed in this study. Since 1.4 to 2.8 m^3 (50 to 100 ft^3) of LH_2 is contained in the start tank, the primary and secondary regions must contain the remainder.

After the start tank has been refilled, gas flow through the standpipe would cease and capillary attraction would then raise a column of liquid in the standpipe, closing off the screen. For this design, the screen mesh used on the standpipe has a lower bubble point than the secondary screen to provide for vapor flow and resealing. As an alternate, the standpipe and screen could be replaced with a valve. During start tank refill, the secondary trap region valve would be opened to allow gas to enter the secondary trap region, while the propellant replaced that withdrawn from the primary region. After refill, the secondary trap region valve would be closed and no liquid would be lost from the primary and secondary trap regions.

After some number of vacuum refill operations have occurred and the secondary trap region has been partially emptied, an engine burn occurs which settles propellant to the bottom of the tank at maximum acceleration. The

secondary trap valve is then opened and vapor displaced up through the valve as liquid enters through the secondary trap region screen. It is not necessary during this operation to replace all of the vapor with liquid since any vapor present in the secondary trap region would not enter the primary trap region.

For the final reentry burn, liquid in the primary trap region could be used to fill the start tank. Vehicle acceleration would settle the remaining propellant which would dynamically refill the start tank through the main refill valve in the usual manner, while supplying continuous propellant flow to the ACPS accumulators.

Auxiliary Acquisition System for Vacuum Refill Start Tank

Reference 1 showed that the principal additional weight associated with the vacuum vent/refill concept is the amount of residual liquid remaining in the start tank which can not be transferred back into the main tank after screen breakdown occurs in the channel. It is therefore necessary to place auxiliary screens on the start tank wall and inside the channels to transfer nearly all of the start tank propellant back into the main tank. The residual liquid remaining in the channel and on the start tank wall after breakdown of the auxiliary screens is primarily a function of the outflow rate to the main tank and the size of the auxiliary screens. Lowering the outflow rate decreases the residual by allowing smaller screen flow areas to be used, but increases the transfer time. Determination of the maximum acceptable vent/refill operation time thus allows the outflow rate to the approximated, and the optimum auxiliary screen configuration to be designed. Appropriate auxiliary channel and auxiliary annular screen sizes have been determined for start tank residual propellant transfer periods of the order of several minutes, as discussed in Section 3.1.2.3.

The cold propellant vapor and helium that is vented overboard is not an additional penalty, since this gas would be vented overboard during a dynamic refill. There could be a small amount of additional helium used to transfer the residual propellant back into the main tank, but in practice this amount is very small. After a normal propellant expulsion from the start tank, which requires cold helium pressurization, equilibrium occurs such that the concentration of the hydrogen vapor in the start tank ullage reaches equilibrium; the hydrogen partial pressure thus adds to the helium initial pressure, raising

the start tank ullage pressure. Furthermore, the main tank pressure decays, after engine cutoff, due to mixing of the propellant and warm pressurant. Thus, in practice, negligible additional helium is required to expel the 15 percent start tank residual back into the main tank.

Surface Tension Breakdown Correction

The vacuum refill technique also offers a means of correcting an unforeseen surface tension breakdown. Correction of screen failure is an advantage which is unique to the start tank and greatly increases reliability. Assume that the screen device in the start tank fails with the liquid level relatively low. In this case, liquid cannot be transferred into the pumps, since the breakdown may have resulted in screen drying or vapor could be ingested, causing pump failure. As a conservative estimate, assume that the propellant volume is one fourth of the start tank volume when failure occurs, and that the start tank size is maximum, associated with no refills other than the dynamic refills which occur during engine operation and vehicle acceleration. The hydrogen start tank volume is 22 m^3 (778 ft^3) and for oxygen, 2.6 m^3 (91.8 ft^3). Thus the hydrogen vented overboard would be 390 kg (856 lb) and the oxygen vented overboard would be 710 kg (1570 lb). Designing the "no-scheduled-refill" system for the total additional propellant weight of 1100 kg (2426 lb) provides a redundant method for correcting screen breakdown and ensuring completion of the mission. The percentage increase in propellant is approximately 5.0 percent.

However, the capability for correction of surface tension breakdown may well be so important to the mission that even the maximum start tank system, sized for dynamic refill alone, would benefit from inclusion of the additional channel and/or wall liner auxiliary screens and flow control valves for expulsion from the start tank back into the main tank. Although vacuum vent/refill could be accomplished without this additional hardware, the additional weight is small compared to the penalty of the above example. Following further verification of this start tank operational mode during the checkout tests of the IDU(NAS8-27571), the use of vacuum vent/refill can be considered in greater detail as an additional capability of the dynamic refill start tank concept.

3.1.2.2 Start Tank Preliminary Design Development

A preliminary design has been evolved for a start tank acquisition system incorporating the vacuum vent/refill concept, which permits a minimum size

start tank, and an all-screen acquisition channel, which results in high retention safety factors with relatively coarse mesh screens. This design concept is schematically shown in Figure 15. Design of the various elements of the system, including primary channels, auxiliary channels, pressure shell, main tank screens, etc., is discussed in the following paragraphs. A comparable start tank design sized for maximum limiting conditions and using only dynamic refill during periods of high acceleration has also been reevaluated for comparison purposes.

Primary Channel Design

The basic ground rule in channel sizing is that a retention safety factor greater than 2.0 must be achieved for all orbital propellant orientations, flowrates, and acceleration levels. A minimum propellant volume of 15 percent is selected as the worst case. This condition is conservative with both the vacuum vent/refill start tanks and the maximum size dynamic refill start tanks; both operate effectively and with no weight penalty between the limits of 100 percent full and 30 percent full or higher. The major impact is that more frequent vacuum vent/refill operation would be required with higher percentages of minimum propellant load and longer start tank vacuum vent periods would be required. The minimum percentage selected is practical and results in a system that achieves retention safety factors greater than 2.0, while maintaining start tank to main tank transfer periods on the order of several minutes.

A channel configuration consisting of two intersecting channels has been selected for the start tank. Two orientations, as shown in Figure 17, were compared. In the first case, Orientation A, the channels were oriented perpendicular and parallel to the vehicle axis such that only one channel contacted the residual liquid in the worst case propellant orientation. In Orientation B, the channels were orientated at 45 deg to the vehicle axis. In this case, two channels contacted the liquid residual.

Both orientations are constrained by the requirement that the start tank sump be located so as to remove all of the propellant during the final landing phase when the 1-g acceleration level is in the -z direction of the vehicle axis.

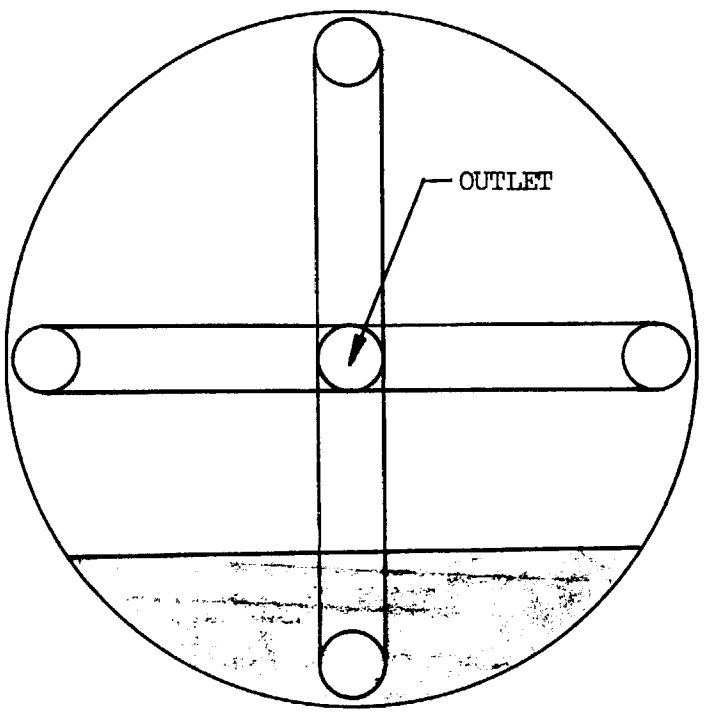

ORIENTATION A

PARALLEL/PERPENDICULAR ORIENTATION

$a = .457\ M/SEC^2$

$(1.5\ FT/SEC^2)$

IN -X DIRECTION
ALONG VEHICLE AXIS

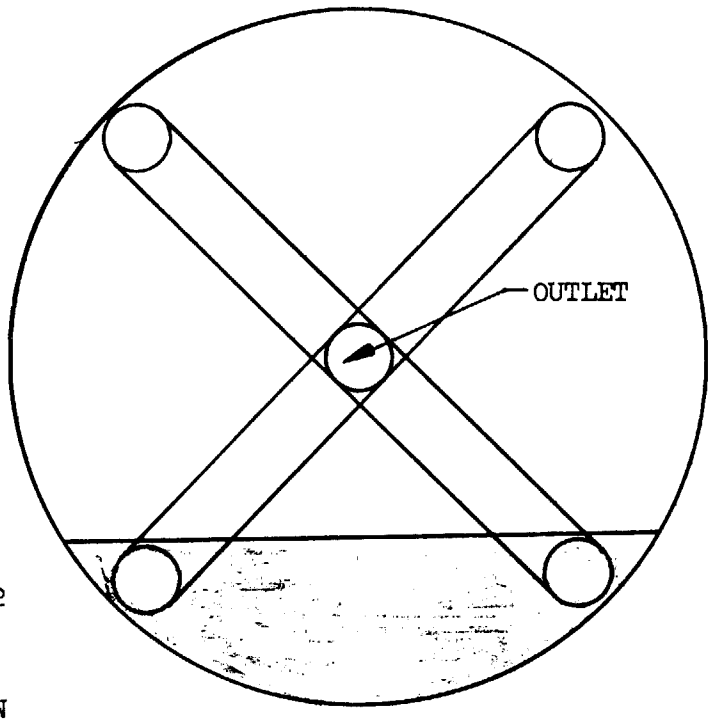

ORIENTATION B

45° ORIENTATION

Figure 17. Orientations of Intersecting Channels

Comparison of the retention safety factors for the two orientations (see Table 13) showed that Orientation B provides 60 percent higher retention safety factor than Orientation A. The improvement results from the fact that with B both channels are in contact with the liquid and the static head is decreased. With flow through two channels, the viscous pressure drop in the channel and the velocity head are both decreased, and since the wetted screen area is also increased, this contribution to pressure drop is also diminished.

Two basic all-screen channel designs have evolved which can be fabricated with existing proven techniques and are optimum for the range of start tank sizes considered in this program. The design philosophy followed in the selection of these channel designs is based on achieving the maximum flow capability in terms of minimum propellant residual, flow losses, and weight within the constraints of the practical and proven fabrication techniques and ease of assembly, disassembly, checkout, inspection, and refurbishment. These channel designs therefore avoid compound screen surface areas, ultra-fine screen mesh sizes, and requirements for complicated channel supports. Although weight improvements may be achieved with more exotic techniques, the preliminary channel system weights determined for these designs are low relative to overall system weights.

The two overall channel configurations are shown in Figures 18 and 19. The basic designs are compatible with any spherical start tank. The square cross section all-screen channel (Figure 18) is contoured to parallel the start tank wall. The screen is applied in the flat state, and roll-spot welded or fusion welded with the overlying strips, as has been done successfully under task B of this program. The straight tube-all-screen channel design (Figure 19) is easily fabricated, and does not require transition joints for the connecting flanges. In addition, this design has the maximum channel cross-sectional area for a given screen surface area; hence, flow losses and system weight are minimized. The tube design offers several alternatives which may be used to advantage in the final design. A weight savings results if bimetallic tubes are used (e.g., aluminum tubes with stainless steel end sections) to which the stainless steel screen is welded. (Bimetallic transition joints are procurable.) Marmon clamps can be used to attach the tubes, thus facilitating assembly and removal from the vehicle.

Table 13

EFFECT OF CHANNEL ORIENTATION ON CHANNEL LH_2 ACQUISITION PERFORMANCE

Channel Orientation	System Pressure Losses, N/m^2 (lb/ft^2)					Retention Safety Factor
	Screen Flow	Channel Flow	Velocity Head	Static Head	Total Loss	
Configuration A Parallel/ Perpendicular	27.15 (0.567)	2.78 (0.058)	52.00 (1.086)	41.33 (0.864)	123.26 (2.575)	1.48
Configuration B 45° Angle	26.33 (0.550)	1.10 (0.023)	13.02 (0.272)	35.40 (0.740)	75.85 (1.585)	2.40

Notes: (1) Acceleration – 0.457 m/sec^2 (1.5 ft/sec^2) negative parallel to vehicle axis (-x direction)

(2) LH_2 Flow rate – 2.7 kg/sec (5.95 lb/sec)

(3) Channel Dimensions – 17.8 x 17.8 cm (7 x 7 in.)

(4) Start Tank Volume – 2.8 m^3 (100 ft^3)

(5) 200 x 600 Mesh Screen – Bubble Point Pressure = 181.9 N/m^3 (3.8 lb/ft^2)

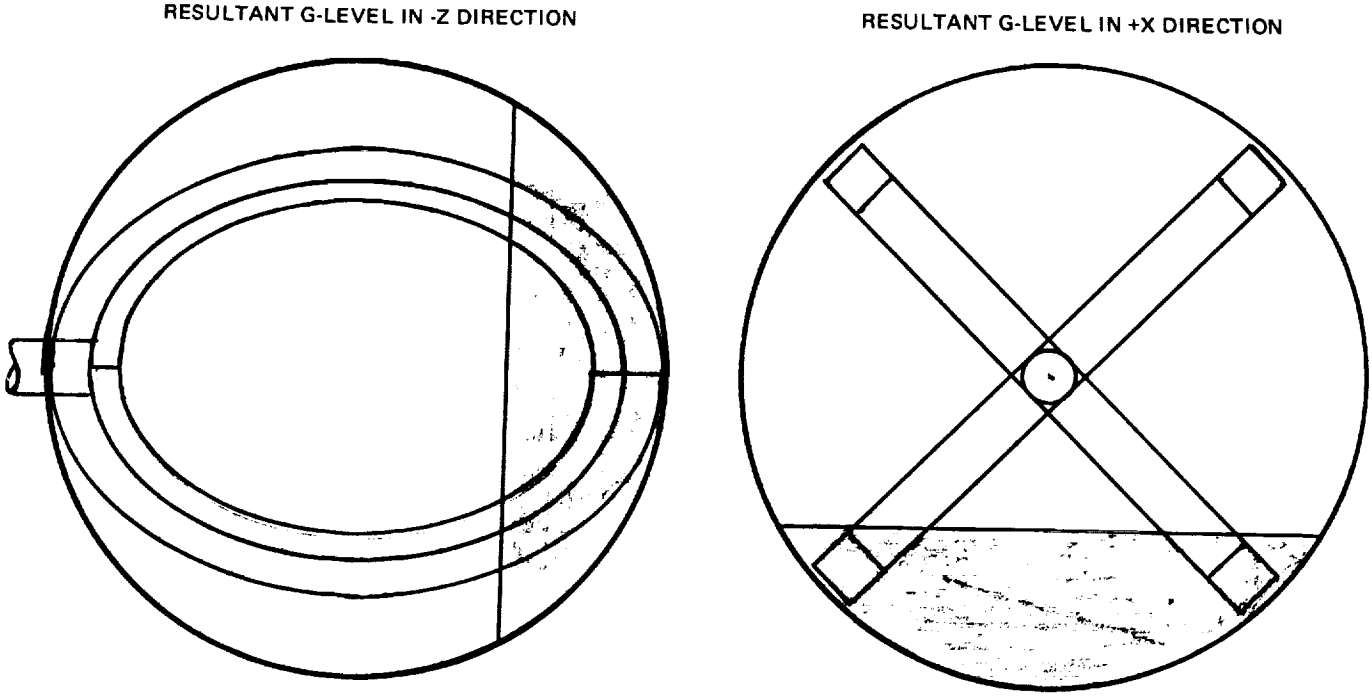

Figure 18. Square Cross Section All-Screen Contoured Channel

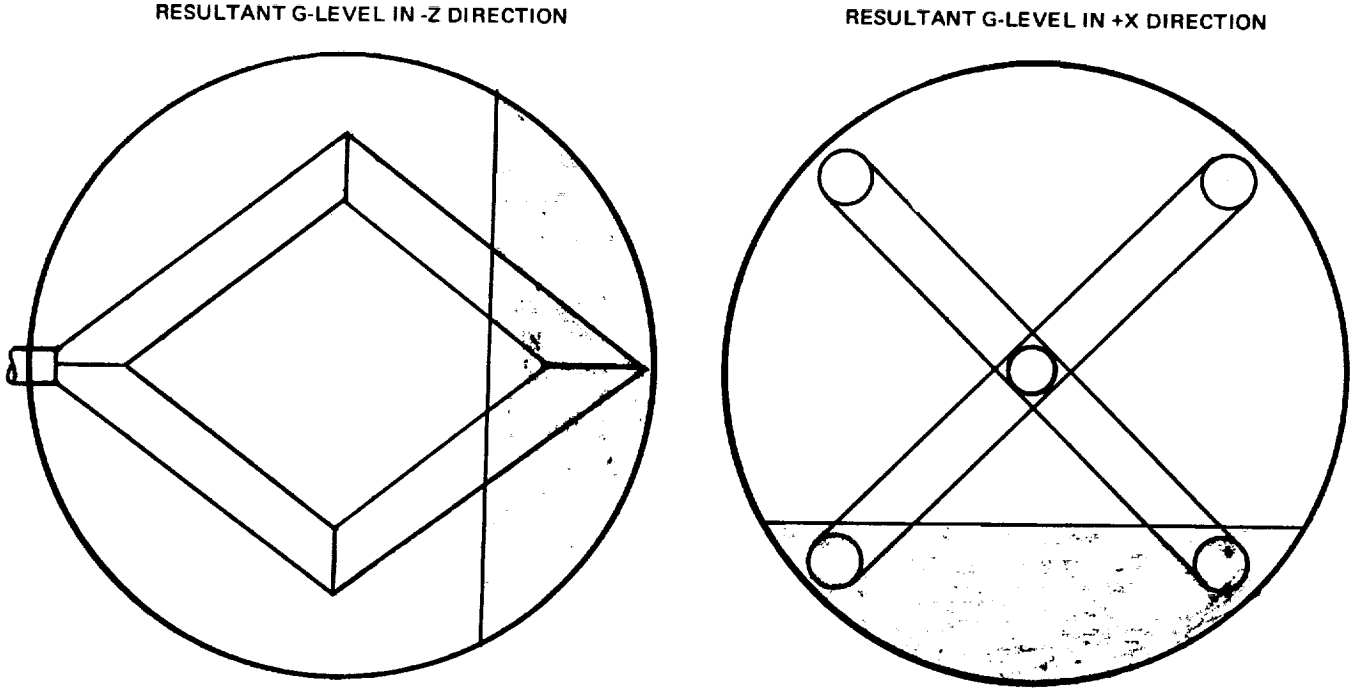

Figure 19. Circular Cross Section All-Screen Straight Channel

The performance characteristics of the primary channel acquisition devices were determined with the aid of MDAC computer codes which calculate pressure losses associated with propellant flow through a screen/duct system. The screen used was 200 x 600 mesh.

The 200 x 600 mesh screen was selected for the channel design based on previous screen mesh comparisons reported in Reference 2. However, recent information indicates that 165 x 800 mesh screen has about the same bubble point as 200 x 600 mesh, but a significantly smaller pressure loss for flow through the screen. Improved designs will therefore be determined based on the 165 x 800 mesh screen during the next reporting period.

The optimum channel size was determined by calculating the retention safety factors as a function of the square cross-section channel width and minimum propellant volume for the 1.4 m^3 (50 ft^3) and 2.8 m^3 (100 ft^3) LH_2 start tanks, and the 0.236 m^3 (8.33 ft^3) and 0.47 m^3 (16.67 ft^3) LO_2 tanks. The results for the LH_2 tanks are shown in Figures 20 and 21. Note that the minimum propellant amount of 15 percent provides a retention safety factor of 2.0 in the worst case with a channel width of approximately 15 cm in both cases. To be conservative, a channel width of 17.8 cm (7 in.) is selected. The corresponding retention safety factor in the next worst case is more than twice as much. This procedure was followed in selecting all other primary channel sizes.

The channel weight was minimized by selecting the smallest channels which provided retention safety factors equal to or greater than 2.0 for the worst case flow condition. The selected channel sizes for each LH_2 and LO_2 start tank for the two worst case conditions are tabulated in Table 14 and 15. The individual pressure losses are itemized. The total acceleration imposed on the LH_2 start tank in the +z direction is 0.293 m/sec^2 (0.96 ft/sec^2) whereas that on the LO_2 start tank is 0.188 m/sec^2 (0.6 ft/sec^2), due to the LO_2 tank being located closer to the vehicle center of gravity.

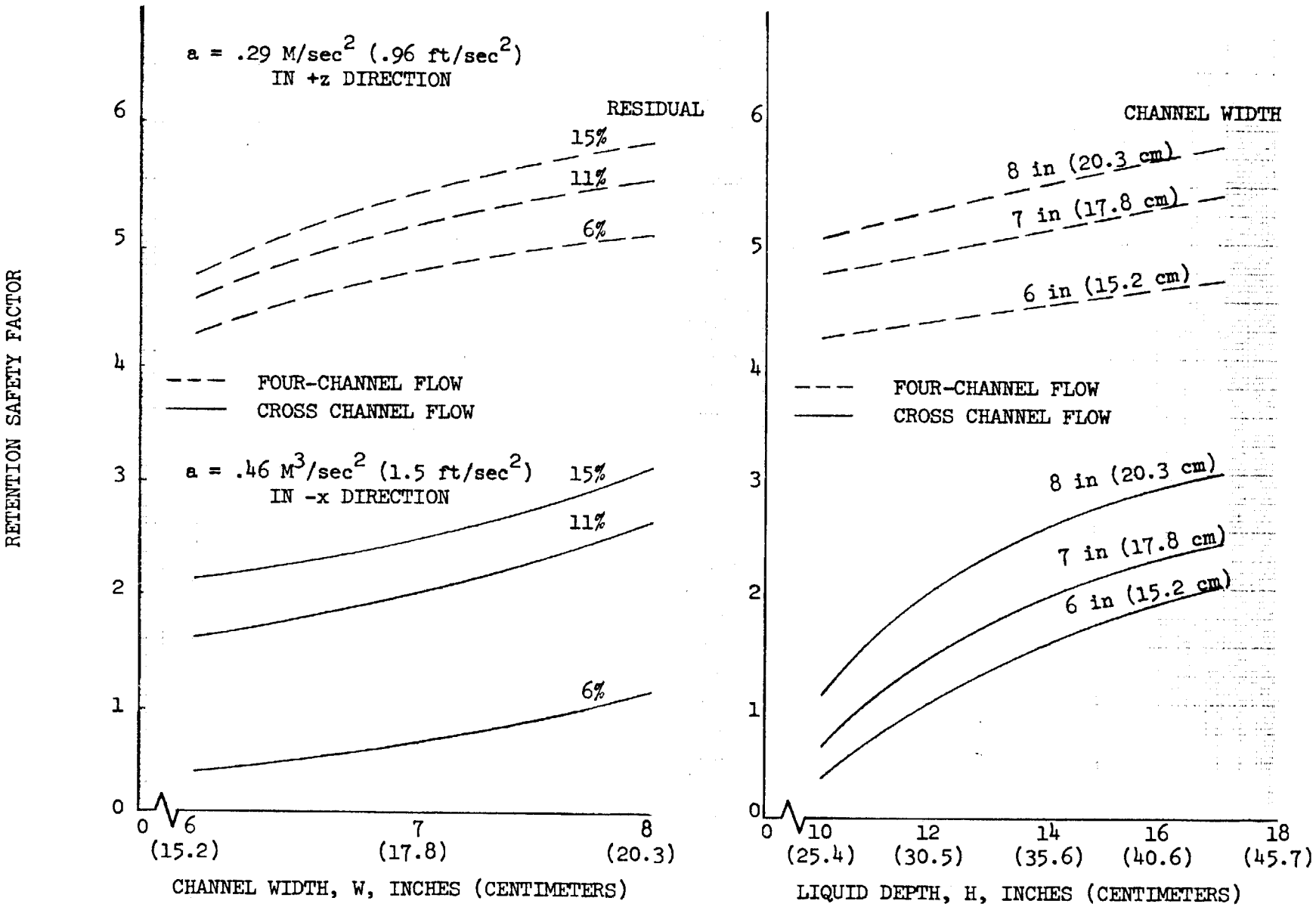

Figure 20. Retention Safety Factor for LH_2 Channels in 2.8 M^3 (100 ft^3) Start Tank

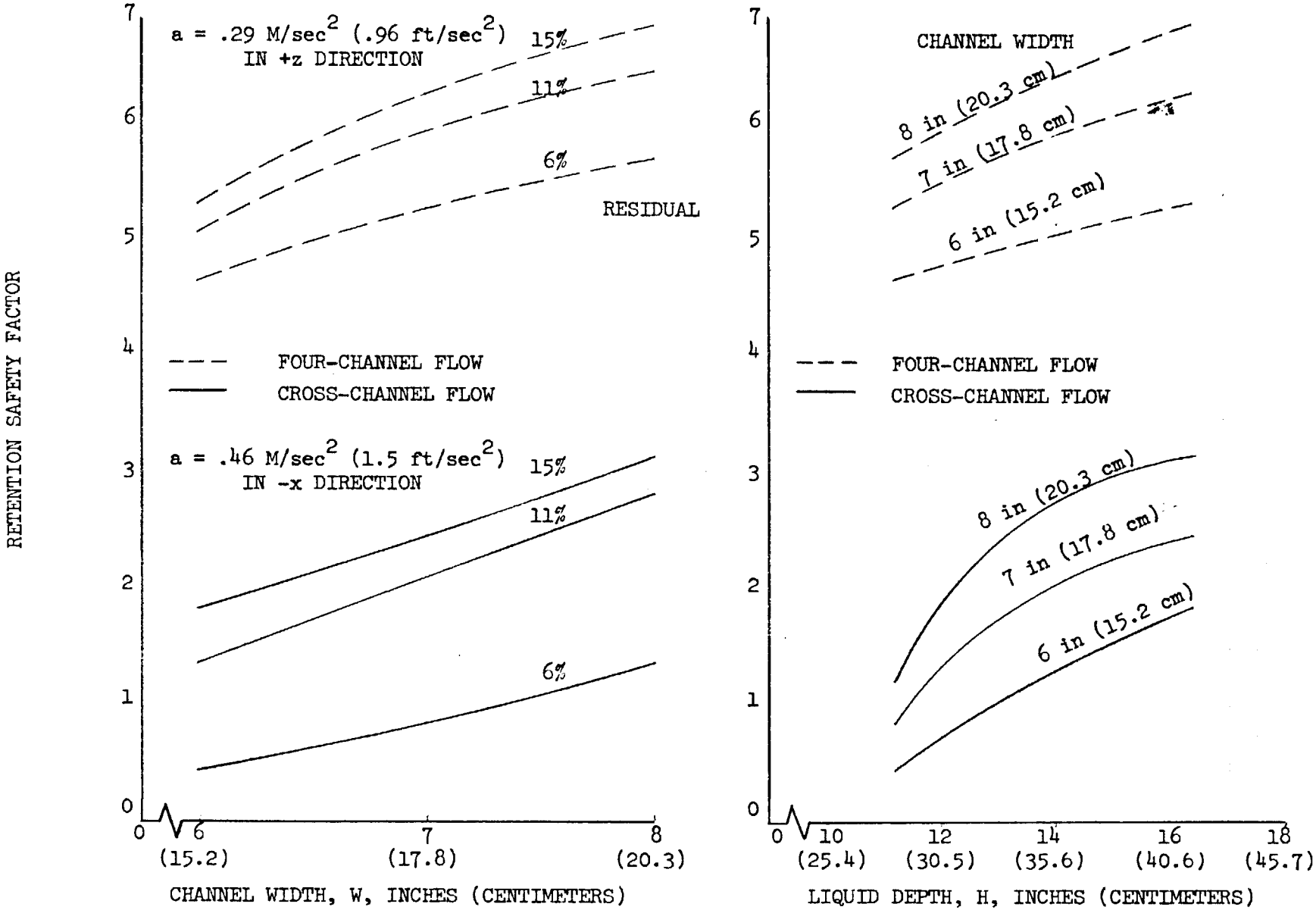

Figure 21. Retention Safety Factor for LH_2 Channels in 1.4 M^3 (50 ft^3) Start Tank

Table 14

CHANNEL ACQUISITION DEVICE PERFORMANCE – LIQUID HYDROGEN START-TANK APPLICATION 200 x 600 MESH SCREEN – BUBBLE POINT PRESSURE = 181.9 N/m^2 (3.8 LB/FT^2)

Start Tank Volume, m^3 (ft^3)	Channel Dimensions cm (in.)	LH_2 Flow, kg/sec (lb/sec)	Acceleration m/sec^2 (ft/sec^2)		System Pressure Losses, N/m^2 (lb/ft^2) Velocity Head	Channel Flow	Screen Flow	Static Head	Retention Safety Factor(3)
1.4 (50)	17.8 x 17.8	2.7 (5.95)	0.457 (1.5)	(1)	13.02 (0.272)	0.91 (0.019)	29.97 (0.626)	29.30 (0.612)	2.5
	(7 x 7)	2.04 (4.5)	0.293 (0.96)	(2)	1.87 (0.039)	0.29 (0.006)	5.55 (0.116)	20.95 (0.438)	6.3
2.8 (100)	17.8 x 17.8	2.7 (5.95)	0.457 (1.5)	(1)	13.02 (0.272)	1.10 (0.023)	26.33 (0.550)	35.40 (0.740)	2.4
	(7 x 7)	2.04 (4.5)	2.93 (0.96)	(2)	1.87 (0.039)	0.34 (0.007)	4.88 (0.102)	26.47 (0.553)	5.4
22.0 (778)	20.3 x 20.3	2.7 (5.95)	0.457 (1.5)	(1)	7.61 (0.159)	1.05 (0.022)	8.56 (0.179)	69.30 (1.448)	2.1
	(8 x 8)	2.04 (4.5)	0.293 (0.96)	(2)	1.10 (0.023	0.38 (0.008)	2.54 (0.053)	53.20 (1.112)	3.2

(1) Cross-Channel Flow - 0.457 M/Sec^2 (1.5 ft/sec^2) Negative Parallel to Vehicle Axis (-X Direction)

(2) 4-Channel Flow - 0.96 Ft/Sec^2 Positive Normal to Vehicle Axis (+Z Direction)

(3) Safety Factor Based on 15% LH_2 Volume in the Start Tank

Table 15

CHANNEL ACQUISITION DEVICE PERFORMANCE – LIQUID HYDROGEN START-TANK APPLICATION 200 x 600 MESH SCREEN – BUBBLE POINT PRESSURE = 1,250 N/m^2 (26.1 LB/FT^2)

Start Tank Volume, m^3 (ft^3)	Channel Dimensions cm (in.)	LO_2 Flow, kg/sec (lb/sec)	Acceleration m/sec^2 (ft/sec^2)		System Pressure Losses, N/m^2 (lb/ft^2) Velocity Head	Channel Flow	Screen Flow	Static Head	Retention Safety Factor(3)
0.24 (8.33)	12.7 x 12.7	13.5 (29.75)	0.457 (1.5)	(1)	77.0 (1.61)	4.35 (0.91)	209.0 (4.37)	254.0 (5.31)	2.3
	(5 x 5)	6.85 (15.1)	0.188 (0.60)	(2)	4.98 (0.104)	0.526 (0.011)	28.8 (0.601)	114.3 (2.39)	8.4
0.47 (16.67)	12.7 x 12.7	13.5 (29.75)	0.457 (1.5)		77.0 (1.61)	5.21 (0.109)	192.3 (4.02)	316.7 (6.62)	2.1
		6.85 (15.1)	0.188 (0.60)		4.98 (0.104)	0.670 (0.014)	21.4 (0.447)	145.0 (3.03)	7.3
2.60 (91.9)	20.3 x 20.3	13.5 (29.75)	0.457 (1.5)		11.8 (0.246)	0.861 (0.018)	32.5 (0.68)	567.0 (11.85)	2.0
	(8 x 8)	6.85 (15.1)	0.188 (0.60)		0.765 (0.016)	0.143 (0.003)	5.31 (0.111)	260.7 (5.45)	4.7

(1) Cross Channel Flow – 0.457 M/Sec^2 (1.5 Ft/Sec^2) Negative Parallel to Vehicle Axis (-X Direction)

(2) 4-Channel Flow – 0.188 M/Sec^2 (0.6 Ft/Sec^2) Positive Normal to Vehicle Axis (+Z Direction)

(3) Safety Factor Based on 15% LO_2 Volume in the Start Tank

The critical start tank operating condition, in terms of propellant acquisition, is that imposed by the relatively high propellant flowrates and the high acceleration level in the negative direction of the vehicle x axis, as indicated in Tables 14 and 15. A major reason for this is that the total propellant flow in each start tank is split into two flow paths, rather than four, which results in greater channel flow velocities and losses. It is necessary to orient the channels so that only two channels contact the minimum propellant amount, because of the requirement that the sump be located so as to minimize propellant residual during landing. Performance is further degraded in this orientation because the total wetted screen area is minimal, as compared to the condition in which both ring channels experience maximum immersion in the propellant liquid.

The retention safety factors calculated for this critical condition are conservative because the flow model assumes that the entire flow in each channel follows the shortest path from the wetted screen to the outlet, while in reality the flow would be proportioned among the four possible paths of flow. The bulk of the flow would still follow the shortest path, however. Thus, the analysis was not further complicated by attempting to solve the complex flow distribution, particularly since the design is more than adequately conservative.

Start Tank Auxiliary Screen Devices

With the gravity-independent vacuum vent/refill start tank, the propellant penalty associated with each vent is minimized if both the channels and the start tank wall are provided with auxiliary screen devices. These auxiliary screen devices allow nearly all of the residual liquid on the start tank wall and inside the channel to be transferred back into the main tank, prior to the vacuum vent operation.

Figures 22 and 23 illustrate screen liners inside a solid duct and all-screen channel design, through which the liquid flows during the expulsion operation from the start tank to the main tank. One difference between these two applications is that with the all-screen channel inner liner the total flow loss

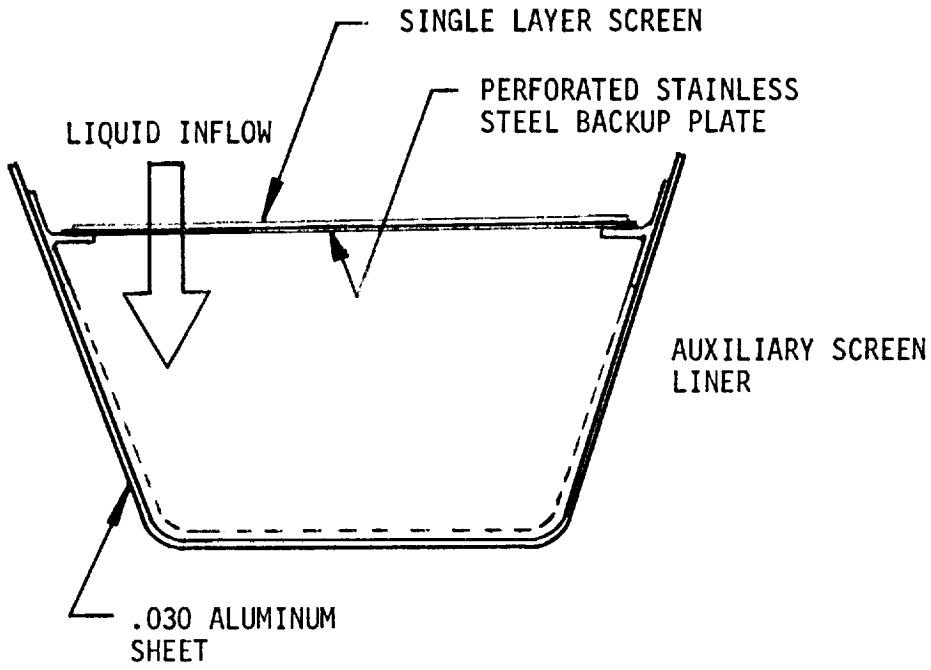

Figure 22. Solid Duct Channel with Auxiliary Screen Liner

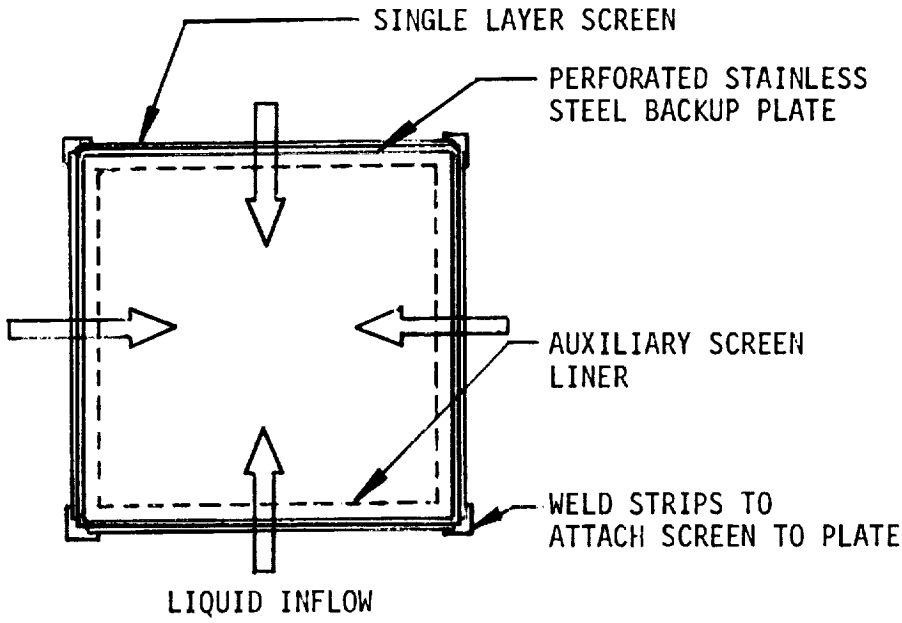

Figure 23. All-Screen Channel with Inner Liner Auxiliary Screen

is increased since the flow loss through the double layer of screen is increased; this loss offsets the advantage of the increased screen area of the all-screen channel relative to the baseline channel. A single screen tube wrapped alternately along the inside of the square cross-section channel was initially considered; a similar approach could be used with the circular cross section channels. However, this concept presents fabrication difficulties in terms of joining and supporting the screen tube to the inner channel wall and was therefore dropped from consideration.

Figure 24 illustrates a more practical concept for emptying the channel by withdrawing liquid from the four corners. This concept appears to be simpler to fabricate than the previous designs (Figures 22 and 23). The triangular sections can be made in two ways. In the first case, the two perpendicular sides are solid and the hypotenuse is covered with a coarser mesh screen than the 200 x 600 used on the channel walls. A coarse mesh screen on the corners is satisfactory since the flow velocities are small and the hydrostatic head is negligible. Screen stability therefore presents no problem. However, the solid walls decrease the flow area available for the channel, and therefore impose a penalty. In the second case, the triangular sections are completely covered with a fine mesh screen, e.g., the 200 x 600. In this case, the effective screen flow area is slightly decreased, due to the use of two fine mesh screens, but the channel performance is slightly better than for the previous triangular section design. In both cases, the fabrication is relatively simple. The channel is assembled with the primary screens and the corner screens temporarily affixed to the channel. The triangular sections are then clamped to the channels and rolled-spot welded or fusion welded as shown in Figure 24. If necessary, square cross section auxiliary channels could be used, rather than triangular, in order to increase the flow rate.

The circular cross section all-screen straight channel, with provision for expelling the propellant back into the main tank through auxiliary screen tubes, is shown in Figure 25. The three auxiliary tubes are first assembled by wrapping the screen around the perforated tubes and welding the straight L-sections to the screen and tube. Roll-spot welding or electron beam welding could be used for this operation. The main channel perforated tube

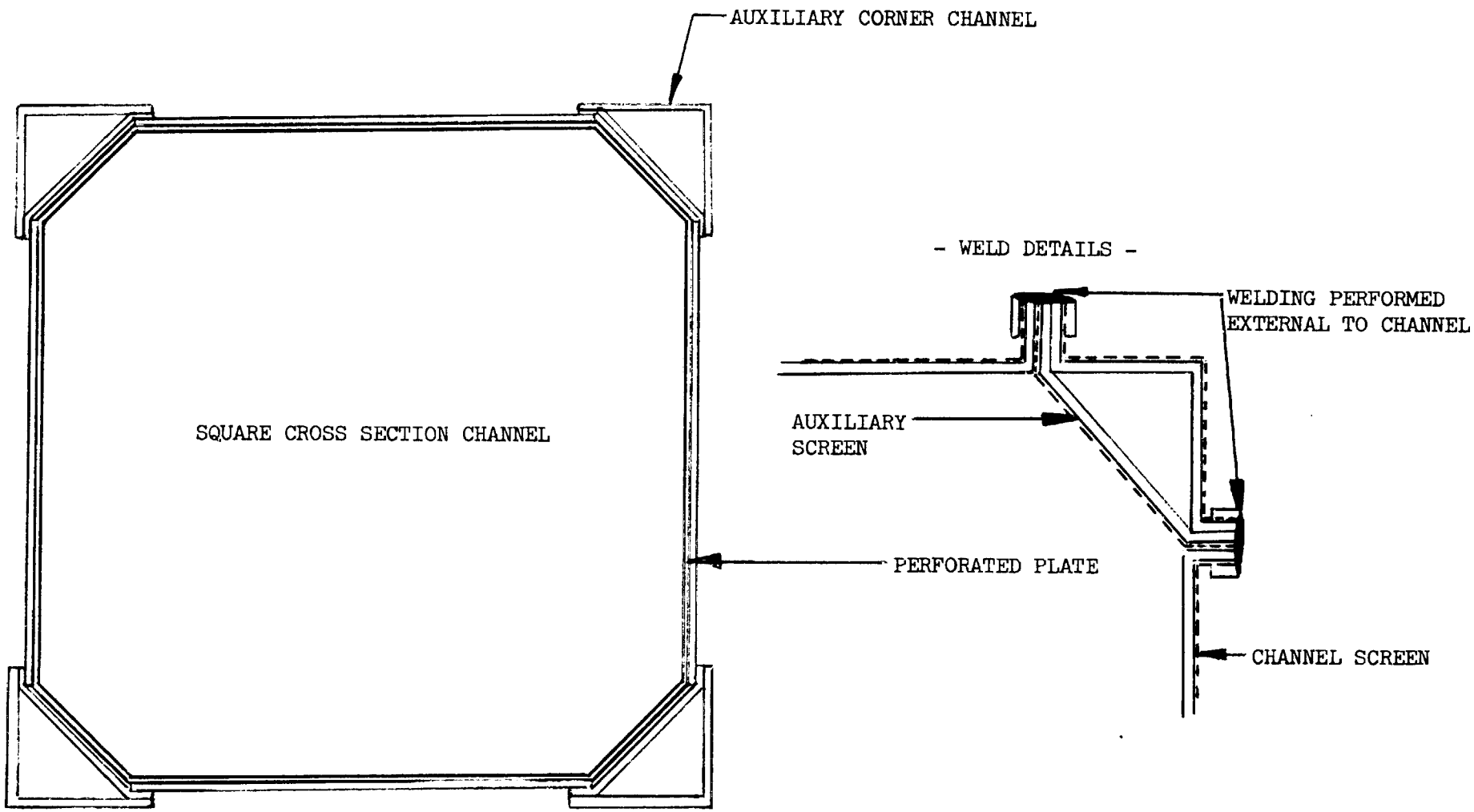

Figure 24. Square Cross Section All-Screen Channel with Auxiliary Corner Channels

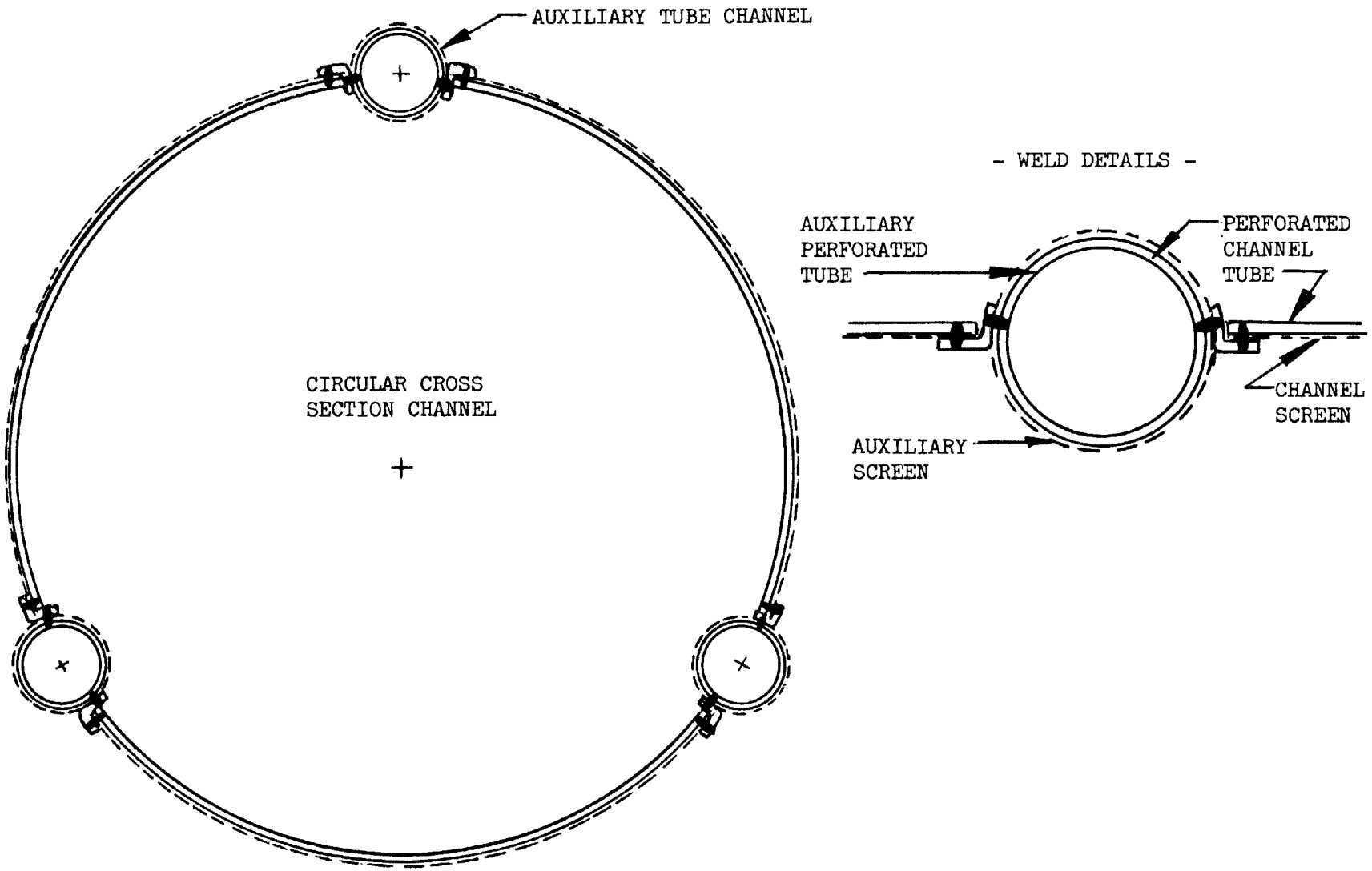

Figure 25. Circular Cross Section All-Screen Channel with Auxiliary Tube Channels

would then be assembled by wrapping the fine mesh screen and coarser mesh support screen around each of the three sections of main channel tube and tack welding the material in place. The auxiliary tubes would then be joined to the sections of main channel tube by rolled-spot welding or electron beam welding, as shown in welding details of Figure 25.

The flow characteristics in the auxiliary screens were determined using the screen/duct sizing analysis computer code.

The purpose of the annular screen device and triangular (or square) auxiliary channels is to empty the start tanks and the main acquisition channels, respectively, in the absence of accelerating forces on the tanks, prior to the vacuum vent operation. The auxiliary channel concepts were initially evaluated for use in the 1.42 and 2.83 m^3 (50 and 100 ft^3) fuel tanks and the 0.236 and 0.471 m^3 (8.3 and 16.7 ft^3) oxidizer tanks with annulus sizes of 0.318 and 0.635 cm (0.125 and 0.25 inch) for the start tanks and with 1.82 cm (0.707 inch) wide screens inserted into each corner of the square main acquisition channels. The performance of these configurations was found to be acceptable at flowrates as great as 0.045 kg/sec (0.1 lb/sec) for the hydrogen (Tables 16 and 17) and 0.454 kg/sec (1.2 lb/sec) for the oxygen (Tables 18 and 19).

The insertion of 1.82 cm (0.707 inch) screens into the four corners of the square main acquisition channels forms a right triangular cross section for the auxiliary flow of propellant, with the screen as the hypotenuse and with two equal sides of 1.27 cm (0.5 inch). This cross section is the smallest which provides acceptable performance in the larger start tanks at the design flowrates, although smaller flow areas may be possible in the smaller start tanks. Thus the resultant residual masses in the channels (Tables 16 and 17) can be further reduced only by reducing the outflow rates so that smaller auxiliary channels can be used.

The main acquisition channels empty in from 6 to 8 minutes and from 2 to 3 minutes for the conditions of Tables 16 and 17, respectively. The time required to empty the hydrogen acquisition channels is at least twice that

Table 16

AUXILIARY CHANNEL PERFORMANCE IN LIQUID HYDROGEN START TANK

Tank Volume m^3	(ft^3)	Screen Radius cm	(in.)	Screen Safety Factor	Residual Mass kg	(lb)	Total Auxiliary Residual Mass kg	(lb)	Total Residual Mass kg	(lb)
1/2-INCH TRIANGULAR AUXILIARY CHANNEL - 7-INCH MAIN CHANNEL RESIDUAL MASS = 0.39 Kg (0.87 LB)										
2.83	(100)	85.0 (outer)	(33.5)	2.10	0.12	(0.26)	0.22	(0.48)	0.61	(1.35)
		67.8 (inner)	(26.7)	2.46	0.10	(0.22)				
1.42	(50)	67.8 (outer)	(26.7)	2.46	0.12	(0.22)	0.17	(0.37)	0.56	(1.24)
		50.5 (inner)	(19.9)	2.98	0.07	(0.07)				
1/2-INCH SQUARE AUXILIARY CHANNEL - 7-INCH MAIN CHANNEL RESIDUAL MASS = 0.39 KG (0.87 LB)										
2.83	(100)	85.0 (outer)	(33.5)	2.73	0.24	(0.52)	0.44	(0.96)	0.83	(1.83)
		67.8 (inner)	(26.7)	3.08	0.20	(0.44)				
1.42	(50)	67.8 (outer)	(26.7)	3.08	0.20	(0.44)	0.73	(0.97)	0.73	(1.61)
		50.5 (inner)	(19.9)	3.53	0.14	(0.30)				

Table 17

AUXILIARY CHANNEL PERFORMANCE IN LIQUID OXYGEN START TANK

1/2-INCH TRIANGULAR AUXILIARY CHANNEL - 5-INCH MAIN CHANNEL RESIDUAL MASS = 2.32 KG (5.11 LB)

Tank Volume m^3	Tank Volume (ft^3)	Screen Radius cm	Screen Radius (in.)	Screen Safety Factor	Residual Mass ② kg	Residual Mass ② (lb)	Total Auxiliary Residual Mass kg	Total Auxiliary Residual Mass (lb)	Total Residual Mass kg	Total Residual Mass (lb)
0.471	(16.7)	45.7 (outer)	(18.0)	2.15	1.80	(3.96)	3.37	(7.43)	5.69	(12.54)
		40.1 (inner)	(15.8)	2.29	1.57	(3.47)				
0.236	(8.3)	35.8 (outer)	(14.1)	2.42	1.42	(3.13)	2.62	(5.77)	4.94	(10.88)
		30.2 (inner)	(11.9)	2.60	1.20	(2.64)				

① Percent residual = Residual volume/start tank volume x 100

② Mass in auxiliary triangular channels.

Table 18

ANNULAR SCREEN PERFORMANCE IN LIQUID HYDROGEN START TANK

LH_2 FLOWRATE: 0.045 KG/SEC (0.1 LB/SEC)

200 x 600 MESH SCREEN - BUBBLE POINT PRESSURE = 181.9 N/M^2 (3.8 LB/FT^2)

Tank Volume m^3	(ft^3)	Separation Distance cm	(in.)	Screen Safety Factor	Percent Residual ①	Residual Mass kg	(lb)
UNPLEATED ANNULAR SCREEN							
2.83	(100)	0.317	(0.125)	2.85	1.08	2.14	(4.71)
		0.635	(0.25)	3.17	2.16	4.26	(9.39)
1.42	(50)	0.317	(0.125)	2.02	1.36	1.35	(2.97)
		0.635	(0.25)	2.17	2.71	2.68	(5.91)
PLEATED ANNULAR SCREEN (Pleated Area/Unpleated Area = 3)							
2.83	(100)	0.317	(0.125)	1.91	0.54	1.07	(2.36)
		0.330	(0.13)	2.10	0.56	1.11	(2.45)
		0.635	(0.25)	6.41	1.08	2.14	(4.71)
1.42	(50)	0.317	(0.125)	1.74	0.68	0.67	(1.48)
		0.343	(0.135)	2.06	0.74	0.73	(1.60)
		0.635	(0.25)	4.87	1.36	1.35	(2.97)

① Percent Residual = Residual Volume/Start Tank Volume x 100

Table 19

ANNULAR SCREEN PERFORMANCE IN LIQUID OXYGEN START TANK

LO_2 FLOWRATE: 1.2 LB/SEC (0.545 KG/SEC)

200 x 600 MESH SCREEN - BUBBLE POINT PRESSURE = 1250 N/M^2 (26.1 LB/FT^2)

Tank Volume m^3	Tank Volume (ft^3)	Separation Distance cm	Separation Distance (in.)	Screen Safety Factor	Percent Residual	Residual Mass kg	Residual Mass (lb)
UNPLEATED ANNULAR SCREEN							
0.471	(16.7)	0.317	(0.125)	3.26	1.96	10.4	(23.0)
		0.635	(0.25)	3.91	3.90	20.7	(45.7)
0.236	(8.3)	0.317	(0.125)	2.44	2.46	6.6	(14.5)
		0.635	(0.25)	2.78	4.89	13.1	(28.8)
PLEATED ANNULAR SCREEN (Pleated Area/Unpleated Area = 3)							
0.471	(16.7)	0.317	(0.125)	1.47	0.98	5.2	(11.5)
		0.368	(0.145)	2.14	1.14	6.0	(13.3)
		0.635	(0.25)	6.30	1.95	10.4	(22.9)
0.236	(8.3)	0.317	(0.125)	1.39	1.23	3.3	(7.3)
		0.381	(0.15)	2.14	1.48	4.0	(8.7)
		0.635	(0.25)	5.13	2.44	6.5	(14.4)

required to empty the oxygen acquisition channels and the hydrogen start tank, but it could be made comparable (3 to 4 minutes) by doubling the outflow rate from the auxiliary screen channels. This would result in higher pressure losses in the triangular channels, but these could be relieved by substituting 1.27 cm (0.5 inch) square auxiliary channels which would double the flow area and increase the screen surface area by 40 percent. However, it would also double the auxiliary hydrogen residual mass. Table 16 shows the square auxiliary channel results. Transfer periods less than 10 minutes are considered acceptable and thus the triangle design is selected for the LH_2 auxiliary channel.

The circular cross section all-screen channel with three circular auxiliary channels, shown in Figure 25, has not yet been evaluated. This design offers an improvement in terms of diminished channel flow loss, due to the more efficient circular cross-sectional area compared to the triangle and square cross sections as well as a decreased residual volume. These design refinements will be made during the next reporting period.

The annular screen (see Figure 15) is employed in the start tank to allow the 15 percent propellant volume to be transferred from the start tank back into the main tank at the same time the channels are being emptied prior to vacuum vent/refill. Since the volume of propellant contained inside the annular region is lost during the vacuum vent operation, it is necessary to minimize this volume. A range of annulus separation distances with both pleated and unpleated screens was considered. Pleated screens offer the advantage of increased wetted screen area and decreased screen flow loss, while being more practical to fabricate. Unpleated screens, however, reduce the pressure loss associated with flow in the annulus.

Tables 18 and 19 present the results for unpleated screens with annulus separation distances of 0.63 cm (0.25 in.) and 0.32 cm (0.125 in.) for the 1.4 m^3 (50 ft^3) and 2.8 m^3 (100 ft^3) liquid hydrogen start tanks. For the screen separation distance of 0.317 cm (0.125 in.), retention safety factors greater than 2.0 are achieved with residuals of approximately 1 percent for the two LH_2 tanks, and residuals of approximately 2 percent, with higher

retention safety factors for the LO_2 start tanks. The pleated annular screen separation distance was determined for a safety factor of 2.0, which halved the percent residual of the unpleated screen. Therefore, pleated screens are selected for the design since the decreased residual weight penalty is much larger than the small increase in screen weight.

Start Tank Pressure Shell

The minimum weight start tank pressure shell is a spherical isogrid structure; this design has been thoroughly analyzed and tested at MDAC and is documented in Reference 6. The weights of the isogrid with a single circumferential weld were determined from the tables of Reference 6 for the range of start tank sizes assuming a maximum crushing pressure of 332×10^3 N/m^2 (48 psi). The properties of aluminum (2219-T87) were used at the appropriate cryogenic temperature (22°K for LH_2 and 90°K for LO_2). The weld seam thickness was assumed to be 2.5 times the effective thickness of the isogrid structure and the width was assumed to be 7.5 cm (3 inches) for all start tank sizes. It should be noted that in Reference 2, six circumferential welds were assumed with the sphere composed of six gore segments. However, the lighter and more practical design is composed of two hemispheres joined by a single circumferential weld. The tank support weight is assumed to be approximately 8 percent of the start tank weight. These new weights are at the end of this section.

For the larger start tanks, a manhole is used to provide access for screen device servicing. Thus, installation and removal of the channels would be accomplished by technicians working within the large start tanks. Repair or replacement of the screens is then performed under laboratory conditions. It is necessary that the channels be easily removable and therefore, Marman clamps are used. The manhole cover design is shown in Figure 26; this design is a refinement of that used on the Saturn S-IVB. The total weight penalty is essentially proportional to the manhole circumference. The flange weight penalty for a 0.9 m (3 ft) diameter flange is 16.8 kg (37 lb) with 2.05 kg (4.3 lb) for the bolts.

Installation of the large start tank within the main propellant tank would probably have to be accomplished during main tank assembly. However, in

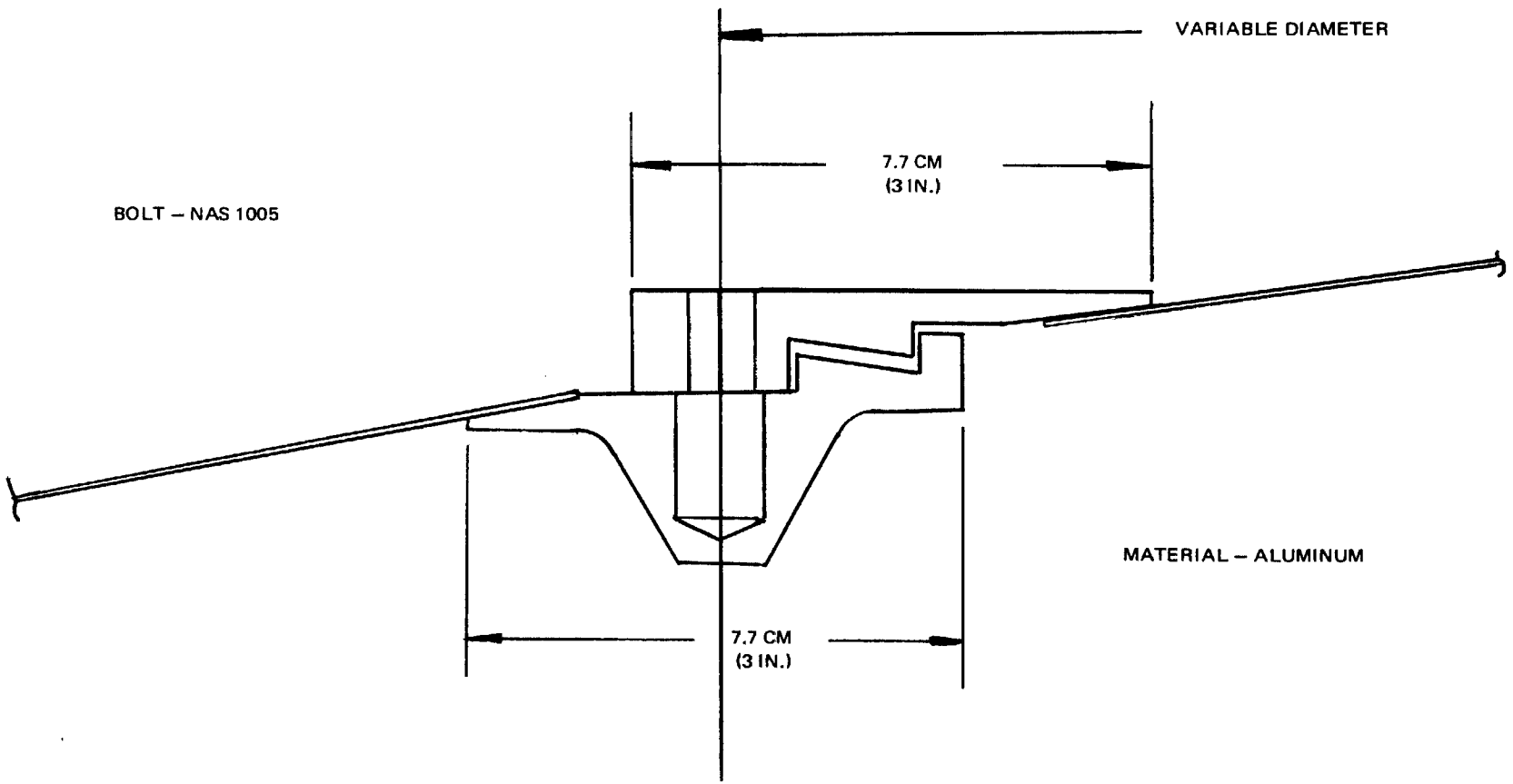

Figure 26. Manhole Cover Flange Design

the case of the small LO_2 vacuum vent/refill start tank (0.24 and 0.47 m^3), the entire start tank can be inserted through the normal manhole access of the liquid oxygen main tank. It is only necessary that the structural supports of the LO_2 start tanks be easily detachable.

Integrated Systems

Total integrated system weights and penalties for the principal start tank concepts have been determined, based on analyses documented in the previous quarterly reports (References 1 and 2) as well as the new concepts and parametric data as discussed in the preceding sections.

The schematic diagram of the overall system and required components for the start tank concept is shown in Figure 27. This layout is developed to the same level as that for the distributed channel system. A list of the components and associated weights for the LH_2 and LO_2 systems is given in Tables 20 and 21. The LO_2 schematic diagram is essentially identical to the LH_2 system, except that the viscojet components are not used.

Pressurization System – The start tank is pressurized with cold helium stored at the bulk liquid temperature of the propellant. The main LH_2 tank is pressurized by the warm GH_2 taken from the high-pressure accumulators. The main LO_2 tank is pressurized by cold helium; these weights are unchanged. System weights have been determined for the start tank system in previous quarterly reports. These analyses have been updated for the vacuum vent/refill start tank.

The total propellant which is expelled directly from the start tank, using the cold helium system alone, has been determined to be 22 m^3 (780 ft^3) for the LH_2 system, independent of the size of the vacuum vent/refill start tank. As a highly conservative estimate, it is assumed that the total pressure in the start tank is 1.72×10^5 N/m^2 at 22 °K (25 psia) prior to vacuum venting, and that the partial pressure of hydrogen vapor is negligible.

Based on these assumptions, the cold helium pressurization system weight is 220 kg (485 lb), including gas, pressure bottles, supports, and a main tank weight penalty associated with the additional volume. As a comparison the system weight associated with an equilibrium mixture of hydrogen and

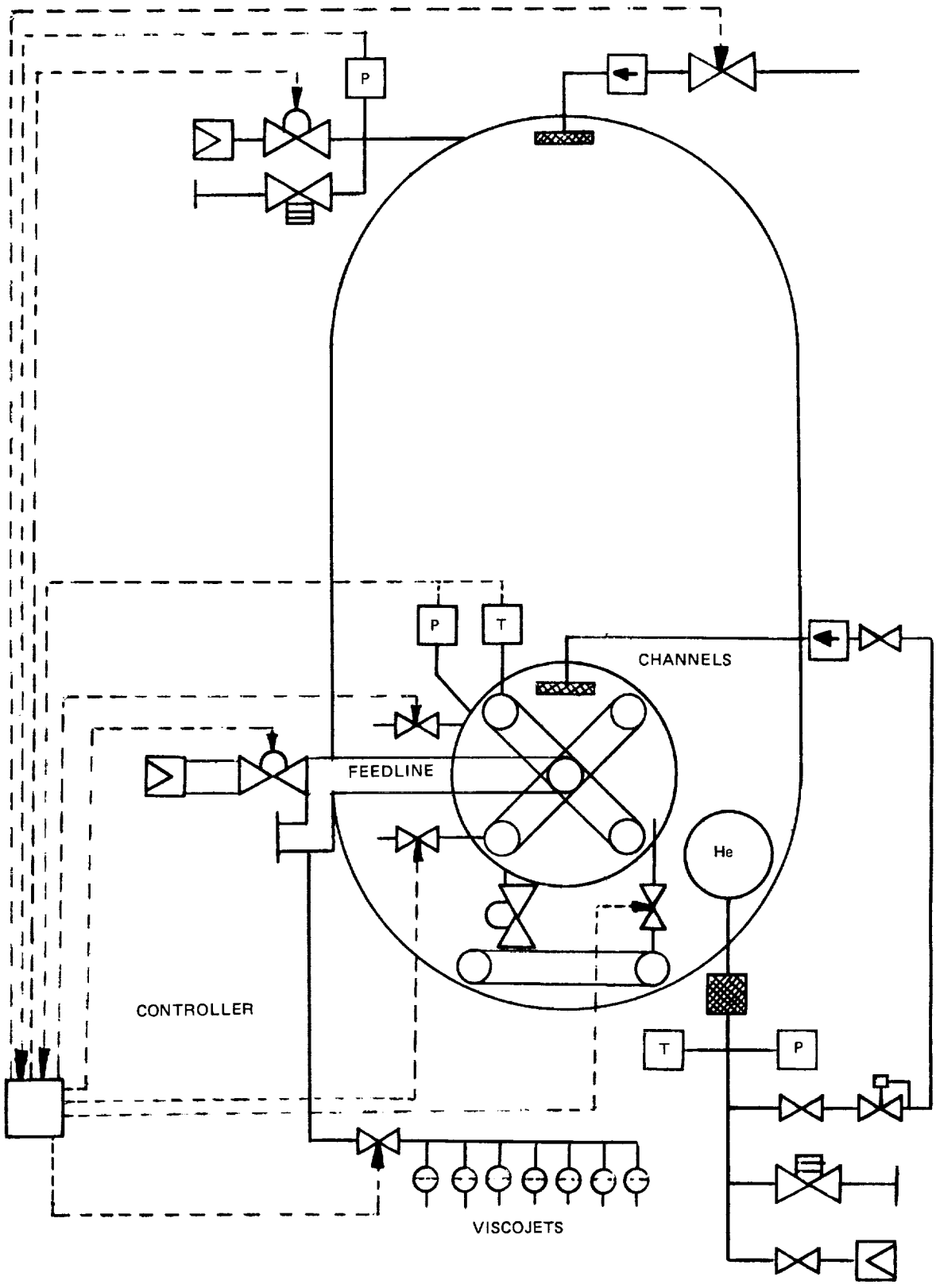

Figure 27. Schematic Diagram of LH_2 Start Tank System

Table 20

LH_2 START TANK SYSTEM COMPONENT WEIGHTS
VACUUM VENT/REFILL DESIGN*

Quantity	Component		
2	Outlet shutoff valves (2-inch ball)	12.70 kg	(28.0 lb)
1	2-Inch quick-disconnect	2.70 kg	(5.0 lb)
1	4-Inch vent valve	9.10 kg	(20.0 lb)
1	4-Inch relief valve	9.10 kg	(20.0 lb)
1	4-Inch gas quick disconnect	2.72 kg	(6.0 lb)
3	Pressure sensors	1.00 kg	(2.2 lb)
2	Pressurization diffusers	0.90 kg	(2.0 lb)
2	Check valves (1 inch)	1.36 kg	(3.0 lb)
1	Solenoid valve (1 inch)	0.91 kg	(2.0 lb)
1	Pressure controller (split with LO_2 tank)	3.19 kg	(7.0 lb)
4	Solenoids (1/2 inch)	1.46 kg	(3.2 lb)
2	Temperature sensors	0.45 kg	(1.0 lb)
7	Viscojets	0.32 kg	(1.1 lb)
1	High-pressure solenoid (1 inch)	1.82 kg	(4.0 lb)
2	High-pressure regulators	4.52 kg	(10.0 lb)
	Component support hardware	4.60 kg	(10.0 lb)
		56.84 kg	(124.5 lb)
	Feed lines (2 inch)	0.91 kg	(2.0 lb)
	Vent lines (4 inch)	5.90 kg	(13.0 lb)
	Pressurization lines (1 inch)	10.56 kg	(23.0 lb)
	Miscellaneous lines	3.18 kg	(7.0 lb)
	Fittings	2.27 kg	(5.0 lb)
	Support and miscellaneous hardware	2.27 kg	(5.0 lb)
		24.99 kg	(55.0 lb)

*Dynamic refill design does not require three 1/2-inch solenoid valves tabulated above.

Table 21

LO_2 START TANK SYSTEM COMPONENT WEIGHTS
VACUUM VENT/REFILL DESIGN*

Quantity	Component		
2	Outlet shutoff valves (2-inch ball)	12.70 kg	(28.0 lb)
1	2-Inch quick disconnect	2.70 kg	(5.0 lb)
1	4-Inch vent valve	9.10 kg	(20.0 lb)
1	4-Inch relief valve	9.10 kg	(20.0 lb)
1	4-Inch gas quick disconnect	2.72 kg	(6.0 lb)
3	Pressure sensors	1.00 kg	(2.2 lb)
2	Pressurization diffusers	0.90 kg	(2.0 lb)
2	Check valves (1 inch)	1.36 kg	(3.0 lb)
1	Solenoid valve (1 inch)	0.91 kg	(2.0 lb)
1	Pressure controller (split with LH_2 tank)	3.18 kg	(7.0 lb)
3	Solenoids (1/2 inch)	1.10 kg	(2.4 lb)
2	Temperature sensors	0.45 kg	(1.0 lb)
1	High-pressure solenoid (1 inch)	1.82 kg	(4.0 lb)
2	High-pressure regulator	4.52 kg	(10.0 lb)
	Component support hardware	4.60 kg	(10.1 lb)
		56.16 kg	(122.7 lb)
	Feed lines (2 inch)	0.91 kg	(2.0 lb)
	Vent lines (4 inch)	5.90 kg	(13.0 lb)
	Pressurization lines (1 inch)	10.45 kg	(23.0 lb)
	Miscellaneous lines	3.18 kg	(7.0 lb)
	Fittings	2.27 kg	(5.0 lb)
	Support and miscellaneous hardware	2.27 kg	(5.0 lb)
		24.99 kg	(55.0 lb)

*Dynamic refill design does not require three 1/2-inch solenoid valves tabulated above.

helium at a total pressure of 25 psia is 110 kg (242 lb). The assumption of nonequilibrium conditions is therefore conservative by a factor of two. The system weights for both main tank warm hydrogen and start tank cold helium are shown as a function of start tank volume in Figure 28. The warm hydrogen (110°K) gas weight decreases with increasing start tank volume since less liquid hydrogen is displaced from the main tank.

Propellant Thermal Protection System – With the start tank concept, it is possible to eliminate the main LH_2 tank foam insulation and store the cryogen within the start tank for the high heat input reentry period. This reduces boiloff loss and total thermal weight penalty for small start tanks. A transient thermal analysis was conducted to establish the optimum thickness of foam insulation for the start tank to minimize the total foam and propellant boiloff weight penalty during the reentry and landing mission phases. Sample results are presented in Figure 29. The total weight penalty was determined as a function of start tank diameter for the optimum condition (Figure 30). A computer program, developed previously under MDAC IRAD funding, was used to make the calculations. The program was written for use with the MDAC version of the CINDA-3G thermal network analysis program. The CINDA program is a preprocessor type program which provides a framework for a user to set up a thermal analog model for his specific problem, furnishes an assortment of network solution routines, and combines the user input data and selected solution routines in a FORTRAN program for the problem.

The main tank insulation was assumed to be 1.25 cm of helium purged MLI. This thickness was found to be optimum as reported in Reference 2 for the on-orbit portion of the mission profile. Property data were taken from References 7, 8, and 9. Vehicle acceleration, temperature and pressure history input data, calculated for reentry of a Space Shuttle class vehicle, were taken from Reference 10.

During entry, the propellant tank was assumed to be at 0.1 atmosphere. Other pertinent input data are the following:

MLI Layer Density	90 layers/inch

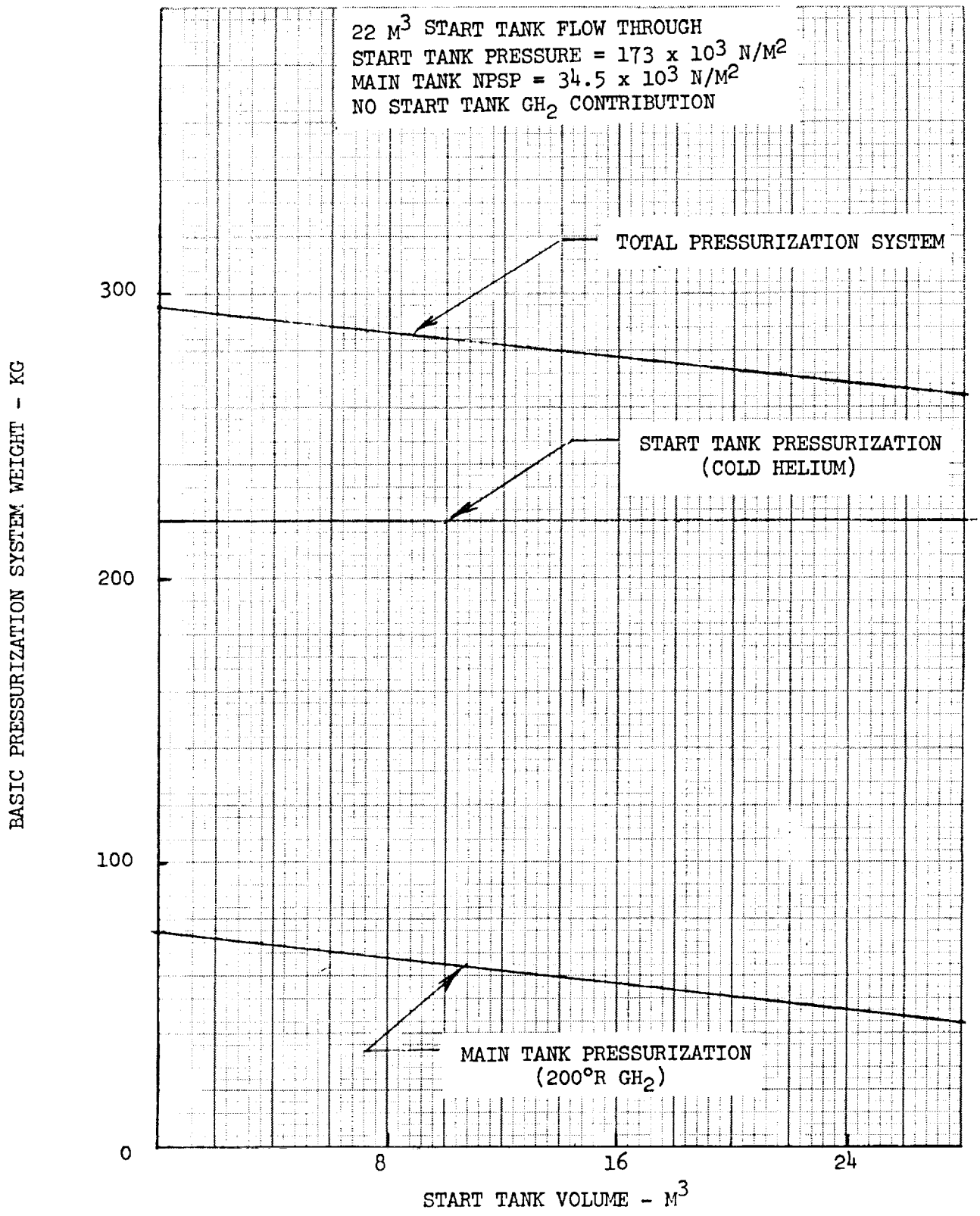

Figure 28. Start Tank Concept Pressurization System Weights

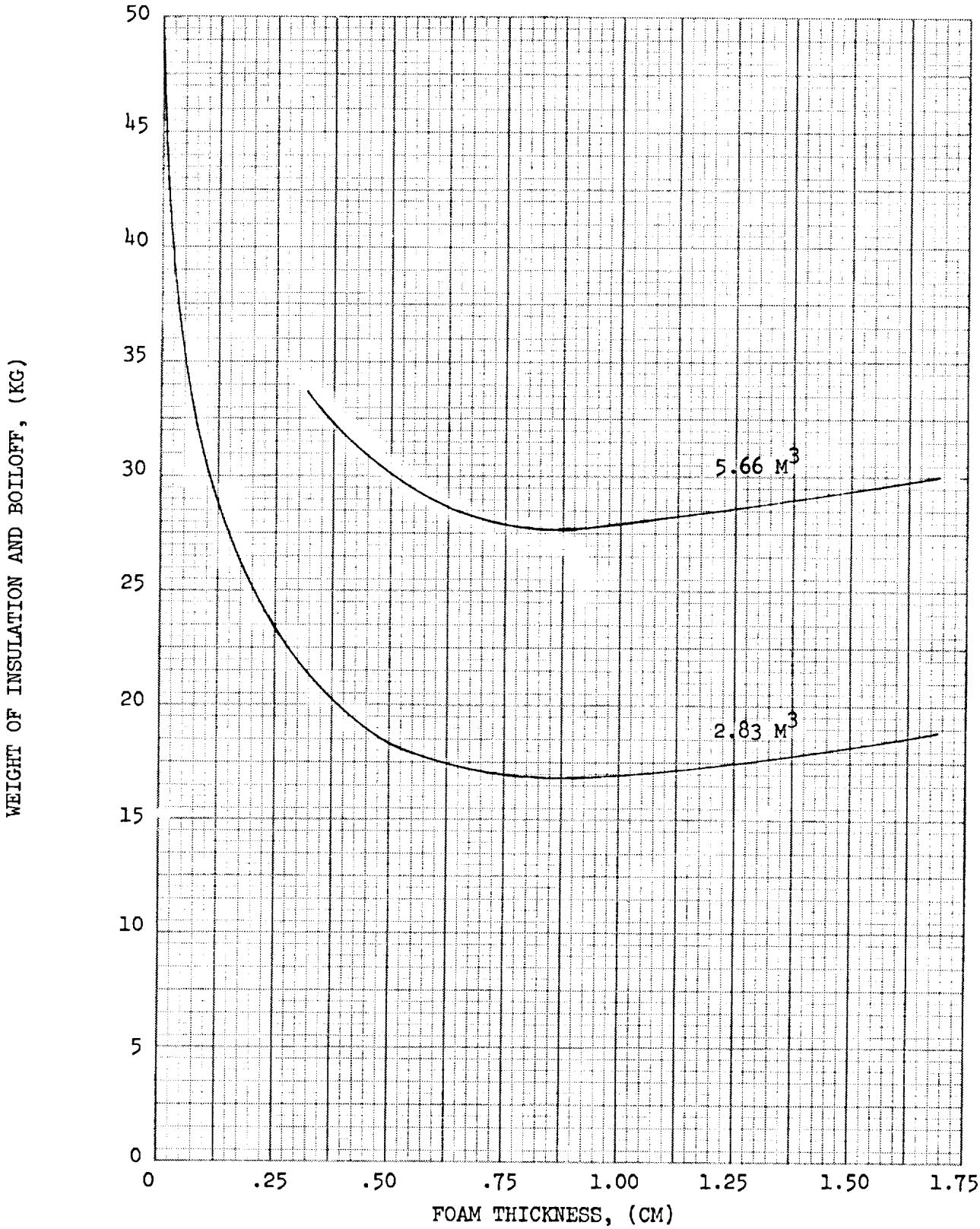

Figure 29. Start Tank Boiloff Penalty

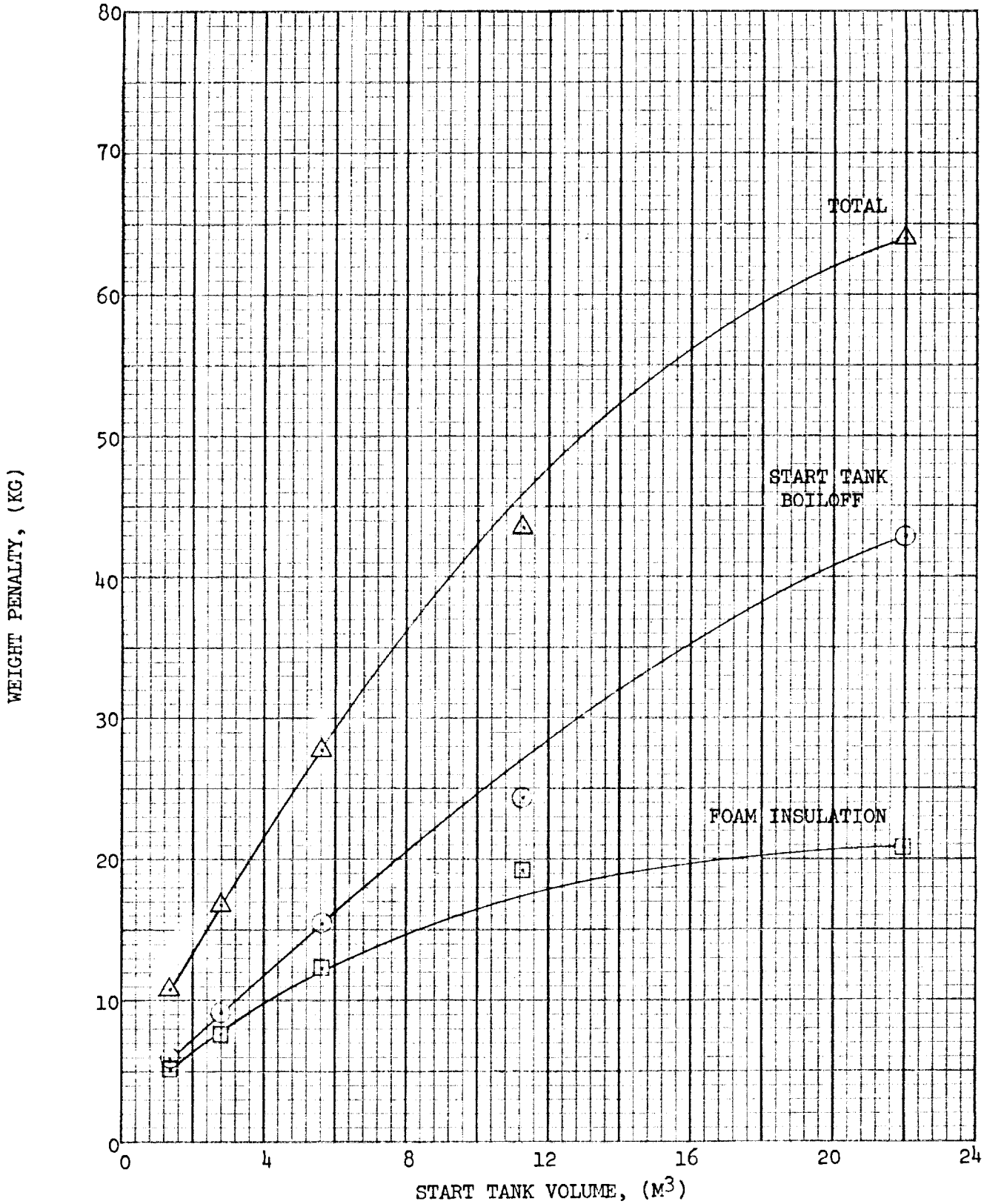

Figure 30. Influence of Start Tank Size and Boiloff Penalty

MLI Evacuated Effective Thermal Conductivity	2.41 joule/M-sec-^{o}K	(1.55 x 10^{-5} Btu/hr-ft^{o}R)
Main Tank Radius	1.83 M	(6.0 ft)
Main Tank Wall Thickness	0.152 cm	(0.06 inch)
Spacing-Purge Bag to MLI	1.37 cm	(0.5 inch)
Purge Bag Thickness	0.015 cm	(0.006 inch)
Start Tank Foam Insulation	Polyurethane foam	
Foam Insulation Density	83.3 kg/m^3	(5.2 lb/ft^3)
Main Tank Residual	34 kg GHe/29 kg GH_2	(75 lb GHe/64 lb GH_2)
Purge Gas Accomodation Coefficient	0.35	

The insulation weight and boiloff losses of the LH_2 start tanks are entered in the weight summary tables at the end of this section.

Acquisition System Weight – The screen acquisition system for the vacuum vent/refill start tank includes the primary channels, auxiliary channels, the start tank annular screen device, and the main tank screens. The dynamic refill start tank contains only the primary channels. The weights of each of these devices were determined based on conservative assumptions. The square cross-section all-screen channel is formed from perforated steel, 0.508 cm (0.02 inch) with a 60 percent open area as shown in Figure 31. Open areas of 80 percent or larger can be achieved by special cutting of sheet stock, but perforated steel of 60 percent open area is commercially available at low cost. An open area of 60 percent or greater has been shown to have negligible effect on the total flow loss through the screen, if a coarse mesh screen overlay is used to support the fine mesh screen. A coarse mesh aluminum screen is used as a standoff support screen, with a weight per unit area of 2.39 N/m^2 (0.05 lb/ft^2). The fine mesh steel screen (200 x 600) has a weight per unit area of 12 N/m^2 (0.25 lb/ft^2). The weld area joining the four channel walls is included in the weight. The weld width is 0.63 cm (0.25 inch) and the thickness is 1.02 cm (0.04 inch). The total length of each weld is approximately that of the channel, and there are eight welds per channel. Eight Marman clamps are used, with transition joints to couple the eight square cross-sectional channels. The auxiliary channels are formed with

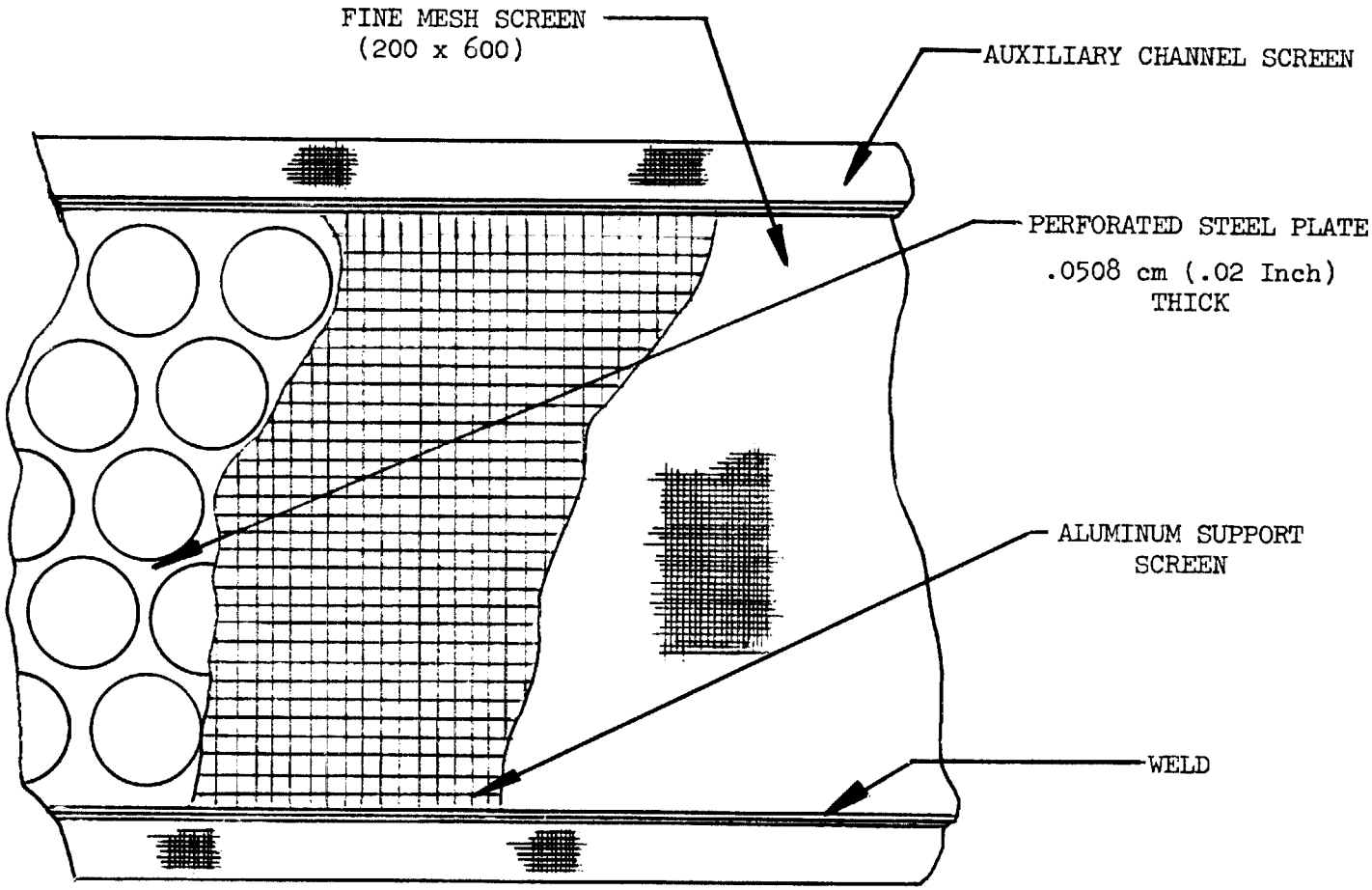

Figure 31. Square Cross Section All-Screen Channel Wall

the same layup of screens and perforated plates. The annular screen device is assumed to be a pleated sphere with a pleated-to-unpleated surface area ratio of 3.0. The 200 x 600 mesh screen is used.

The main tank screen weights were estimated based on the areas required to contain approximately 19.6 m^3 (700 ft^3) of LH_2 and 2.6 m^3 (92 ft^3) of LO_2. The screen areas were 14 m^2 (150 ft^2) for LH_2 and 7 m^2 (75 ft^2) for LO_2. The screen weight is therefore approximately 20 lb for LH_2 and 10 lb for LO_2. However, these weights were doubled to account for the support structure.

The main tank refill channel weight used for vacuum refill is the same as one channel in the corresponding vacuum vent/refill start tank. These weights are given in the start tank acquisition system weight summaries.

The acquisition device weight summary for the 2.8 m^3 (100 ft^3) LH_2 start tank is given in Table 22 as an example; the acquisition device weights associated with the other start tank sizes are summarized in Table 23. The screen weights are determined from the geometrical areas of the channels, with the weights per unit area given above.

Weight Summary – The start tank system weights and penalties are tabulated in Tables 23 to 27. Tables 23 and 24 contain all weights associated with the acquisition system and include an estimate for the main tank screen of 18 kg (40 lb) for the LH_2, and 9 kg (20 lb) for LO_2. It should be noted that the pump bypass penalty is no longer assessed against the start tank, since this fluid can be returned to the main tank, thereby reducing the pressurant requirements from the accumulators. Table 27 summarizes the total weight penalty for the LH_2 and LO_2 systems.

There are additional design changes which offer significant weight savings that will be considered during the next reporting period. The LO_2 start tank can be integrated with the main tank wall such that approximately half of the pressure shell is a common wall of the main tank and start tank. This change presents no heat transfer problems, since the LO_2 tank is cooled by the LH_2 thermodynamic vent. The weight savings would be approximately 13 kg (28.5 lb). An even greater weight savings would be achieved if the

Table 22

ACQUISITION DEVICE WEIGHTS FOR 2.8 M^3 (100 FT^3)
LH_2 START TANK

(EXCLUDING PRESSURE SHELL)

Item	Weight	
	kg	(lb)
Perforated steel wall	16.00	(35.00)
Steel screen (200 x 600)	6.60	(14.6)
Aluminum screen	1.66	(3.65)
Welding joints	0.95	(2.07)
Auxiliary channels	2.50	(5.50)
Auxiliary annular screen	7.10	(15.60)
	34.81	(76.42)

Table 23

START TANK ACQUISITION SYSTEM WEIGHTS (LIQUID HYDROGEN)

System Weight Penalties Acquisition Hardware	Start Tank Size 1.4 m^3 kg	(50 ft^3) (lb)	2.8 m^3 kg	(100 ft^3) (lb)	22 m^3 kg	(778 ft^3) (lb)
Pressure shell (spherical isogrid)	13.8	(30.0)	29.3	(64.4)	212.0	(465.0) ①
Support structure for start tank	2.3	(5.0)	3.6	(8.0)	20.5	(45.0)
Access manhole (3-ft ID)	18.7	(41.0)	18.7	(41.0)	18.7	(41.0)
Channel (stainless steel, square cross section)	19.6	(43.4)	25.2	(55.3)	68.0	(150.6)
Marmon Clamps (8 stainless steel)	8.2	(18.0)	8.2	(18.0)	9.3	(20.5)
Auxiliary channels (stainless steel)	2.0	(4.3)	2.5	(5.5)	0	0
Auxiliary annular start tank screen (pleated)	5.5	(12.2)	7.1	(15.6)	0	0
Foam insulation	5.0	(1.0)	8.2	(18.0)	19.5	(43.0)
Main tank refill channel	10.0	(22.0)	12.7	(28.0)	0	0
Main tank screen	18.1	(40.0) ②	18.1	(40.0) ②	18.1	(40.0) ②
Channel supports	0.45	(1.0)	0.7	(1.5)	1.4	(3.0)
	103.65	(227.9)	134.3	(295.3)	367.5	(807.5)
Start Tank In-Flight Losses						
Boiloff during reentry	5.9	(13.0)	9.1	(20.0)	42.8	(94.0)
Residual within channels	8.5	(18.6) ③	4.3	(9.5) ④	0	0
Residual within annular screen	20.4	(45.0) ③	15.0	(33.0) ④	0	0
	138.45	(304.5)	162.7	(357.8)	410.3	(901.5)

① Weight reduced from Figure 14 of Reference by assuming one circumferential weld, rather than six.

② Main tank screen weight is approximate at this time.

③ Calculated for 15 vacuum vent/refill cycles.

④ Calculated for 7 vacuum vent/refill cycles.

Table 24

START TANK ACQUISITION SYSTEM WEIGHTS (LIQUID OXYGEN)

System Weight Penalties Acquisition Hardware	Start Tank Size					
	0.236 m^3 kg	(8.33 ft^3) (lb)	0.47 m^3 kg	(16.67 ft^3) (lb)	2.6 m^3 kg	(91.9 ft^3) (lb)
Pressure shell (spherical isogrid)	1.82	(4.0)	3.64	(8.0)	27.2	(60.0)
Support structure for start tank	2.72	(6.0)	5.48	(12.0)	29.5	(65.0)
Access manhole	0	0	0	0	18.4	(41.0)
Channel (stainless steel, square cross section)	7.03	(15.7)	9.30	(20.4)	30.5	(67.5)
Marmon clamps (8 stainless steel)	5.90	(13.0)	5.90	(13.0)	9.30	(20.5)
Auxiliary channels (stainless steel)	0.73	(1.6)	0.91	(2.0)	0	0
Auxiliary annular start tank screen (pleated)	1.40	(3.1)	1.91	(4.2)	0	0
Foam insulation	0	0	0	0	0	0
Main tank refill channel	3.64	(8.0)	4.64	(10.2)	0	0
Main tank screen	9.0	(20.0)	9.0	(20.0)	9.0	(20.0)
Channel supports	0.45	(1.0)	0.68	(1.5)	1.36	(3.0)
	32.79	(72.4)	41.46	(91.3)	125.26	(277.0)
Start tank in-flight losses						
Boiloff during reentry	0	0	0	0	0	0
Residual within channels	74.5	(164.0)	40.0	(88.0)	0	0
Residual within annular screen	59.0	(130.0)	42.2	(93.0)	0	0
	133.5	(294.0)	82.2	(181.0)	0	0
TOTALS	166.3	(366.4)	123.7	(272.3)	125.3	(277.0)

Table 25

LIQUID HYDROGEN START TANK SYSTEM WEIGHT SUMMARY

	Start Tank Size					
	1.4 m^3	(50 ft^3)	2.8 m^3	(100 ft^3)	22 m^3	(780 ft^3)
	Weights (kg)					
Acquisition system						
Hardware	99.0		126.1		348.0	
Residual losses	28.9		19.3		0	
		127.9		145.4		348.0
Pressurization system						
Start tank	220		220		110	
Main tank	73		72		51	
Feed system penalties	27		25		20	
		320.0		317.0		181
Feed system components		82.0		82.0		81
Insulation system						
Main tank	138.7		138.7		138.7	
Start tank	5.0		8.2		19.5	
		143.7		146.9		158.2
Thermal induced boil-off						
Main tank	100		100		100	
Start tank	5.9		9.1		42.8	
		105.9		109.1		142.8
Basic tankage ①		678.0		678.0		678.0
Low-g pressure control ②		41.8		41.8		41.8
Cryogen loss for cooling		60.2		60.2		60.2
TOTALS		1559.5		1580.4		1691.0
Pump bypass loss ③		0		0		0

① Does not include penalties incurred by other subsystems; these are included with the system of concern
② Assumes vapor-cooled shroud thermodynamic vent system.
③ Assumes all pump bypass directed back into main tank; decreased tank weight penalty not subtracted for this analysis.

Table 26

LIQUID OXYGEN START TANK SYSTEM WEIGHT SUMMARY

	Start Tank Size					
	0.236 m^3	(8.33 ft^3)	0.47 m^3	(16.67 ft^3)	2.6 m^3	(91.9 ft^3)
	Weights (kg)					
Acquisition system						
Hardware	32.8		41.5		125.3	
Residual losses	133.5		82.2		0	
		166.3		123.7		125.3
Pressurization system						
Start tank						
Main tank	91.0		91.0		91.0	
Feed system penalties	7		6		5	
		98.0		97.0		96.0
Feed system components		81.0		81.0		80.0
Insulation system						
Main tank	46.3		46.3		46.3	
Start Tank	0		0		0	
		46.3		46.3		46.3
Thermal induced boiloff						
Main tank						
Start tank		0		0		0
Basic tankage ①		265.0		265.0		265.0
Low-g pressure control ②		20.9		20.9		20.9
Cryogen loss for cooling		0		0		0
TOTALS		677.5		633.9		633.5
Pump bypass loss ③		0		0		0

① Does not include penalties incurred by other subsystems; these are included with the subsystem of concern.

② Assumes vapor cooled shroud thermodynamic vent system.

③ Assumes all pump bypass directed back into main tank; decreased tank weight penalty not subtracted for this analysis.

Table 27

TOTAL START TANK SYSTEM WEIGHT SUMMARY

Start Tank System Combination	Refill Operation	Total Weight (kg)
1.4 m^3 LH_2 and 0.236 m^3 LO_2	Vacuum vent/refill	2,237.0
2.8 m^3 LH_2 and 0.47 m^3 LO_2	Vacuum vent/refill	2,214.3
22 m^3 LH_2 and 2.6 m^3 LO_2	Dynamic refill	2,324.9
1.4 m^3 LH_2 and 2.6 m^3 LO_2	LH_2 vacuum vent/refill LO_2 dynamic refill	2,193.0

LH_2 start tank wall were integrated with the LH_2 main tank. In this case, a savings of approximately 100 kg (220 lb) would be gained. This savings would be somewhat offset by additional boiloff during reentry and landing. However, the total thermal degradation of the integral wall start tank concept does not appear to be significant. One of the most significant weight reductions will occur as a result of the refined requirements for hydrogen thermodynamic vent coolant. The LH_2 start tank size will be reduced from 22 m^3 (778 ft^3) to 15.5 m^3 (550 ft^3). Furthermore, if all hydrogen coolant is removed from a channel device beneath the main tank screen, the start tank size is further reduced to 6.4 m^3 (226 ft^3). The circular cross-section all-screen channel design offers a small weight improvement, but a significant improvement in ease of fabrication.

3.1.3 All-Screen Channel Surface Tension Stability Verification Test Procedure

Two qualification test procedures are outlined below for the bubble point verification of large-scale all-screen devices. Both procedures are based on the principle that a film of liquid on the screens seals each screen pore and that the hydrostatic head, relative to a screen device filled with liquid, is negligible. Screen devices larger than the supportable heights of liquid columns can therefore be tested using films of wetting liquids. This procedure is practical with screen devices in tanks, whereas, submerging large screen devices in a test liquid and performing standard bubble point test (e.g., SAE ARP 901) cannot be done with the large-scale screen devices assembled within propellant tanks. These procedures are used primarily to verify that a large-scale screen device maintains indefinitely a stable sealing interface at a pressure slightly less than the breakdown bubble point pressure of the screen. The procedures are used during the qualification testing of the tank final assembly and as a checkout test of the screen devices during routine maintenance. Failure of the screen device to meet the design capillary pressure difference would necessitate removal and replacement (or repair) of the screen device, which requires access to the tank. However, both procedures developed below do not require tank access, and can be performed with the vehicle in either a horizontal or vertical orientation.

3.1.3.1 Isothermal Liquid Film Pressure Difference Test Procedure for the Start Tank

The isothermal liquid film pressure difference test procedure is used for

relatively small screen devices which can be initially surrounded with the test liquid in a practical manner. For example, filling a 1 to 3 m^3 start tank with the test liquid is practical, but completely filling the large-scale main tank with test liquid so as to wet the distributed all-screen channels is not recommended from a loading and cost standpoint.

Figure 32 is the schematic diagram for one method of screen device bubble point verification for the start tank, which in principle would be used with other localized devices. Following start tank cleaning procedures, the test liquid (e.g., isopropyl alcohol, methanol, Freon 114) is pumped into the start tank at ambient temperature through the connections upstream of the start tank main feed line valve, while the start tank is vented through the auxiliary overboard vent. When full, the test liquid supply valve is closed. The supply gas (N_2, He, etc.) is then bubbled through the alcohol accumulator to displace the test liquid in the start tank with a gas mixture saturated with alcohol vapor at the ambient temperature of the system. The drain valve is opened and test liquid is slowly displaced from the start tank by the incoming gas mixture.

The gas enters the tank through the overboard vent line and through the feed-line so that there is no pressure difference between the inside of the channel device and the start tank which could break through the liquid film covering the screen. Since the system is isothermal and there are no test fluid concentration gradients in the ullage, the film of liquid remains on the screen as the bulk liquid drains from the tank.

When empty, the test liquid drain valve is closed and the bubble point pressure is checked by introducing a gas mixture through a transparent vessel containing the test liquid into the channel device. The gas entering the channels is saturated at the appropriate partial pressure of the test liquid to alleviate mass concentration gradients in the channels which could lead to evaporation of the liquid film. The transparent vessel allows direct observation of the gas bubbles entering the channel and thus can be used to verify that there is no leakage from the channel through unsealed screen pores into the start tank. The pressure difference between the inside of the channels and the start tank is monitored with manometer No. 1, and the gage pressure of the start tank is monitored with manometer No. 2.

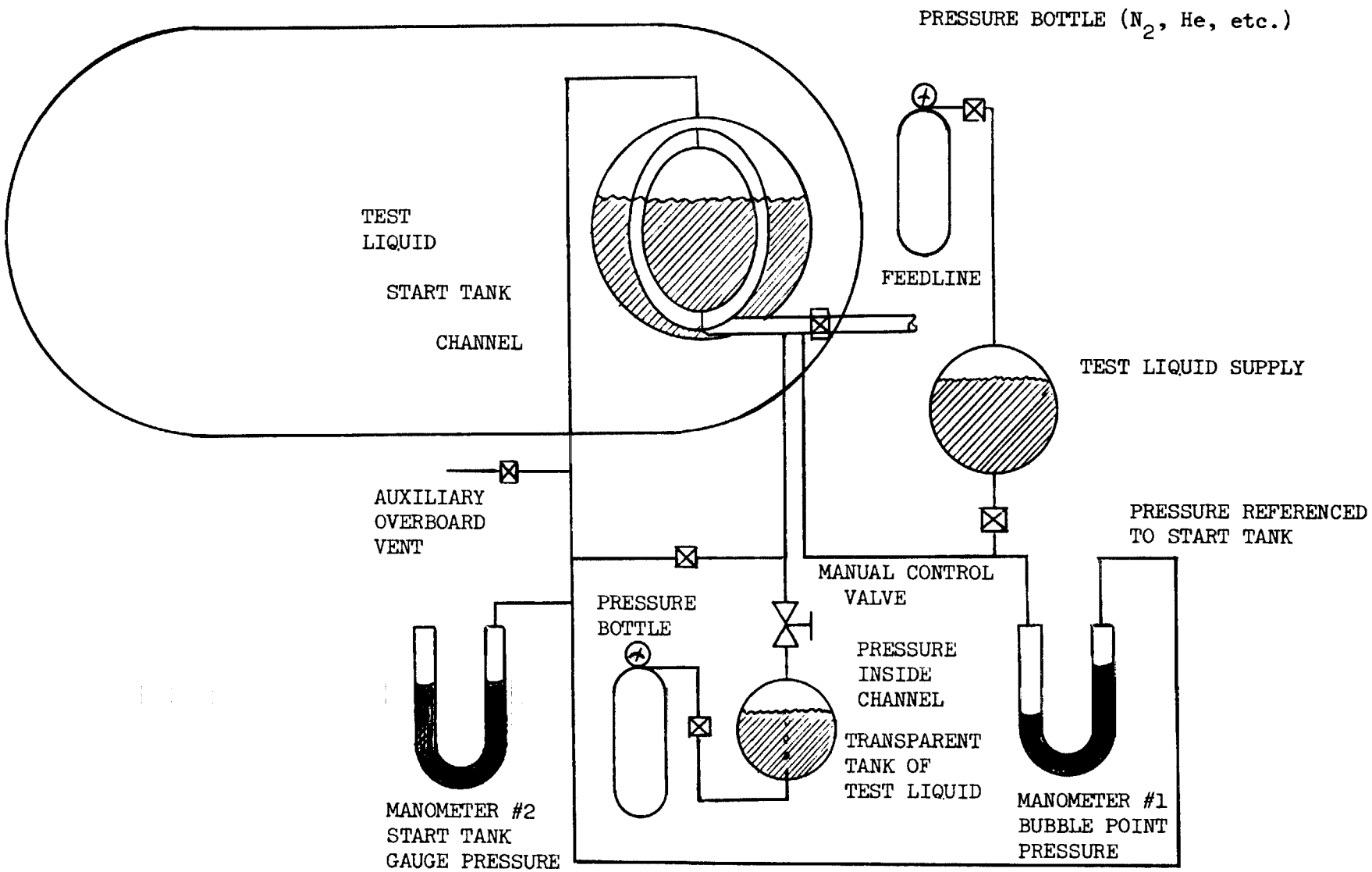

Figure 32. Bubble Point Verification Procedure

After reaching the design pressure for which screen stability must be assured, the transparent test vessel and start tank gage pressures are observed for approximately 10 minutes to 1 hour; if no additional gas enters the channels and/or the start tank pressure is constant during this period, no leakage has occurred through the screen. The design pressure for screen stability is thus verified.

3.1.3.2 Condensing Liquid Film Pressure Difference Test

The condensing liquid film pressure difference test departs from the preceding isothermal test only in the manner in which the liquid film is formed on the screens. Rather than filling a tank to wet the screens, a saturated vapor flow of the test fluid is introduced into the tank at a temperature slightly above the tank temperature. Condensation thus occurs on the tank walls and screen device, as demonstrated by the test discussed in Section 3.2.9. During the condensation flow process, the vapor enters both through the channels and directly into the tank so as to maintain a negligibly small pressure difference across the screens. The fluid enters at the top of each channel so that the falling condensate film enhances the wetting of the screens.

Although the bench test described in Section 3.2.9 demonstrated the feasibility of the condensing film technique, further tests are required to establish such parameters as the saturated vapor inflow rate and time required to totally wet the screen, and to determine the most appropriate test fluid. In addition, analyses are required of the interrelationships of the saturation temperature and pressure, heat transfer through the tank walls, and initial temperature of the tank.

A candidate procedure which eliminates much of the transient heat transfer problem involves initially cooling the tank below the ambient temperature. A saturated vapor having a vapor pressure equal to or greater than 1 atmosphere at the ambient temperature is then transferred into the tank at approximately 1 atmosphere or above. As condensation occurs, the tank internal temperature will rise, eventually reaching a steady-state temperature equal to the ambient temperature. This condition can be maintained indefinitely, thus allowing long-term bubble point tests to be conducted. Pressures equal to or greater than 1 atmosphere are used to avoid problems of crushing pressure loads on the tank wall.

3.2 PHASE II, TASK B — BENCH TESTING

Work began during the third quarter and was continued during the fourth quarter on a series of bench tests conceived to resolve critical design problems relative to the candidate acquisition system preliminary designs. The planned tests and their current status are summarized in Table 28. As can be seen, most of these have been completed except for repeating of important LH_2 bubble point tests and an additional test warranted by the new emphasis on advance cryogenic spacecraft applications. Details of each test are reported in the following sections.

3.2.1 Test I - Tests to Establish Heat Transfer Effects on Screen Bubble Point in LH_2

Tests were completed to evaluate the effects of heat transfer from a warm ullage gas to a representative screen retaining LH_2. These were accomplished by measuring the changes in bubble point performance for a given screen retaining LH_2 with a warm pressurant gas on the other side of the screen. Gas temperatures above the screen and the resulting heat flux were also measured in the experimental apparatus shown in Figures 23 and 24 of Reference 1. Figure 33 shows final details of the screen sample installation in the test apparatus.

In late 1971, as part of the MDAC IRAD Program, essentially the same apparatus had been tested with LN_2 and it was found that heat transfer rates up to 9.5×10^3 watts/m^2 (the highest that could be obtained with the test system) had no effect on bubble point performance with screen meshes from 450 x 2750 to 165 x 800 (see Reference 11). However, our latest results with LH_2 showed significantly different characteristics.

Two screens were bubble point tested in LH_2; 200 x 1400 and 250 x 1370 dutch twill. Based on a preliminary bubble point test in isopropyl alcohol (σ = 21.4 dyne/cm at 294°K), the expected bubble point in LH_2 (σ = 1.95 dyne/cm at 20.3°K) would be 36.9 mm of water column (W.C.) for the 200 x 1400 mesh. None of the test data used to compute the net heat transfer to the screen is reported here since a leak in the electrical feedthrough and a cracked O-ring seal were discovered during assembly. The vent rate, though suspect, showed

Table 28

BENCH TESTING STATUS

Test No.	Description	Purpose	Status
I	Basic screen bubble point test in LH_2 with simulated warm gas heating (also possible liquid heating).	To demonstrate if a typical screen can actually maintain retention with heat transfer occurring across the screen.	Completed
II	Attach screen material coupons to backup and support structure by various techniques.	To evaluate fabrication techniques for joining screen materials.	Completed.
-	Large-size channel segment fabrication and bubble point and pressure tests.	To establish reasonable assurance that a large-size channel can be built to satisfy design requirements.	Deleted - Basic objectives were achieved under tests II and IX.
III	Bubble point test with LH_2 for selected screen mesh.	To clear up uncertainty in bubble point measurements.	Planned test completed. Modification and retest being planned.
IV	Flow loss tests with composite screen/backup structure.	To provide ΔP data to assess interactions of screen and backup materials.	Completed
V	Bubble point test with representative screen with vibration present.	To establish if there is retention degradation within a vibration environment.	Completed
VI	Bubble point tests with controlled screen deflection and distortion.	To establish structural design criteria for screen rigidity requirements.	Completed

Table 28

BENCH TESTING STATUS (Continued)

Test No.	Description	Purpose	Status
VII	Bubble point and flow performance of pleated screens.	To explore potential problems and benefits of screen pleating.	Completed.
-	TVS heat transfer experiment for a cooled finned tube.	To evaluate basic heat process in a cooled wall element.	To be done under NAS 8-27571 with expanded scope.
VIII	Channel duct joining tests.	To evaluate joining techniques.	Completed
IX	Film bubble point test.	To assess the feasibility of using only a thin film over a screen in measuring bubble point.	Completed
X	Pressure-change-induced screen breakdown tests.	To evaluate the influence of pressure changes on screen breakdown in LH_2.	Being planned.

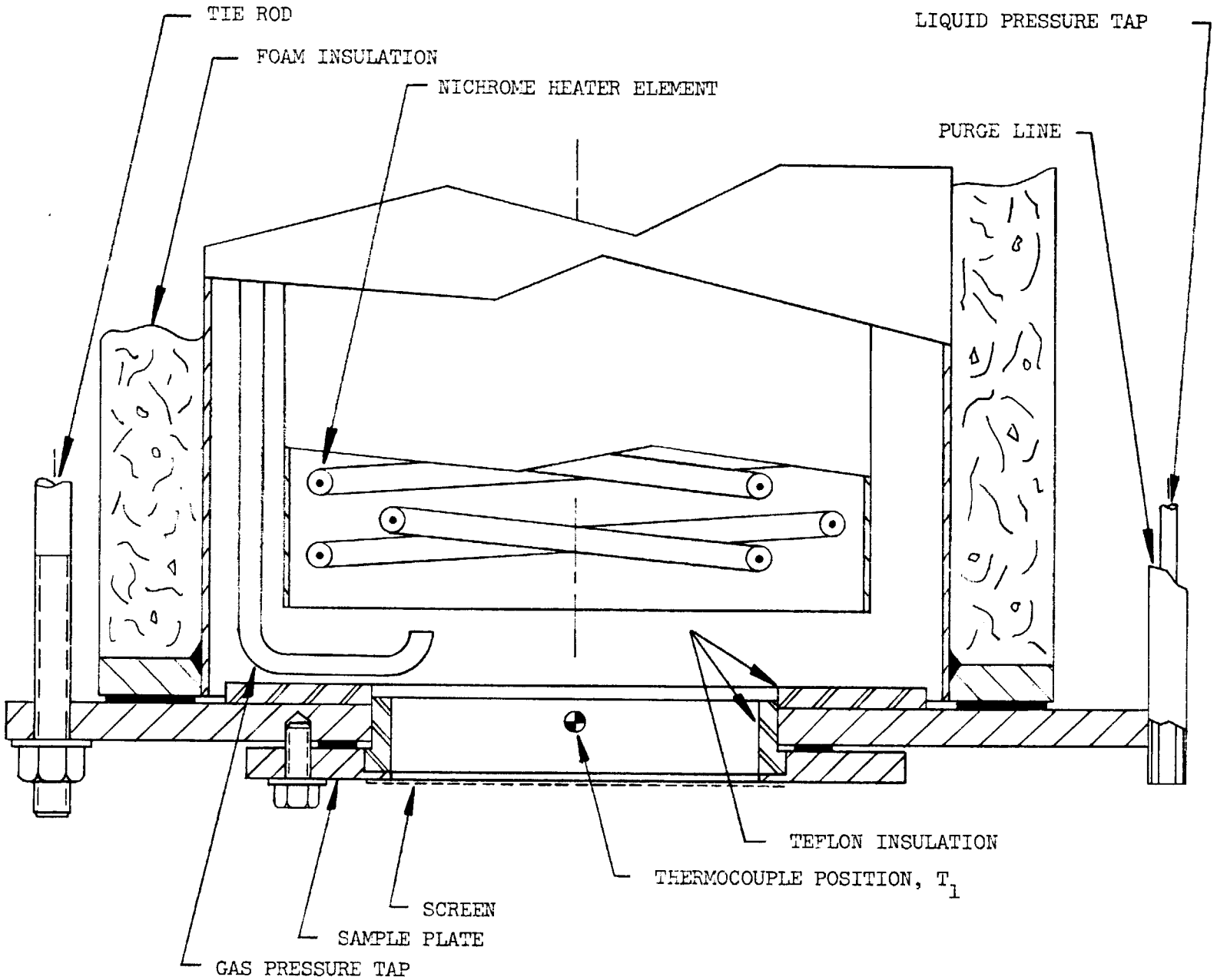

Figure 33. Section View of Screen Sample Plate (Full Scale)

a net heat transfer coefficient of approximately 25 x 10^5 joules/m^2 sec ^oK. The data for the 200 x 1400 mesh screen indicates a serious reduction in bubble point with an increasing rate of heat transfer to the screen. Reductions of up to 50 percent in bubble point were recorded.

The test data for the 250 x 1370 mesh screen are shown in Figures 34 and 35. During the installation of this screen, the leaking components were repaired. An increased vent rate was observed with this screen as the heat transfer coefficient approached the range of 40 to 60 x 10^5 joules/m^2 sec ^oK as shown in Figure 34. As with the 200 x 1400 specimen, the foam insulation cylinder would not pressurize itself when the vent line was closed off. An acceptable explanation for this occurrence has not been discovered. During disassembly no potential leak paths were uncovered. The heat transfer coefficients were computed based on data taken with the vent line open and a small ΔP (<2.5 mm W.C.) across the screen. This heat transfer coefficient does not change as the ΔP across the screen increases (this was demonstrated in the LN_2 tests). Therefore, the plot of bubble point versus gas temperature in Figure 35 can be converted to a plot of bubble point versus heat transfer using a coefficient of approximately 50. Note that there again is a rapid dropoff in bubble point pressure with increasing gas temperature.

The test data shown in Figure 35 were generated in one of two fashions. At the fixed values of T_1, the heater was activated to rapidly increase the pressure above the screen to the breakdown point. The temperature T_1 did not change during this operation. This procedure was used to replace the planned technique of throttling the vent to raise the pressure. The disadvantage in using the heater to raise the pressure is that there is a loss of control of the pressure increase rate. The heater caused the pressure to rise in a rapid fashion which may have exceeded the response rate of the fluid-filled inclined manometer that recorded the ΔP across the screen and temperature T_1 resulted in a small, continuous failure of the screen. The steady-state pressures observed at those points should be very close to the bubble point pressure. The LH_2 bubble point for the 250 x 1370 mesh would be 43.2 mm (1.7 in.) W.C. based on isopropyl alcohol tests. The test data for gas temperatures below 27.6^oK is within 10 percent of this value.

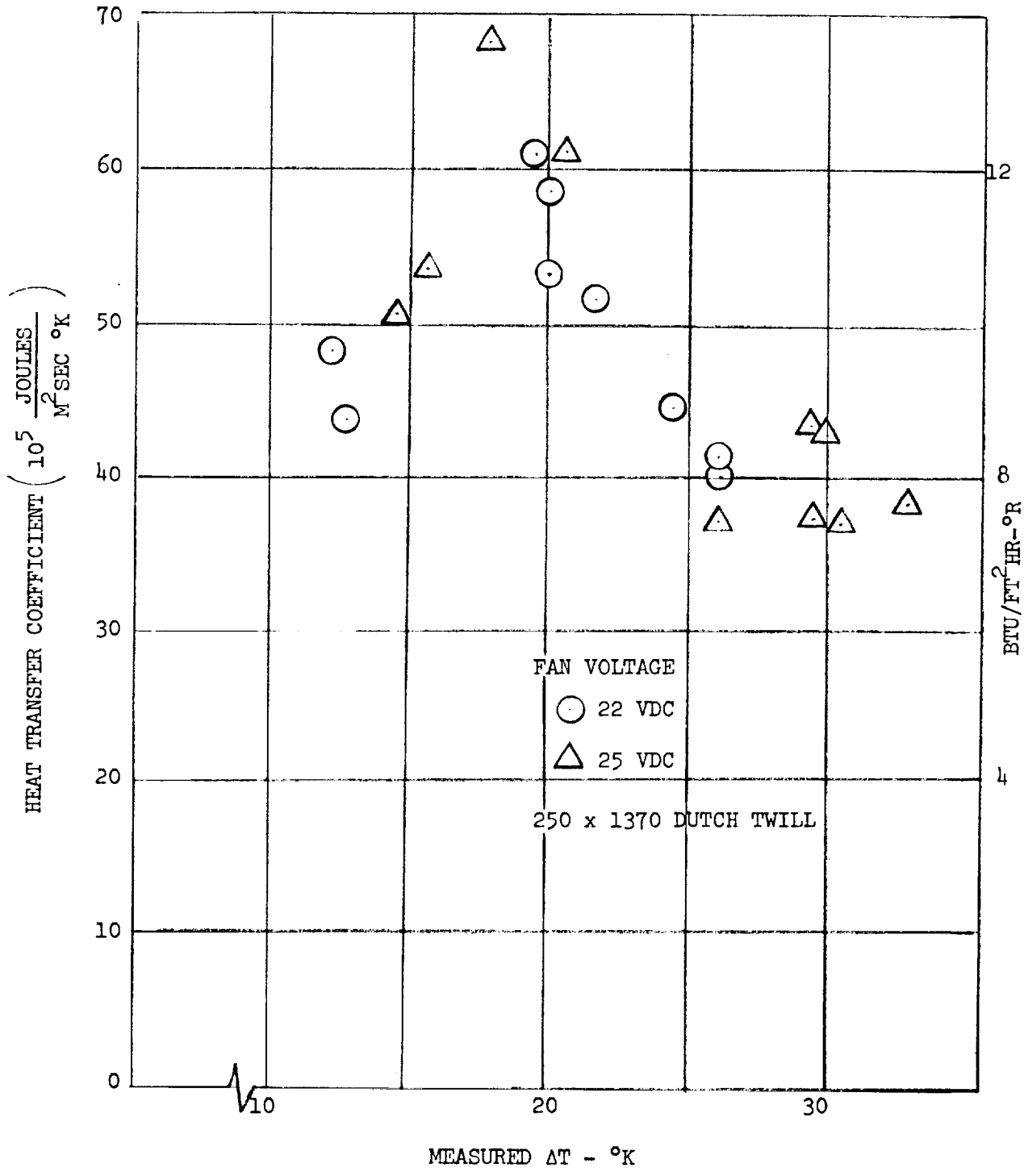

Figure 34. Forced Heat Transfer Coefficient at Screen

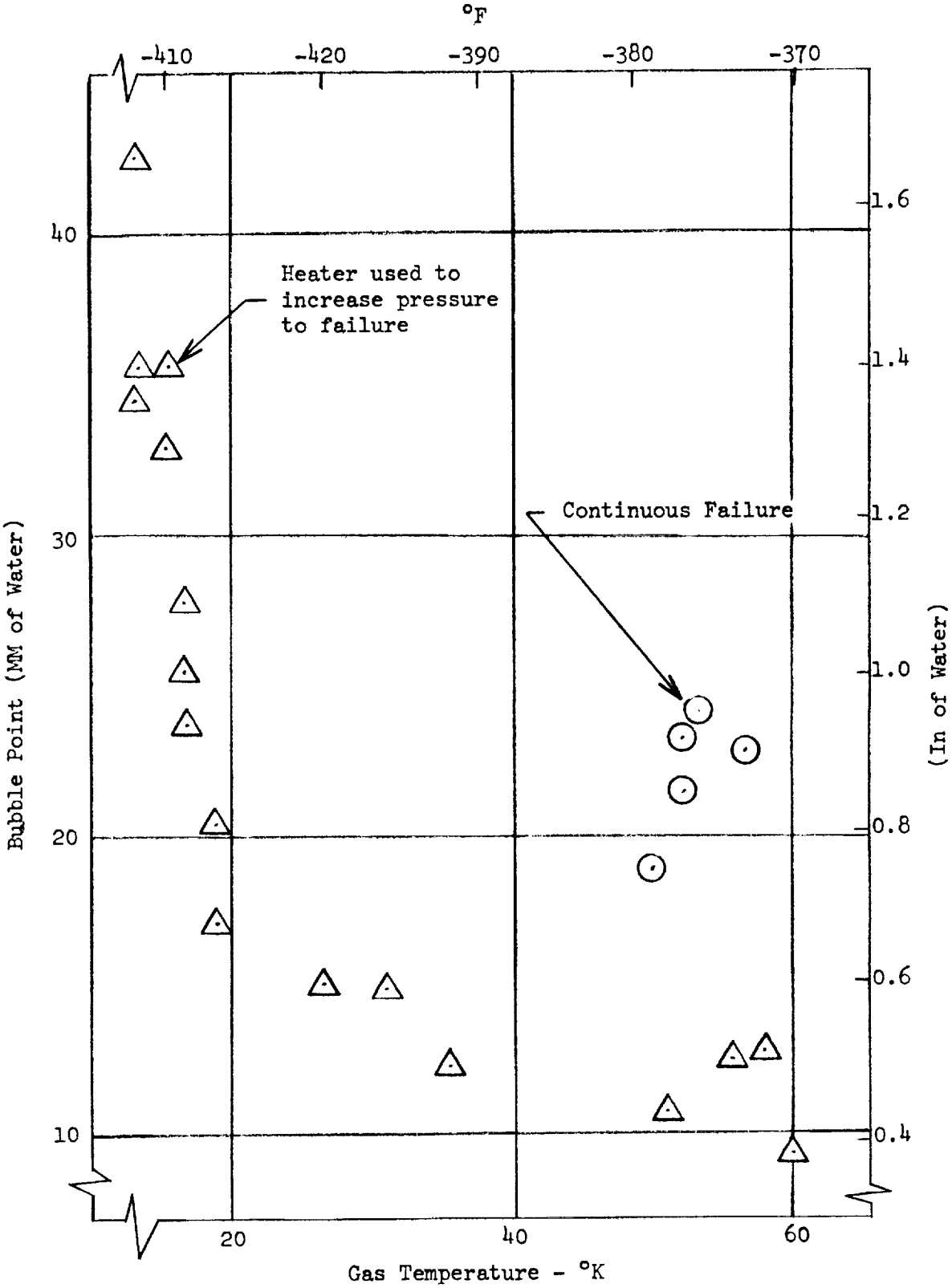

Figure 35. Bubble Point Data for 250 X 1370 Mesh in LH_2

In conclusion, it has been shown that the presence of a warm gas pressurant can seriously reduce the bubble point performance of a screen. This result is in direct contradiction to that observed during testing with LN_2 in which there was no significant bubble point change.

The thermally induced failure observed in these tests was very similar to that observed during MDAC IRAD expulsion demonstration tests on a 10-gallon LH_2 screen acquisition system using warm gas pressurization, in a representative system situation (Reference 5).

The results from the acquisition test are shown plotted in Figure 36 along with the latest bench tests in terms of the common ratio of measured head retention to the ideal head neglecting any heat transfer. Although the indicated temperatures were measured at different points and there was a low-temperature calibration shift on the demonstration test, the same degradation trend is evident in both tests.

Although the previous LN_2 tests indicated that a screen might be capable of sustaining high heating rates without head retention loss, these combined LH_2 results cast strong doubt on the practical feasibility of using screen acquisition devices where direct contact occurs between the screen and a warm pressurant gas. Extensive experimental research would be required to firmly establish design criteria and operational limits before warm gas pressurization could be confidently applied to any specific screen system for an LH_2 tank.

3.2.2 Test II - Screen Element Welding Tests

This effort consisted essentially of fabricating a series of retention screen elements consisting of a perforated steel backup plate, the fine mesh steel screen, and a thin steel "picture" frame. These were welded together by both fusion and roll-spot welding techniques. Material thicknesses of 0.051 cm (0.020 in.) and 0.081 cm (0.032 in.) were successfully fabricated. Although distortion was more of a problem with roll-spot welding, both techniques could be used. The completed 12.7 cm square screen elements are pictured in Figure 37. All specimens were bubble point tested using the apparatus

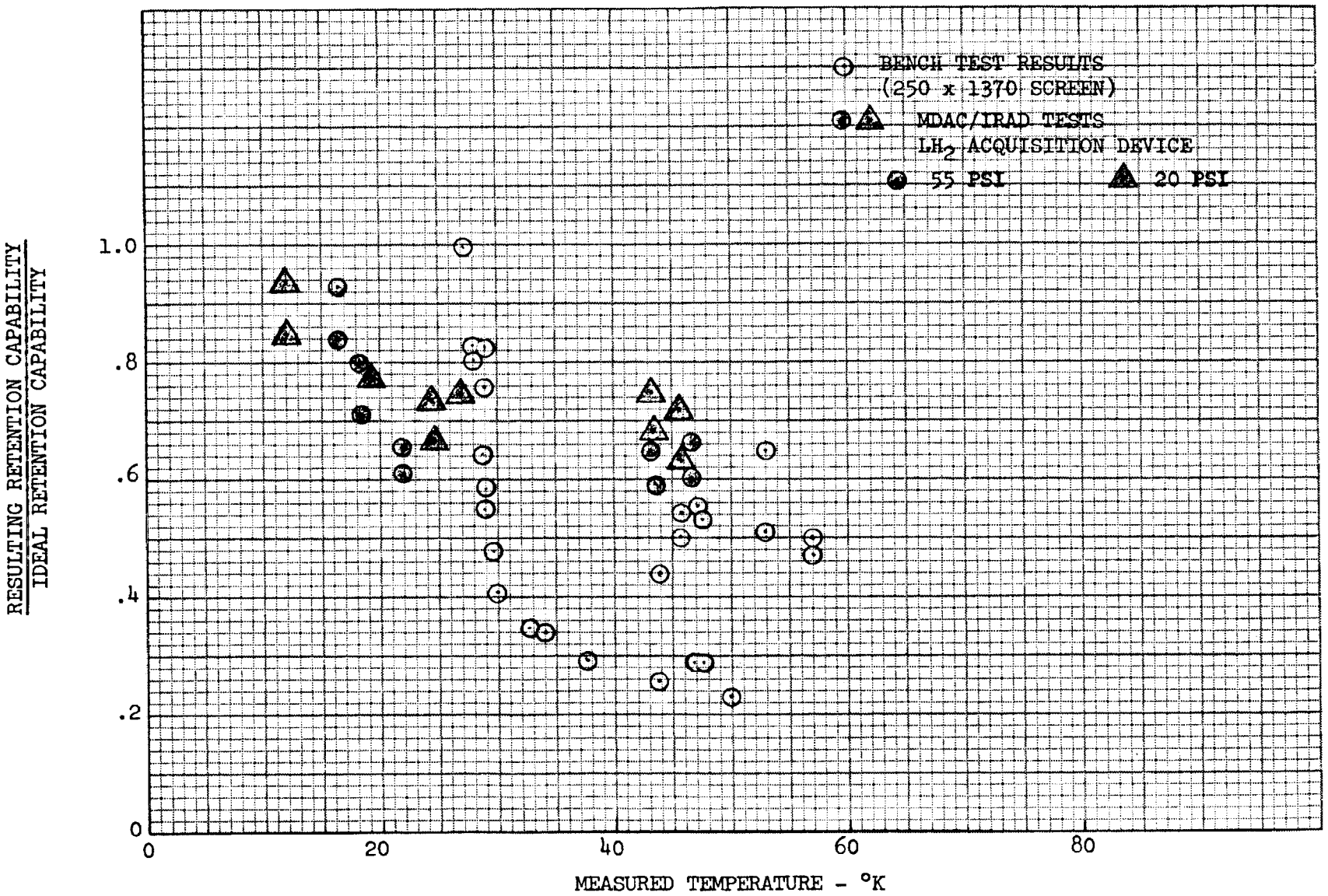

Figure 36. Comparison of Bench and Subsystem Screen Heat Transfer Experiments

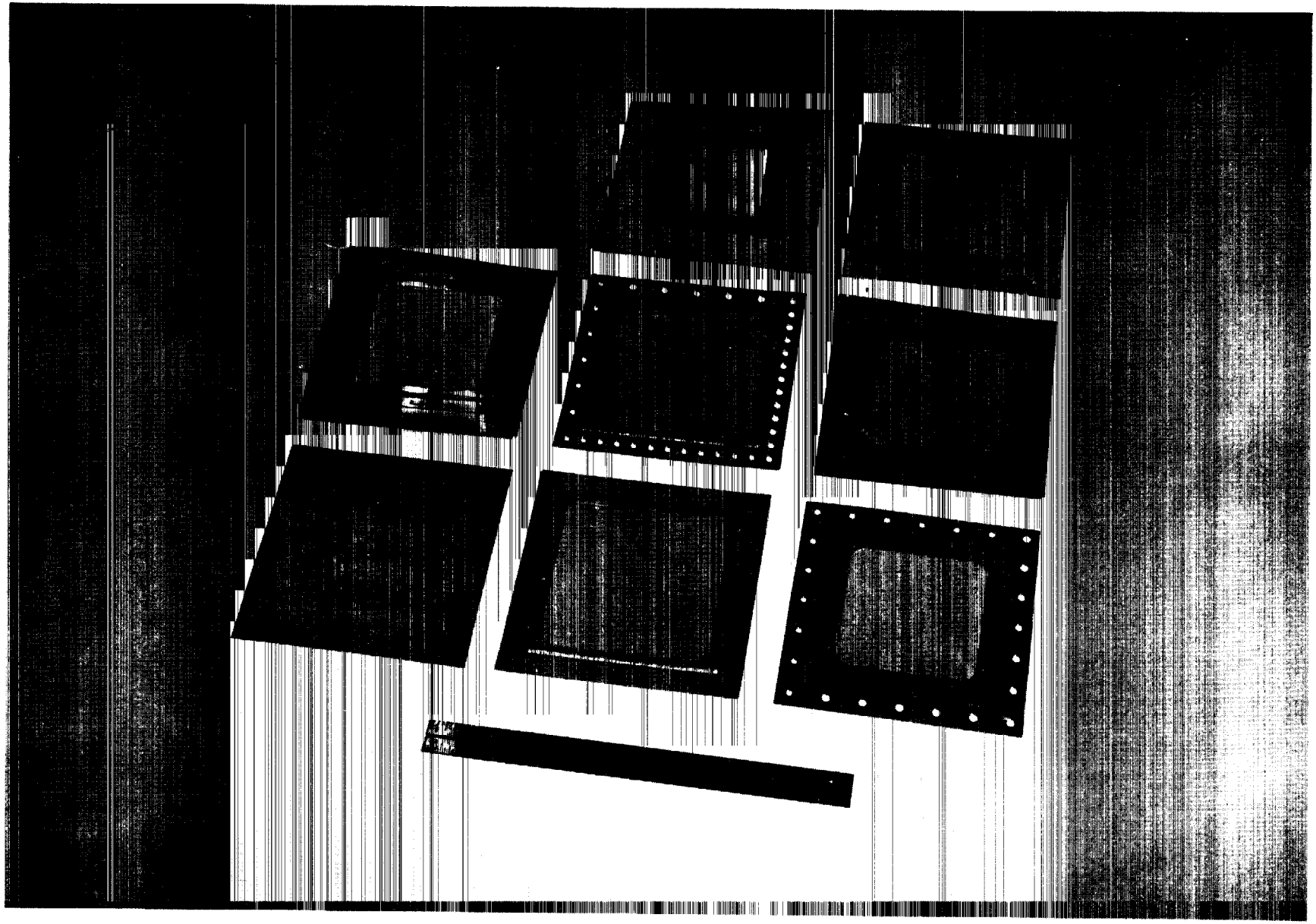

Figure 37. Fabricated Screen Elements

shown in Figure 27 of Reference 1. All specimens passed the bubble point test and from this standpoint both fabrication techniques are acceptable. Figure 37 and 38 are photos of the completed specimens.

3.2.3 Test III - Screen Bubble Point Tests with LH_2

The measurement of the isothermal bubble point pressure of five types of stainless steel fine mesh screens in LH_2 constituted one of the major bench tests. The specific objectives of the test series were:

A. To compare LH_2 and isopropyl alcohol bubble point pressure results for specific screens.

B. To determine the influence of the helium partial pressure on the bubble point in LH_2.

The tests were intended to be isothermal with saturated LH_2 conditions existing at atmospheric pressure, but this was not achieved.

A schematic of the LH_2 test setup is shown in Figure 39. The five screen specimens (165 x 800, 200 x 600, 200 x 1400, 325 x 2300, 450 x 2750) were each 2.85 cm in diameter and adhesively attached to individual elbows on the lower end of short sections of 2.5 cm diameter aluminum tubes suspended within the LH_2. The tubes created a region where the composition of the pressurizing gas could be controlled. Breakdown of the screen was observed by viewing through one of four windows in the lower portion of the dewar. A 25 cm inclined water manometer monitored the pressure differential between the gas pressure within the tube and the dewar ullage. Both GH_2 and GHe were available for pressurizing each tube in turn. A flowmeter was used to monitor the rate of GHe addition.

A single bubble point measurement consisted of first filling one of the five tubes with LH_2 and then displacing a portion of this liquid with a measured amount of GHe. The line sizes and lengths were selected so that at least 95 percent of the GHe added was located within the aluminum tube attached to the screen being tested. Following the addition of GHe, the pressure within the tube would rise slowly due to LH_2 evaporation. The LH_2 would be completely displaced from the tube within a period of 1 to 10 minutes at which

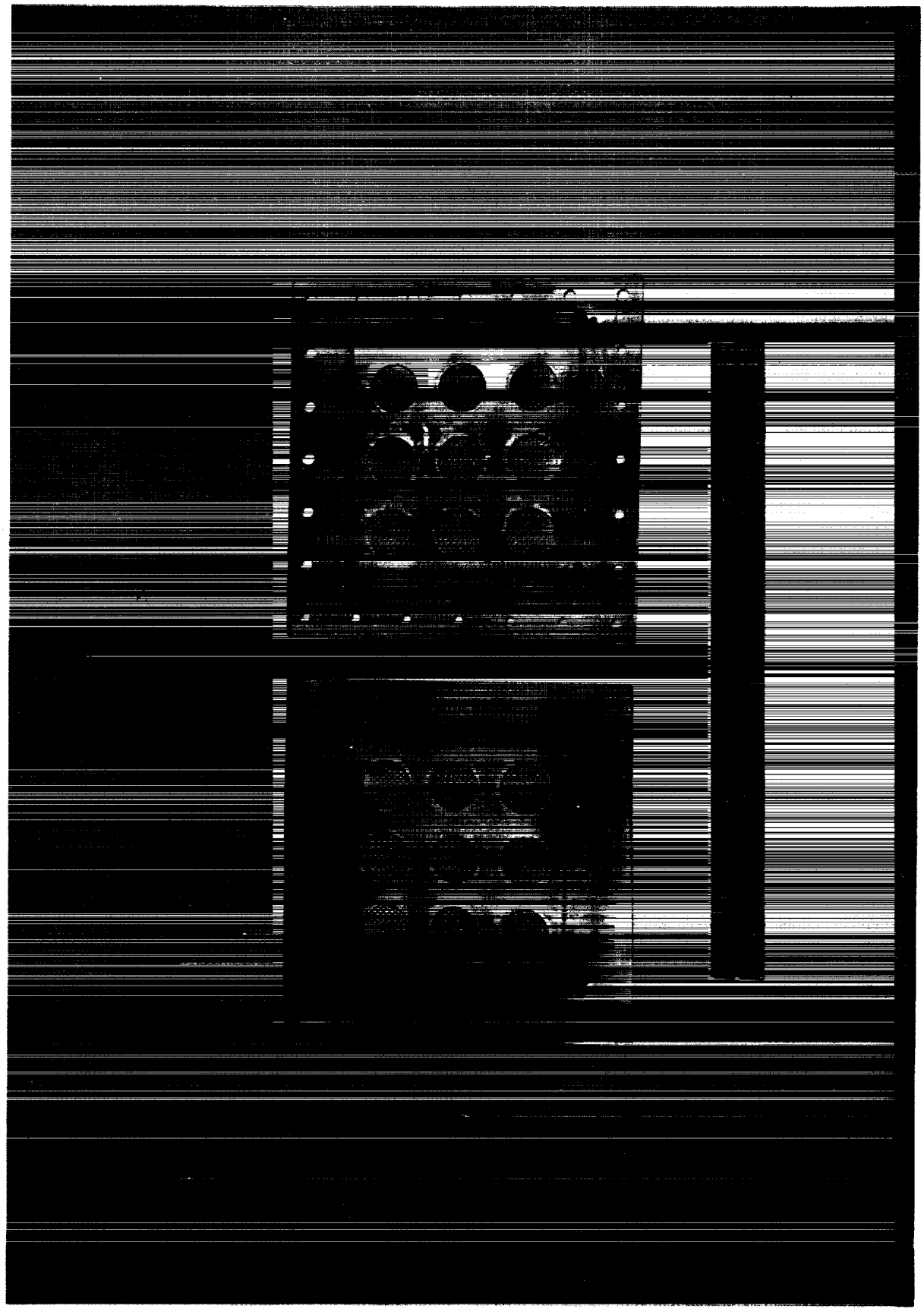

Figure 38. Screen Elements -- Rear View

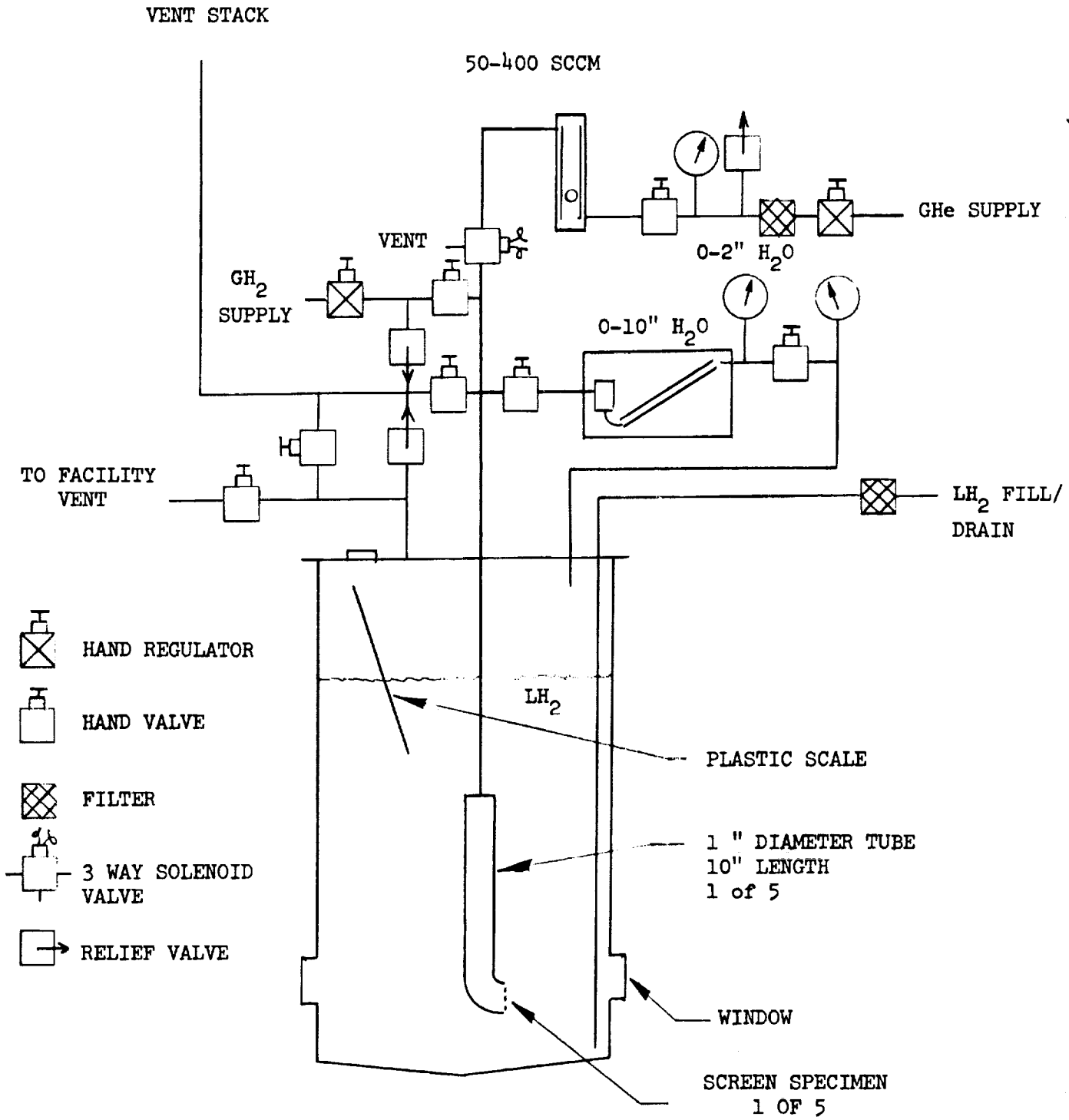

Figure 39. LH_2 Bubble Point Test

time the pressure would rise rapidly until screen failure occurred. The more rapid pressure rise was probably due to the fact that the ullage volume was no longer increasing as the liquid was displaced. This rapid rise precluded an accurate measurement of the pressure at screen failure. Subsequently, the tube was vented during that phase when the tube emptied to modulate the rate of pressure rise. This technique, however, resulted in the loss of an unknown quantity of GHe which prevented the partial pressure from being accurately computed. Under equilibrium conditions, the partial pressure of the GHe will be as the difference between the total pressure and the hydrogen vapor pressure. For nonequilibrium conditions, both the measured amounts of GHe and the partial pressure determinations will give only approximate values of the conditions at the screen interface.

The same throttling technique discussed above was used when pressurizing the screen with GH_2 alone. The results of the bubble point tests with GH_2 are shown in Figure 40. The bubble point was calculated by subtracting the LH_2 head from the manometer reading at the point of breakdown. The expected correlation between the isopropyl alcohol and LH_2 data is based on these values for surface tension:

LH_2 at 20.2°K	1.95 dyne/cm
Isopropyl alcohol at 296°K	21.4 dyne/cm

Four of the five screens are in good agreement with the expected correlation of the two sets of bubble point data based on the ratio of the respective surface tensions. The 325 x 2300 mesh will be rechecked in alcohol to verify that its exceptional behavior in LH_2 is not simply caused by a spurious measurement in alcohol.

Test data for one of the screens tested with varying amounts of GHe is shown in Figure 41. The data scatter prevents the possibility of drawing definite conclusions regarding the influence of GHe on the bubble point. The feasibility of using LN_2 or LH_2 prechillers on the GH_2 and GHe pressurizing gas is being investigated. It is expected that lowering the gas temperature would moderate the evaporation of LH_2 that is causing the excessively rapid rise in pressure within the tube attached to each screen.

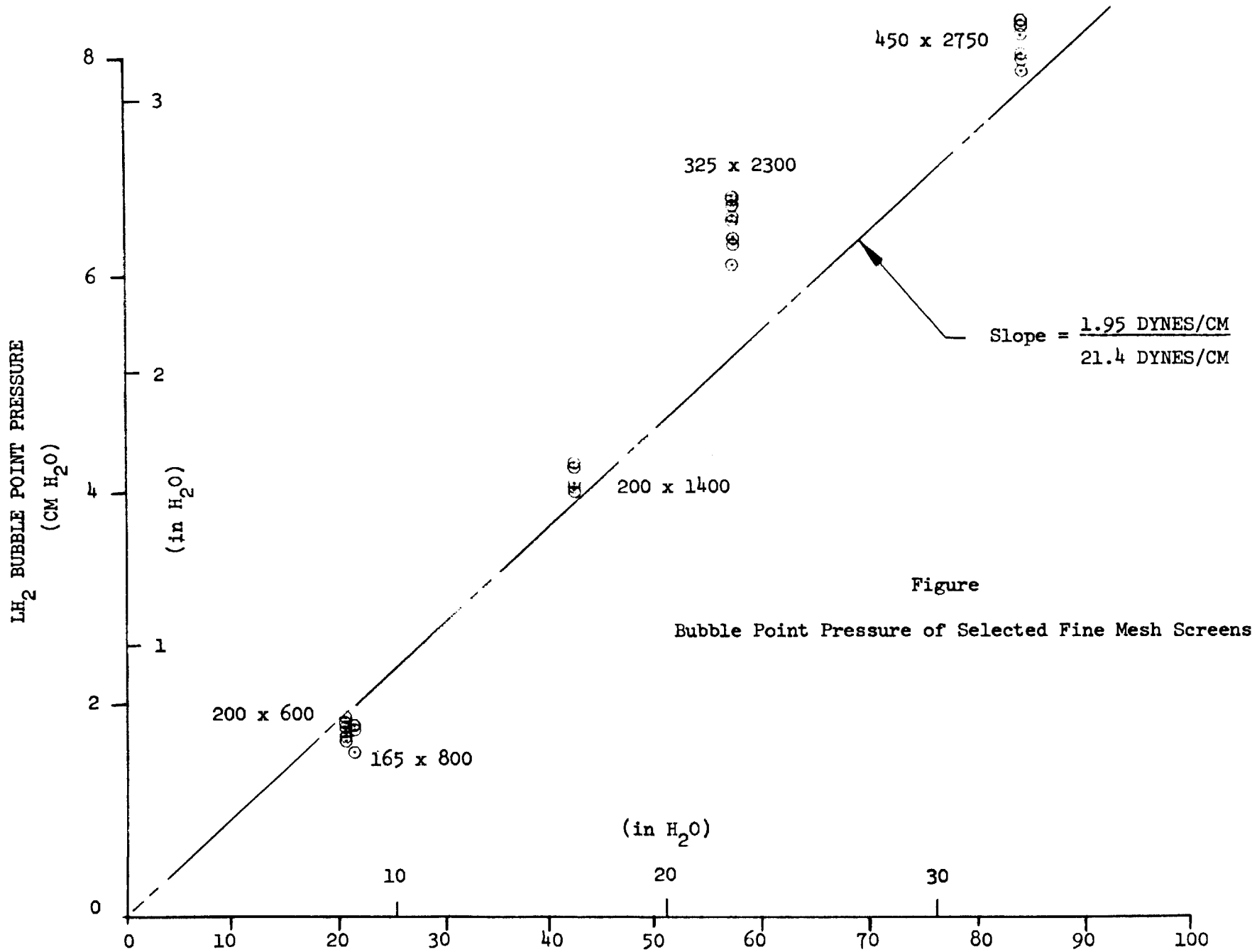

Figure

Bubble Point Pressure of Selected Fine Mesh Screens

Figure 40. Bubble Point Pressure of Selected Fine Mesh Screens

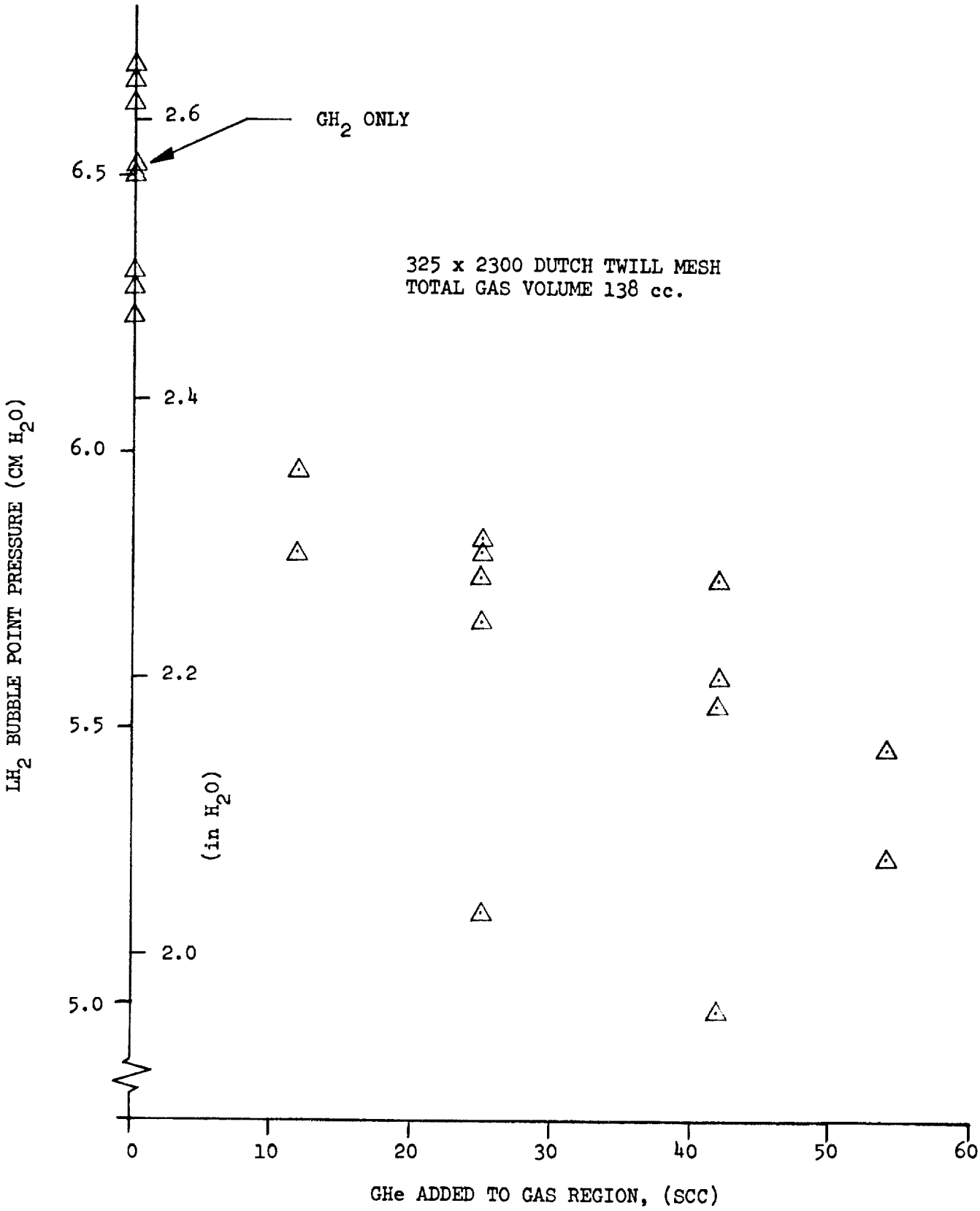

Figure 41. LH_2 Bubble Point with GHe Present

Until further experimental steps are taken, it will be assumed that the bubble point in LH_2 can be estimated based on isopropyl alcohol tests regardless of the quantity of GHe present.

3.2.4 Test IV - Flow Loss Tests for Screen Elements

Most of the flow loss tests were performed in the third quarter and reported in Reference 1.

The flow tests conducted in this quarter were made to determine the pressure losses associated with flow through robusta type screens and to compare these to the results for dutch twill screens. An additional dutch twill screen (200 x 600 mesh) was also tested because it is reported to have low flow loss characteristics. Two fine (850 x 155 and 720 x 140) and two coarse (280 x 70 and 175 x 50) mesh sizes were selected for the robusta tests.

The Armour and Cannon correlation equation is again successful in aligning the data points for particular screens, but the data do not lie uniformly below (or above) the correlation curve because of the range of pore sizes tested. The data for the two fine robusta screens aligned with those of the previously tested dutch twill screens below the curve, whereas those for the two coarse robusta screens and the 200 x 600 dutch twill screen lay on or slightly above the correlation curve. This indicates that the correlation equation is conservative when applied to screens with high pressure loss characteristics, but that it more nearly predicts the performance of screens with lower pressure loss characteristics.

3.2.5 Test V - Bubble Point Tests with Vibration

Bench tests were conducted to establish the influence of vibration on the bubble point pressure of various fine mesh screens. This interaction is of interest because there are several sources of oscillatory inputs to the propellant tank and screen device. These sources include rotating machinery, acoustics, and flow dynamics. If the retention capability of the screen is compromised, provisions must be made for mechanical isolation or reduction in operational safety factor of the acquisition device.

The objective of the bench test was to subject small, wetted screen elements to a controlled pressure differential while providing a sinusoidal displacement input to the screen and fluid column supported by the screen. The independent variables were:

A. Axis of Vibration
   1. Parallel to screen surface
   2. Perpendicular to screen surface
B. Vibration Frequency — 5 to 1000 Hz
C. Vibration Acceleration — 1/4 to 4 g's as measured by an accelerometer on the shaker platform.
D. Liquid depth above screen (isopropyl alcohol) — 1/4 to 15 inches.

A sketch of the test apparatus is shown in Figure 42 and photos of the completed apparatus are shown in Figures 43 and 44. The flat screen elements were sandwiched between 1.6 mm (1/16 inch) thick rubber sheets. The 1 cm diameter holes in these two sheets matched the 1 cm in the plexiglass block above the screen. This transparent block permitted screen breakdown to be detected by an observation of bubbling up through the liquid above the screen. Pressurization of the screen took place in the shallow cavity created by the rubber sheet between each screen specimen and the flat metal baseplate. If the alcohol liquid depth was to be increased beyond the 5 cm limitation of the holes in the transparent block, then an extension piece was clamped to the top of the apparatus. The extension piece consisted of a series of 50 cm vertical metal tubes which were positioned directly over the holes in the block.

The first test sequence was vertical sinusoidal vibration perpendicular to the surface of four screen specimens (325 x 325, 850 x 155, 200 x 600, 250 x 1370). The isopropyl alcohol liquid depth above each screen was 2 cm or less in all cases. As an initial step, the static bubble point of each screen was measured. Next a ΔP somewhat less (10 to 20 percent) than the static bubble point was placed across each screen and the frequency range 5 to 100 Hz was swept at 2 octaves/minute at a fixed g-level. The frequencies at which gas breakthrough occurred were recorded. Customarily, once failure took place, it continued as the frequency increased to 1 kHz. The results of these shallow depth tests are shown in Figures 45 and 46. The vertical separation

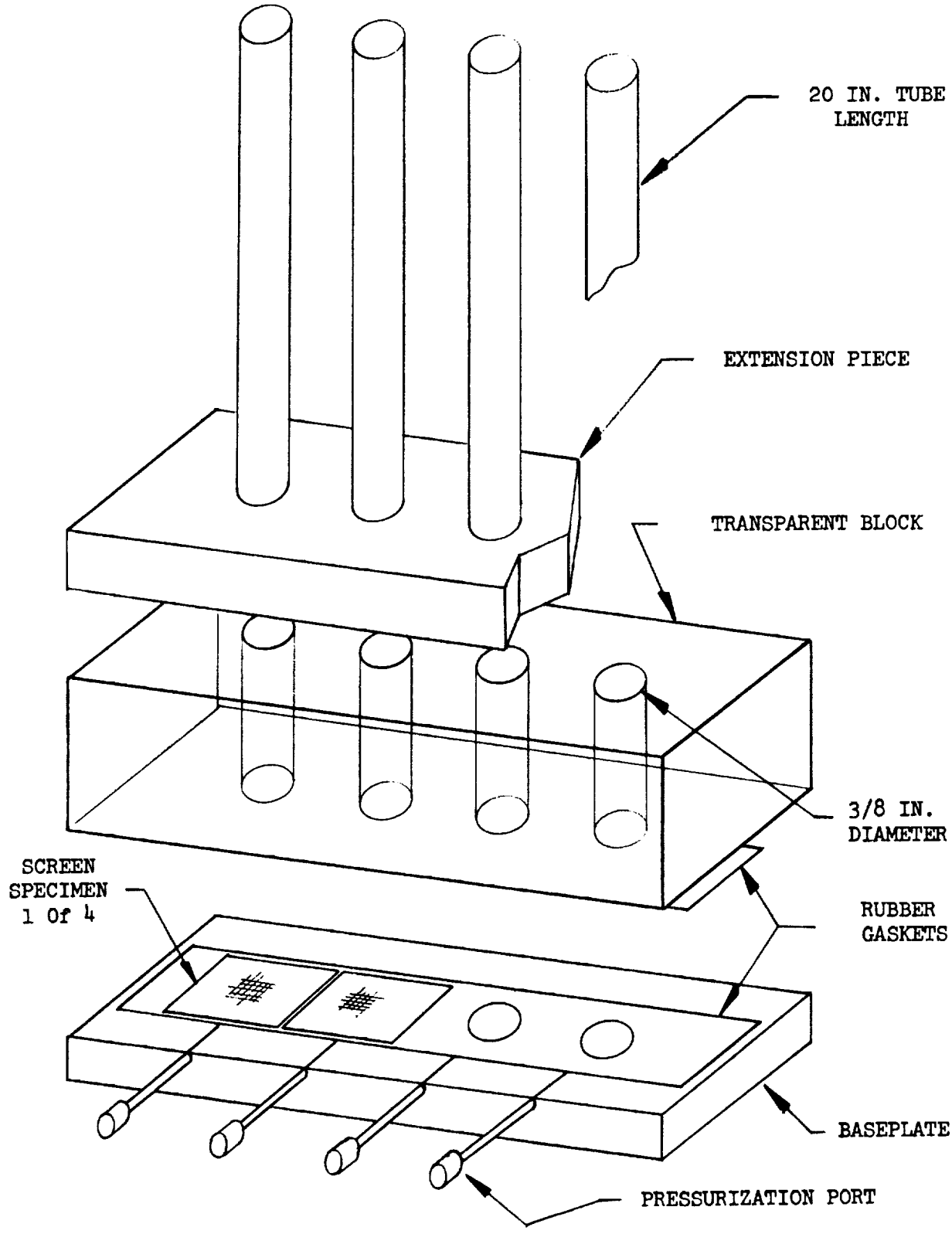

Figure 42. Vibration Test Apparatus

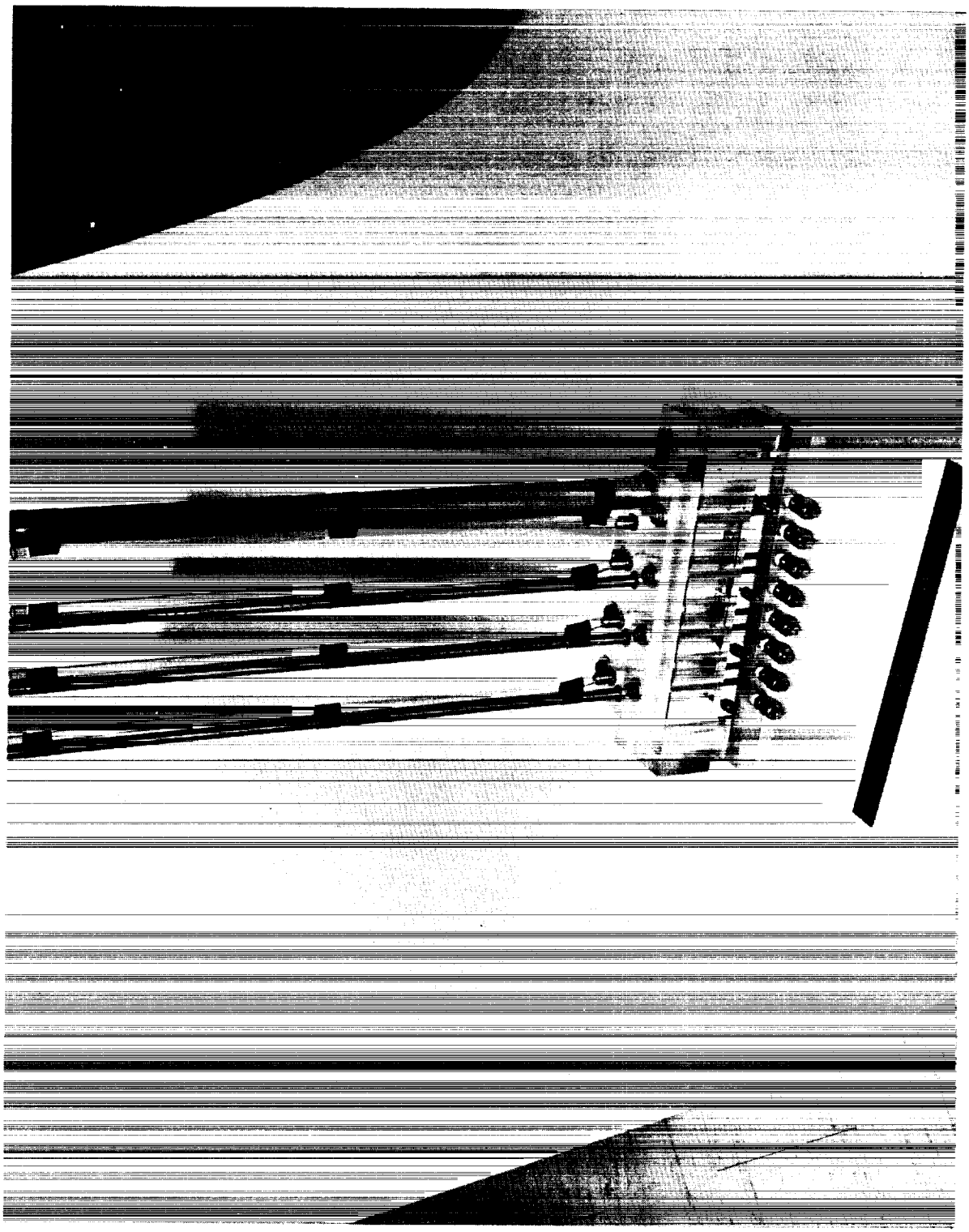

Figure 43. Vibration Test Apparatus

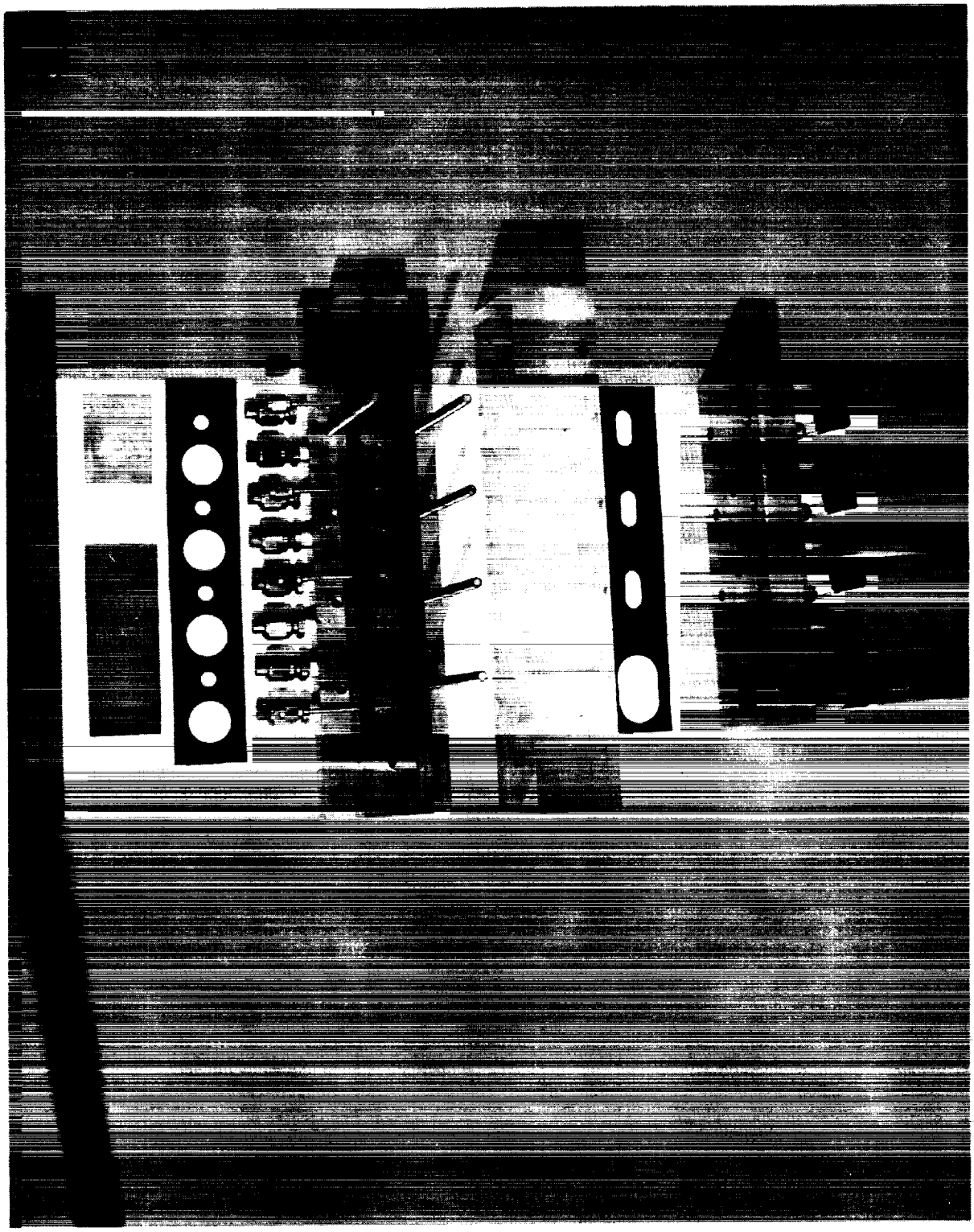

Figure 44. Vibration Test Apparatus Disassembled

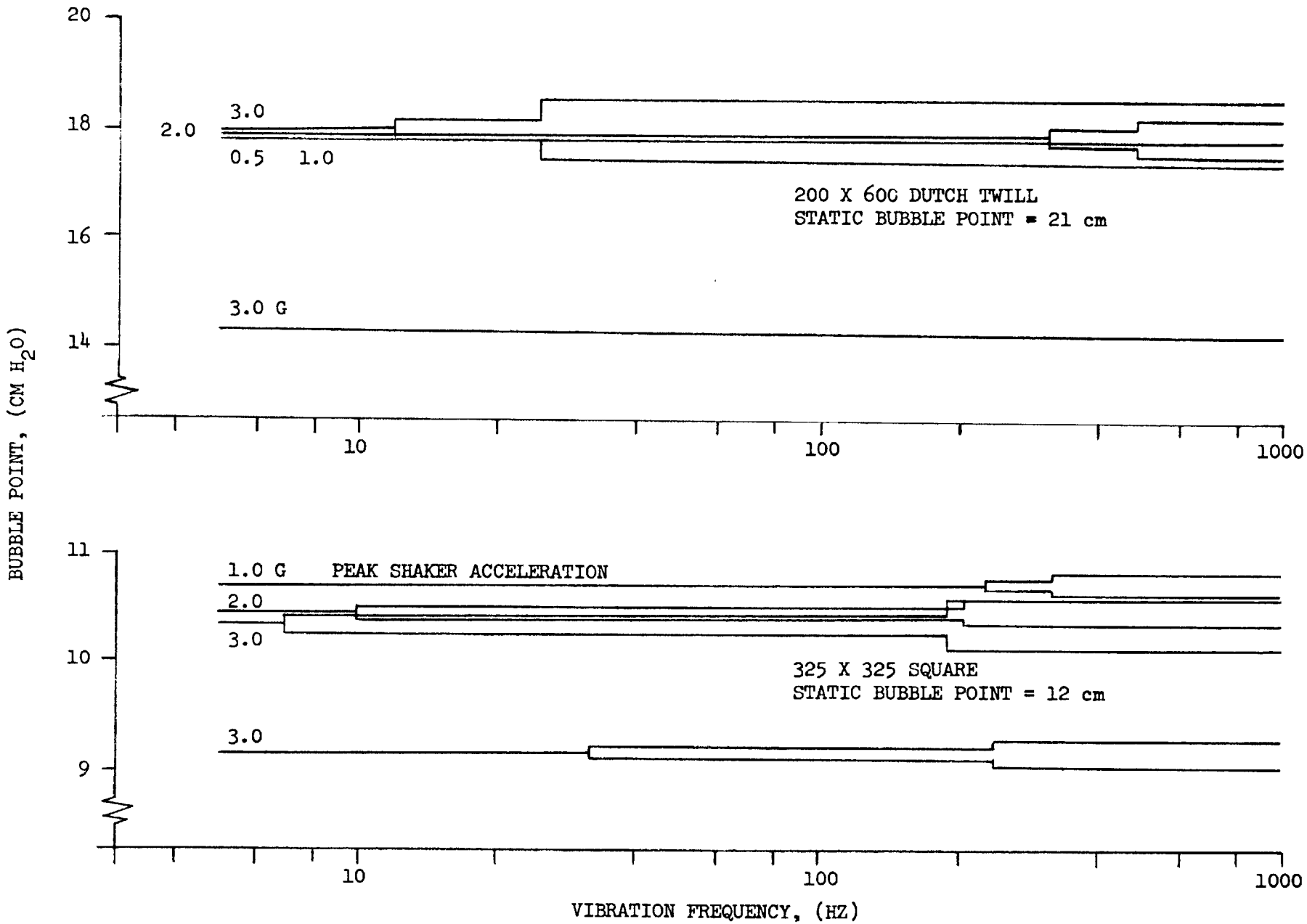

Figure 45. Vertical Sinusoidal Vibration – Shallow

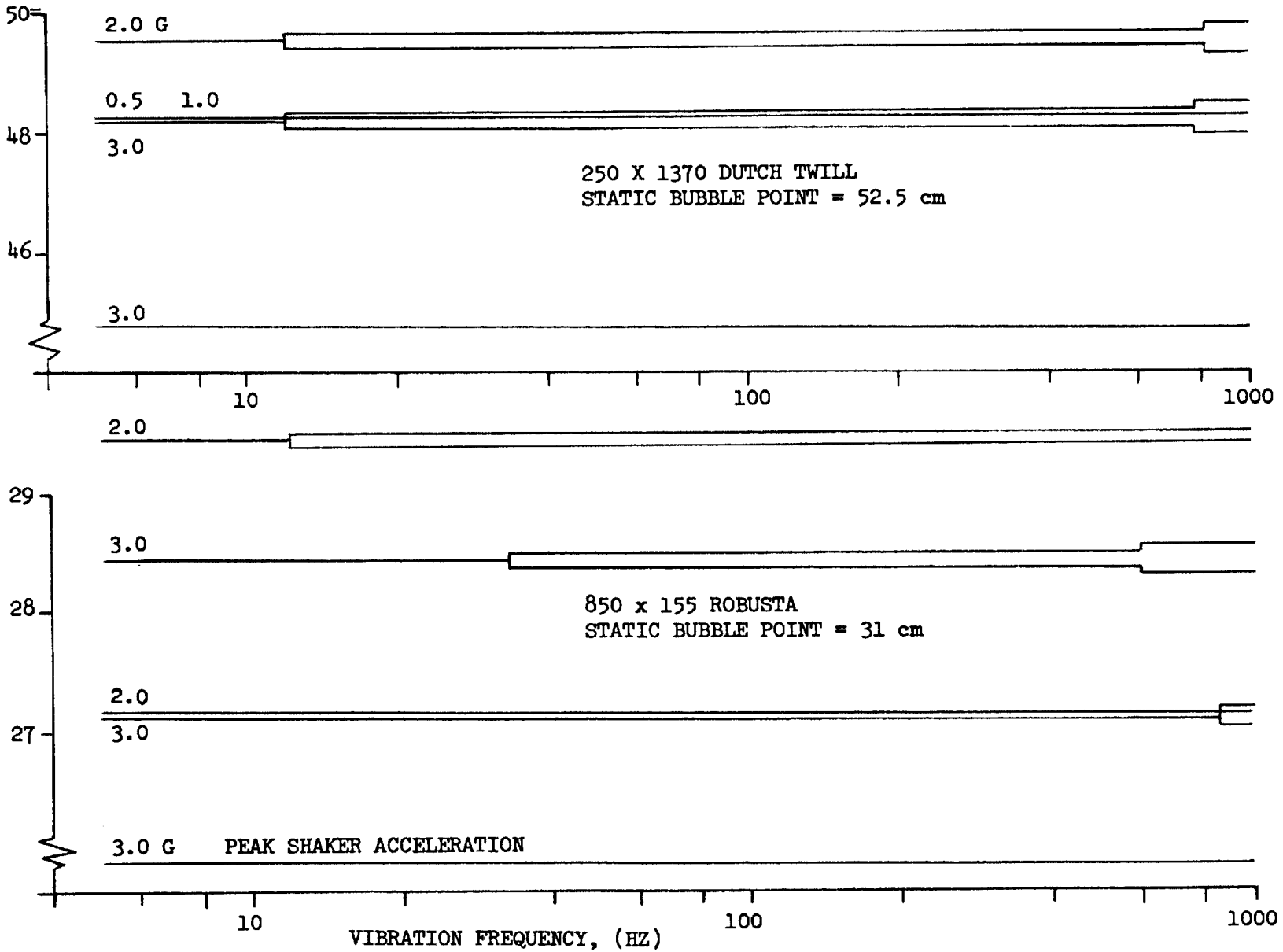

Figure 46. Vertical Sinusoidal Vibration -- Shallow

of the two lines associated with any particular g-level is a qualitative measure of the amount of gas breakthrough; a single line denotes no failure.

The data indicate that vibration results in premature gas breakthrough in all four specimens. Also, increasing g-level results in increased bubble point reduction. The extent of the bubble point reduction will be discussed more thoroughly in combination with the large liquid depth tests.

The second test sequence was conducted with sinusoidal vibration acting parallel to the screen surface with a small liquid depth (<2 cm). The procedure was changed such that the ΔP across the screen was slowly increased to failure at fixed values of frequency and g-level. The test data is shown in Figures 47 and 48. Vibration in this axis has a very slight effect on the bubble point pressure. This indicates that the vibration does not alter the nature of the numerous interfaces within the pores of the screen. It is proposed then that the primary effect of the oscillations is to alter the pressure field within the liquid. The evidence supporting this hypothesis will become more apparent in the last test series when a large liquid depth was combined with vertical excitation.

In the first test series, the combination of experimental technique and shallow liquid depth failed to emphasize the importance of the reduction in liquid pressure above the screen. When this occurs the head acting in opposition to the gas pressure below the screen is reduced allowing more ready passage of the gas.

The third and last test sequence was conducted with a large (23 to 39 cm) liquid column above three screens with the axis of vibration perpendicular to the screen. Again the procedure consisted of slowly increasing the gas pressure breakdown at fixed values of g level and frequency. The test data are shown in Figures 49 through 51. The data are shown as an effective g-level (g_{eff}) which is defined as:

$$\Delta P_{BP} = P - \frac{\rho_{ALCOHOL}}{\rho_{H_2O}} H (1 - g_{eff})$$

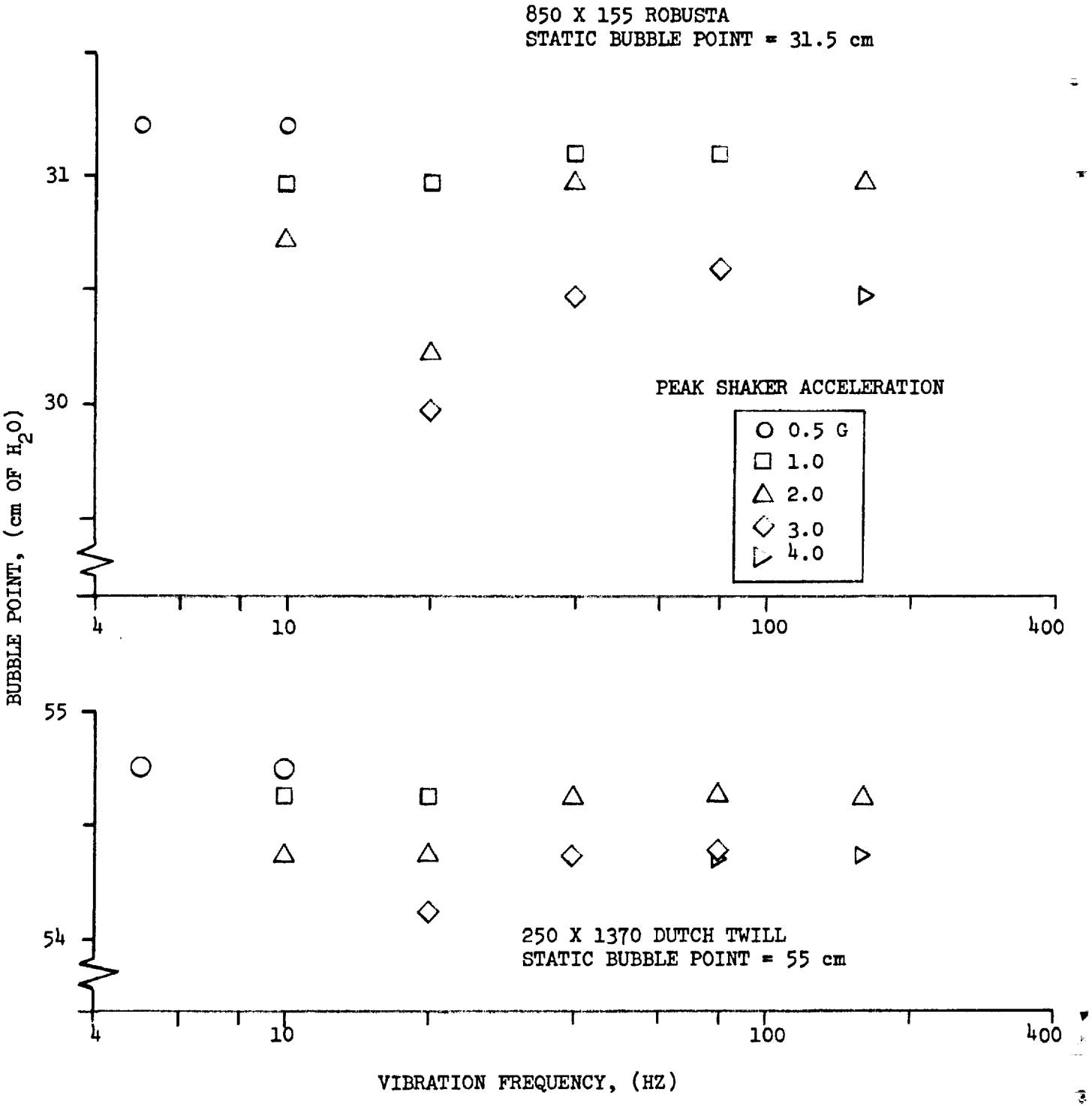

Figure 47. Horizontal Sinusoidal Vibration

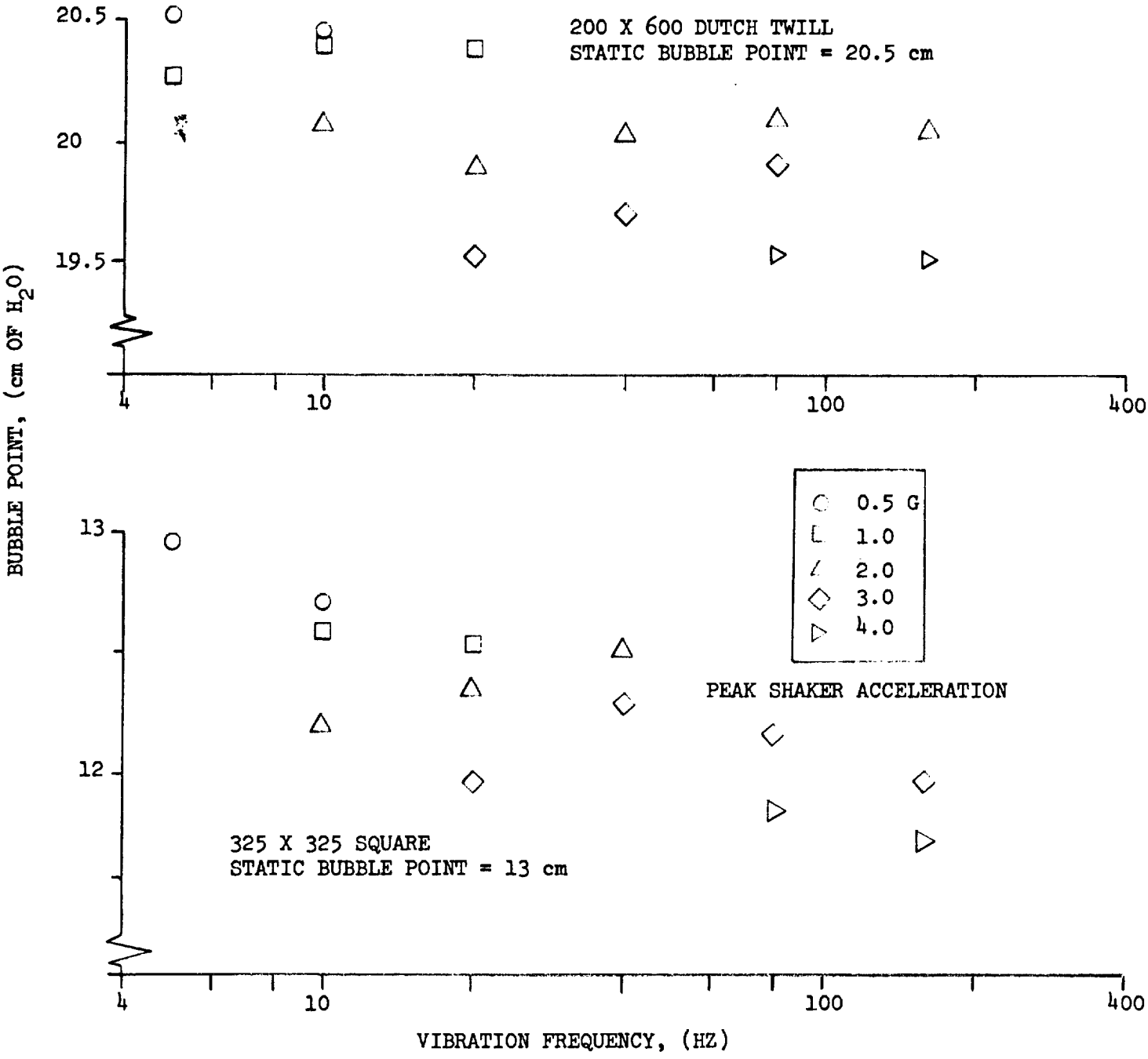

Figure 48. Horizontal Sinusoidal Vibration

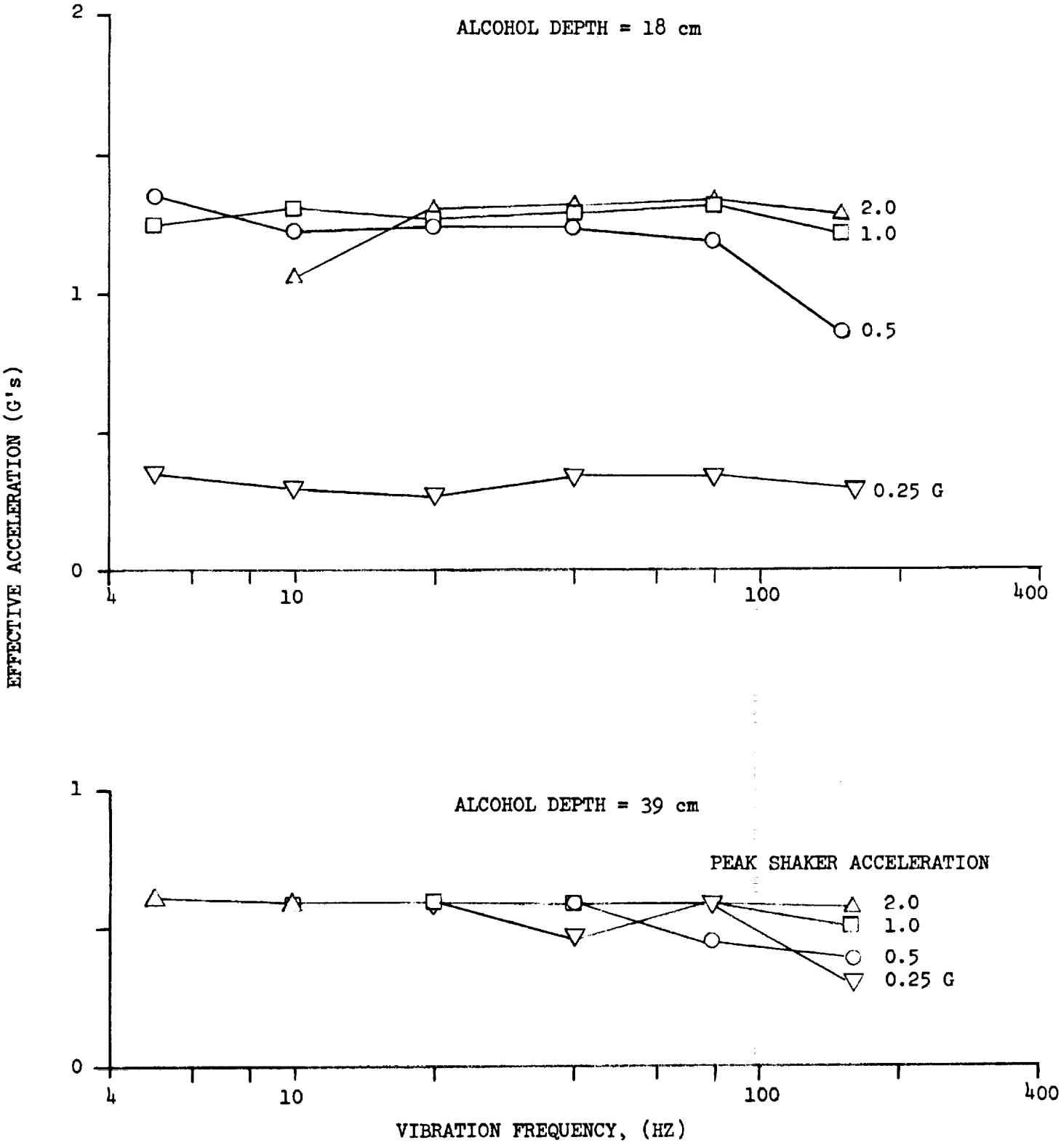

Figure 49. Vertical Sinusoidal Vibration -- 200 X 600 Dutch Twill

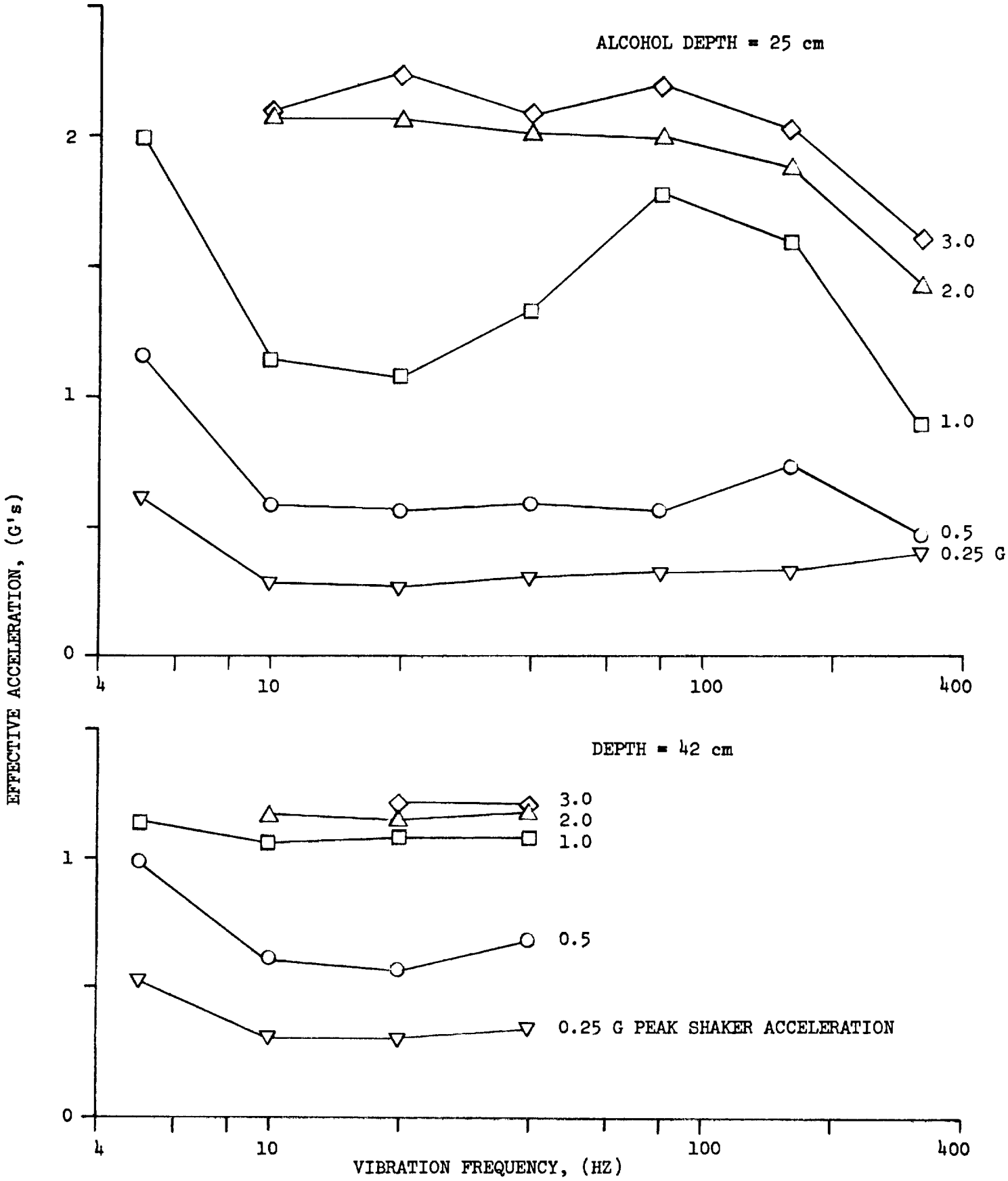

Figure 50. Vertical Sinusoidal Acceleration -- 200 X 1400 Dutch Twill

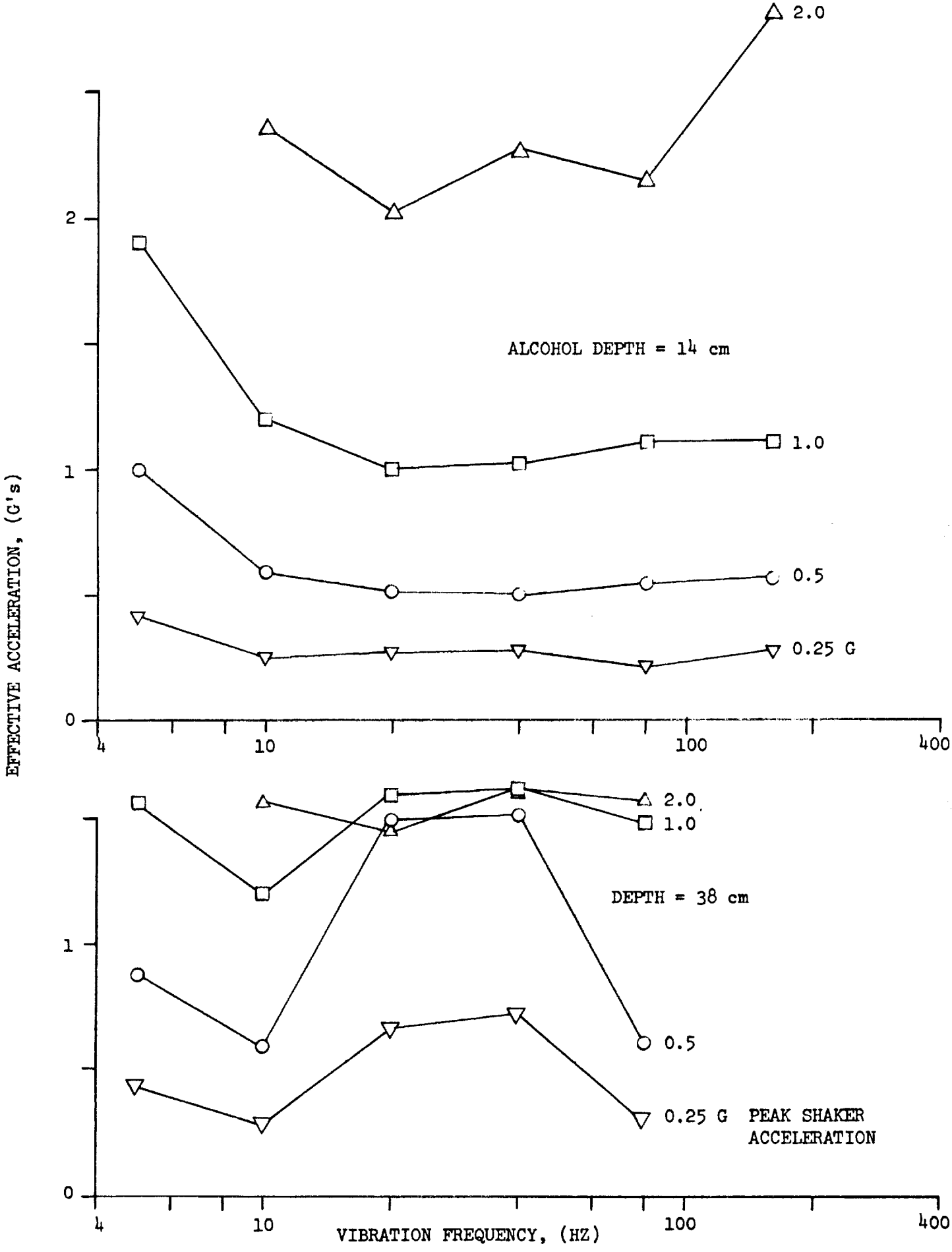

Figure 51. Vertical Sinusoidal Vibration -- 250 X 1370 Dutch Twill

where:

ΔP_{BP} = Static bubble point (cm W. C.)

H = Alcohol depth (cm)

P = Manometer pressure at breakthrough (cm W. C.)

ρ = Liquid density

This mathematical model assumes that the vibration reduces the head above the screen. The quantity g_{eff} can be thought of as a gravitational level (in g's) acting in opposition to normal gravity. When g_{eff} equals 1.0, the vibration induced and gravitational forces cancel and the bubble point corresponds to that set by surface tension forces alone. For g_{eff} larger than 1.0, a negative pressure situation appears with the effective hydrostatic pressure above the screen less than atmospheric. The pressure field is similar to that responsible for the phenomenon of sinking bubbles. In this latter case, the treatment of the pressure oscillations as a one-dimensional acoustic wave has yielded satisfactory results.

Figures 49 through 51 indicate that the vibration environment can have a dramatic effect on the bubble point pressure at all of the frequencies tested. Values for the effective acceleration greater than 1.0 indicate that the sinusoidal vibration reduces the pressure above the screen to less than atmospheric pressure. The data also shows that g_{eff} can be considerably larger or smaller than the peak vibration on the shaker platform. It is anticipated that the nature of the pressure waves within the liquid will be dependent upon the shape of the supported liquid column. The experimental apparatus was designed to minimize this effect by using straight, vertical liquid columns.

The vehicle vibration environment needs to be specified so that the retention capability of the screen device can be ascertained. It may then be necessary to conduct full-scale vibration tests with flight type devices so that the influence of geometry on the bubble point can be fully investigated. This bench test has indicated an important parameter that has not received adequate treatment in the design of surface tension acquisition device. Mathematical techniques may be useful in analyzing the pressure field within the liquid column which seems most important in setting the bubble point.

3.2.6 Test VI - Screen Deflection Tests

The 12.7 cm square screen elements samples fabricated for the element fabrication tests (Test II) were used in controlled deflection tests with the apparatus shown in Figure 38 of Reference 1. Samples were tested over a wide range of conditions with amplitudes ranging from 0.11 to 0.51 cm and cycles up to 13,800, with no significant degradation in bubble point. One of the fusion welded samples failed at the forcing arm attachment point at 2,550 cycles, but none of the other samples was damaged. Although quantitative data were not intended to be generated by these tests, qualitative demonstration of the toughness of the candidate screens was obtained.

3.2.7 Test VII - Bubble Point Degradation

Pleated screen samples had been fabricated as shown in Figure 39 of Reference 1. Tests to assess the bubble point degradation caused by conventional screen pleating were completed during the quarter. The results are shown in Figure 52. Note that the actual degradation is surprisingly small, less than 20 percent in all cases. From these results, it would appear that the use of pleating could result in increased design retention safety factor.

Another effect on screen performance is the change in pressure drop that might result from pleating. Therefore, the flow loss characteristics of several pleated screen samples were measured using the test setup shown in Figure 29 of Reference 1.

Four pleated screen units were made up from 250 x 1370 dutch twill mesh. The flat screen size was 5.1 x 15.3 cm. The pleating pattern had a pleat height of 0.48 cm and a bend radius of 0.038 cm. Two specimens were cut with the long dimension parallel to the warp wires and two parallel to the chute. Pleating took place across the shorter dimension of each piece. The two units with pleats parallel to the warp direction were markedly more rigid than the other two units. Two of the units (one of each type) were adhesively bonded into plexiglass frames for flow testing (see Figure 53). When complete, the two units had increased the effective flow area by factors of 3.6 and 3.8 with a pitch of approximately 10 pleats/cm.

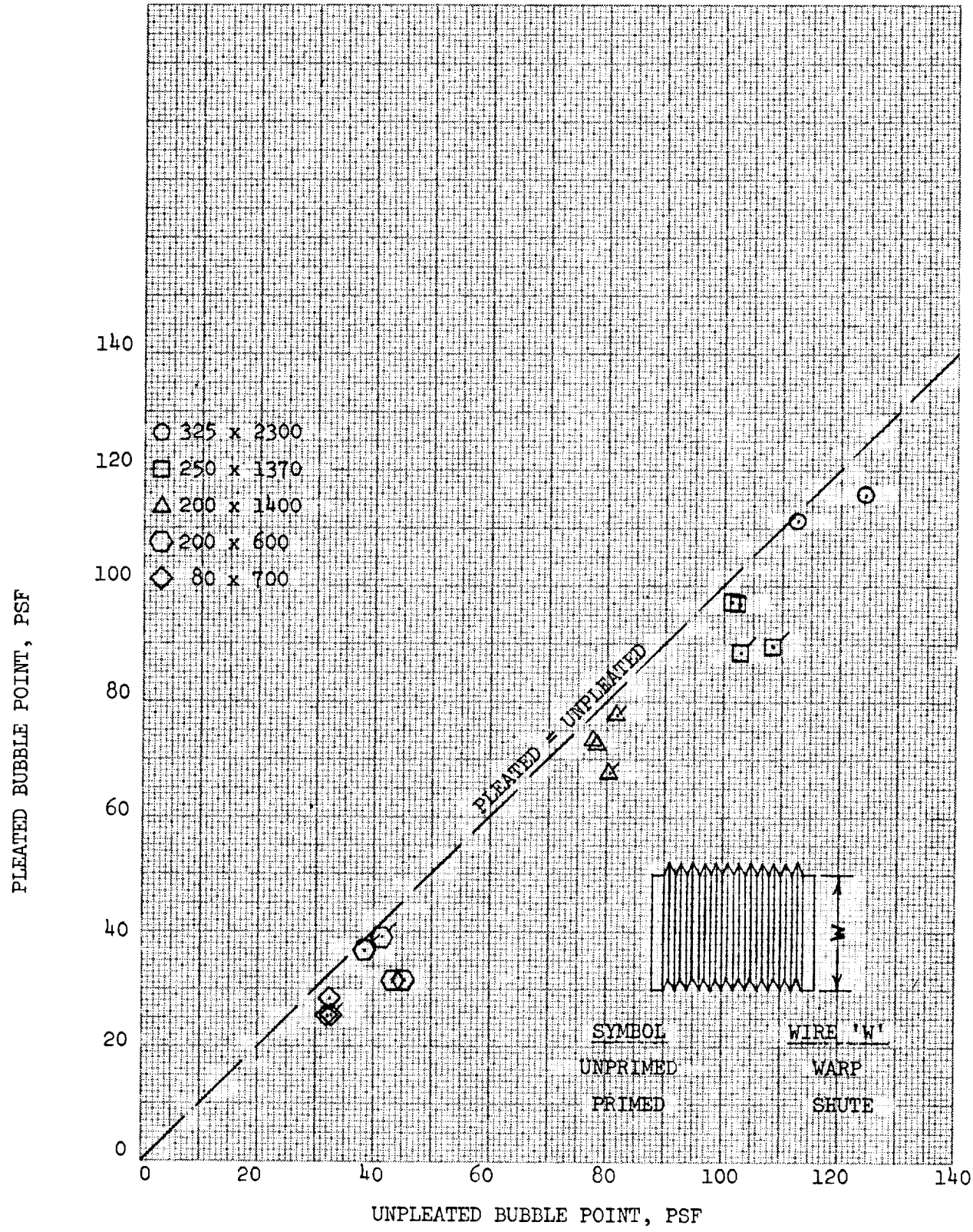

Figure 52. Bubble Point Performance of Pleated Screens

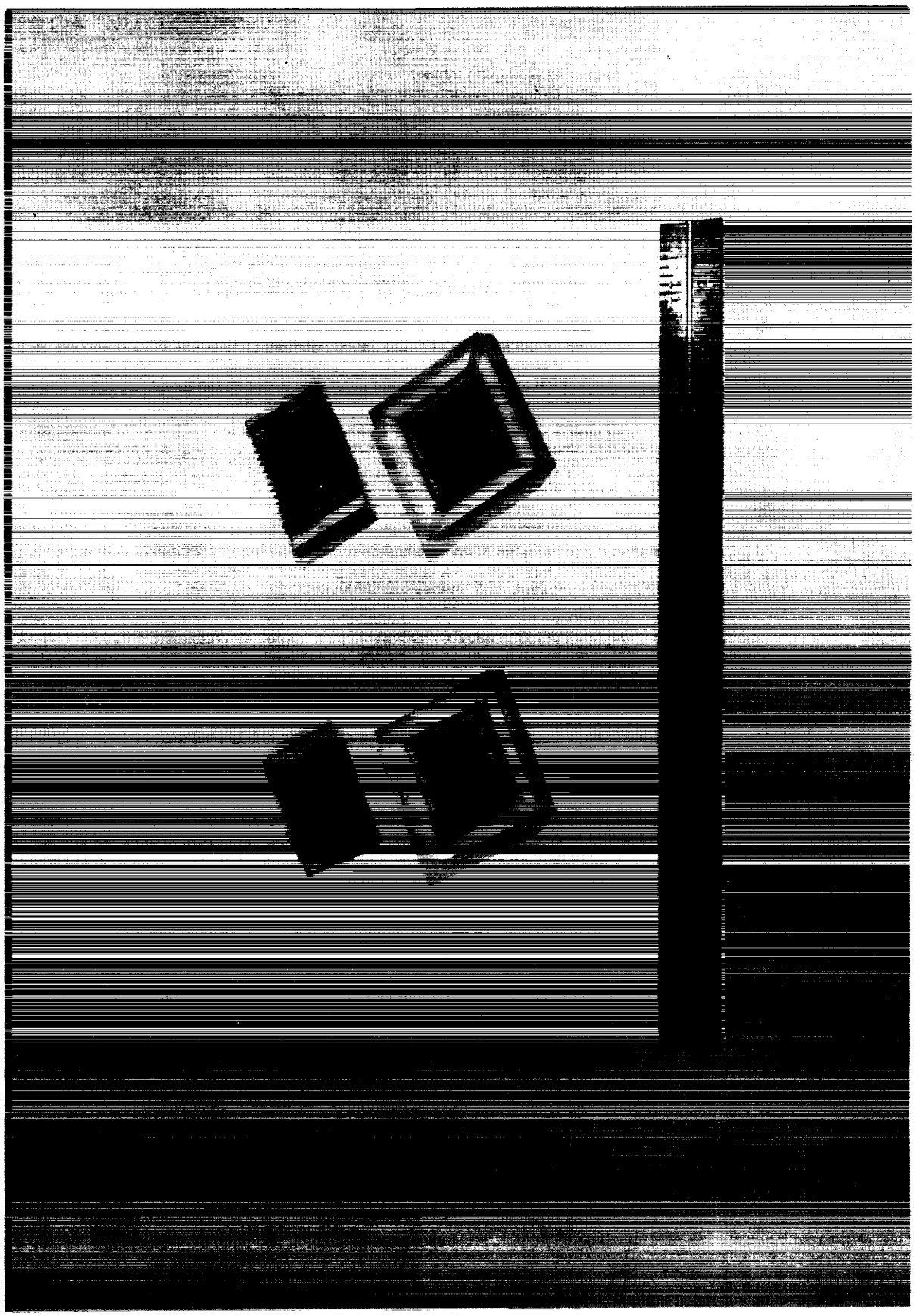

Figure 53. Pleated Screen Sample

The pleated flow test units were tested in the large pressure drop test apparatus with GHe and GN_2. All of the test data fell in the laminar flow regime. The data is plotted in Figure 54 using the Armour and Cannon correlation parameters. The flow area was taken as the total screen area. The test data for both units fall in line with that for unpleated screen of the same type. This indicates that the pleating did not result in a significant flow blockage or interference.

Based on the bubble point and flow loss tests, it is concluded that pleating can be effectively used to increase retention performance. Table 29 shows the typical potential retention safety factor improvement possible with pleating as related to the pleated to unpleated area ratio.

3.2.8 Test VIII - Duct Fabrication/Joining Tests

3.2.8.1 Duct Section Joining

To evaluate duct section joining techniques and to gain an insight into overall acquisition duct fabrication problems, a near full cross-section duct about 1.1 meter long was fabricated from 0.051 cm (0.02 inch) sheet 6061-T4 aluminum. (A solid aluminum blank was used in place of a screen in this assembly.) A prime candidate fabrication technique for building up the channels within the tank was to use conventional riveting; therefore, this was used in fabricating the duct section.

In cross-section, the assembly unit was of the following dimensions:

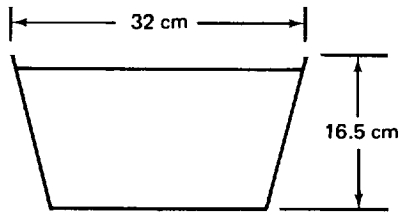

The top of the channel was left solid in the region where customarily it would be cut out beneath the screen. Both ends of the segment were capped so that leak tests could be conducted. No. 40 soft aluminum (Type A) rivets were used throughout the unit. These rivets could be set with a hand squeezer where the location permitted; otherwise, a small hammer and backup block were used.

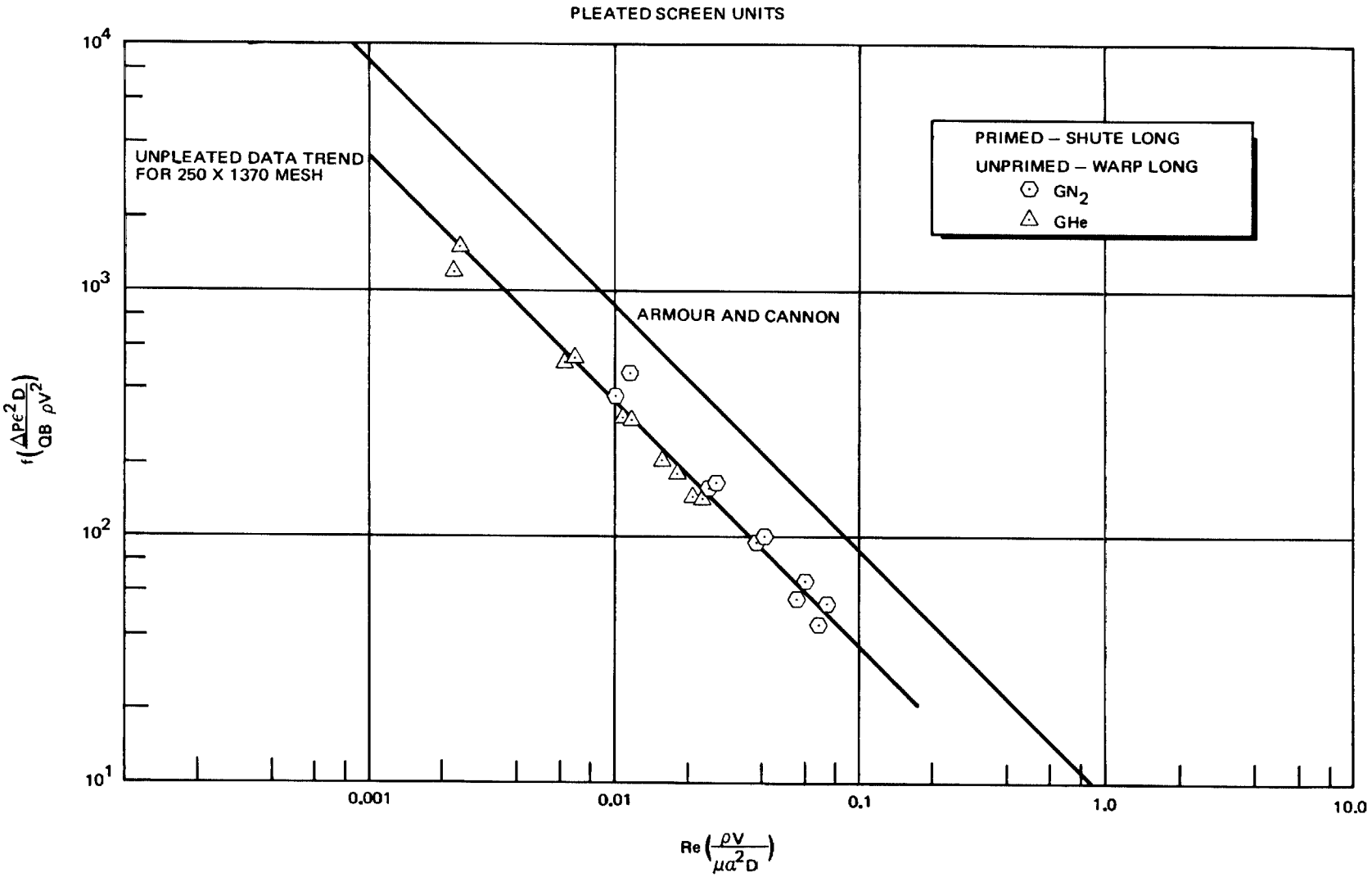

Figure 54. Pleated Screen Flow Loss Measurements

Table 29

INFLUENCE OF PLEATING ON RETENTION CAPABILITY

Channel Flow Retention Safety Factors*			
	Pleated Area/Unpleated Area		
Screen Mesh	1	2	4
200 x 1400	0.697	0.959	1.165
250 x 1370	0.705	1.114	1.504
325 x 2300	0.883	1.307	1.703

LO_2 Tank - Bottom channel

Screen 1/4 covered

1.5 ft/sec^2 positive acceleration

*Channel not optimized for a specific minimum acceptable safety factor.

The segment consisted of three subsegments joined at two nested joints. Both joints (2.5 cm overlap) utilized a rivet pattern of two rows with 1.27 cm spacing, each row having a rivet spacing of 1 cm. The rivets were staggered in the two rows. In one joint a 1/16 inch diameter indium-tin wire was routed between the two rows of rivets as a gasket. The top cover of the channel was riveted to the sides with a single row of rivets having 1.27 cm spacing; no sealing material was used. The completed duct is shown in Figure 55.

Prior to attaching the end caps on the segment as the final phase of assembly, a visual check was made of the two channel joints. Light leaks could be seen at both joints in four locations.

Following the completion of assembly, the joints between the top and sides of the channel were leak checked by pressurizing while submerged in isopropyl alcohol. Leak tightness to a ΔP of 51 cm W.C. is required to match the retention property of 250 x 1370 mesh on the channel. Leaks at several locations were evident at 10 cm W.C. Although sealants could have been used in the joint, this would raise compatibility problems, particularly with the LO_2.

In conclusion, it is apparent that the riveted, trapezoidal channel segment has inherent weaknesses that cannot be simply corrected. The corners in the bottom of the channel could be more gently rounded to eliminate leakage there, but on top this is not possible. A greater bend radius there would preclude access required for close rivet spacing. Thus, riveting to achieve a leak-tight joint against bubble point pressures does not appear feasible. The unit does exhibit a surprising degree of overall rigidity even though assembled from light gage material, and the use of 0.051 cm (0.020 in.) sheet material seems justified.

3.2.8.2 Screen Element Mechanical Attachment

The combination of screws and nutplates has been proposed for mechanically attaching the screen elements (screen/backup plate combination) to the aluminum frame that constitutes the top of the acquisition channel. A bench test was conducted to determine the effectiveness of this type of attachment.

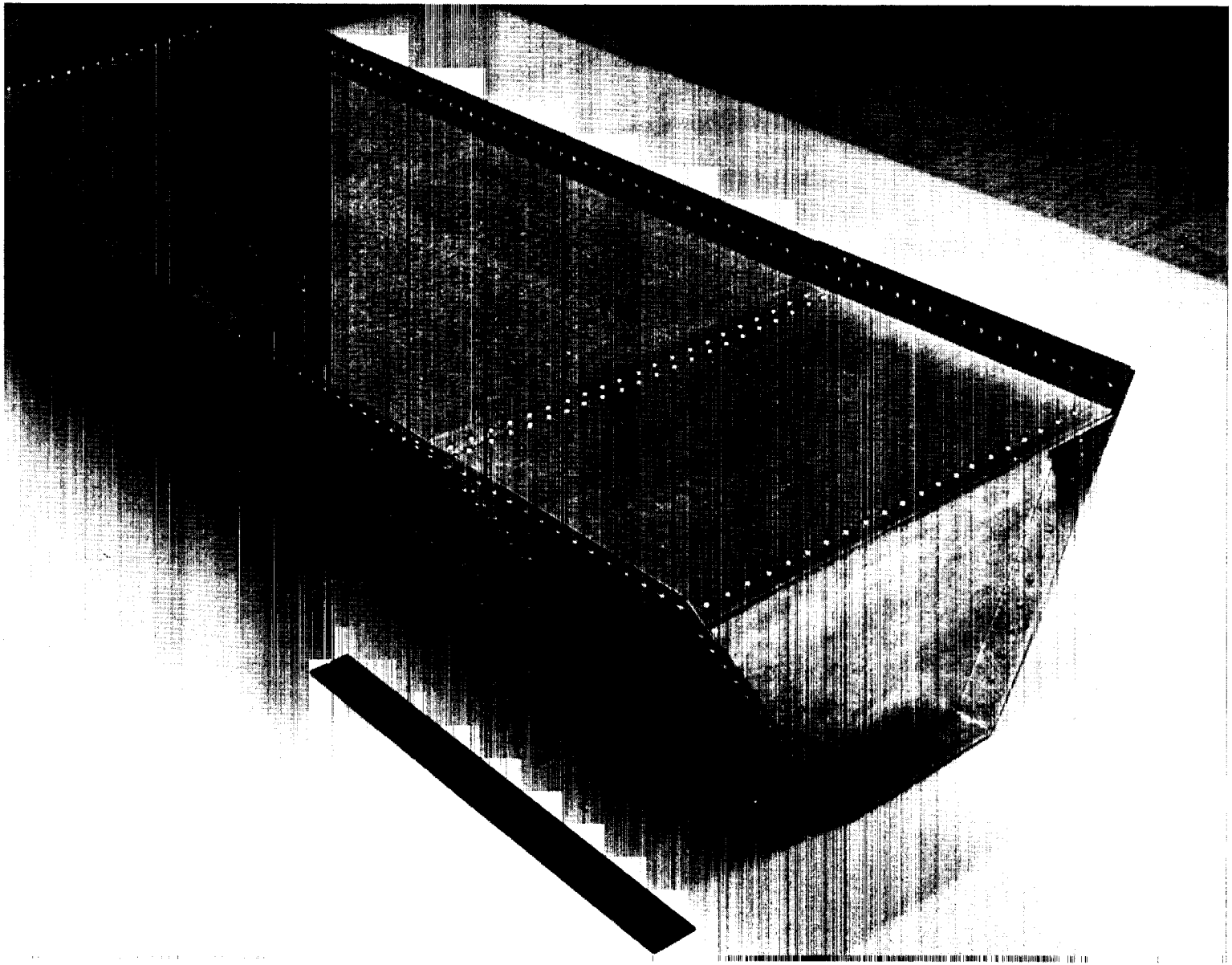

Figure 55. Fabricated Solid Duct

The objectives were to determine the necessary screw spacing and to determine if a gasket material was necessary to effect a leak-tight joint. The joint must be leak tight when submerged in isopropyl alcohol and subjected to a ΔP of 51 cm W. C. This ΔP corresponds to the bubble point of a 250 x 1370 dutch twill screen mesh in isopropyl alcohol.

The two screen elements used were the 0.051 cm stainless steel specimens fabricated as part of the welding bench test (see Figure 38). One specimen had seven holes with a spacing of 2.65 cm along each of the four edges. The second specimen had this same pattern on two adjacent edges and 13 holes with 1.32 cm spacing along the remaining two edges. The acquisition channel frame/nutplate combination was simulated by an aluminum baseplate with a sufficient number of tapped holes to match those in the screen/backup specimens. The various test components are illustrated in Figure 56.

Neither specimen when attached directly to the baseplate proved to be leak tight. Both 10-32 and 6-32 screws were used. When leak tested, there were numerous small leaks. This occurred between screws on all four edges of both specimens.

Next, a 1.6 mm diameter indium-tin wire (Cerroseal 35) was used as a gasket with both specimens. The ends of the wire were overlapped as near as possible to one of the screws. The first specimen was leak tight at the required ΔP of 51 cm W. C. The second specimen had a single leak at the point of overlap on the indium-tin wire.

The indium-tin wire thus appears to be a viable solution to sealing the screen to the channel in a nonpermanent fashion. This material would have to be closely controlled to assure compatibility with liquid oxygen. Also, the frame on the acquisition channel must be sufficiently rigid to prevent deflection between screws, as was the case with the baseplate used in the bench test. If the channel frame distorts significantly under the loading caused by the attachment screws, then the positive results of the bench test would be invalidated.

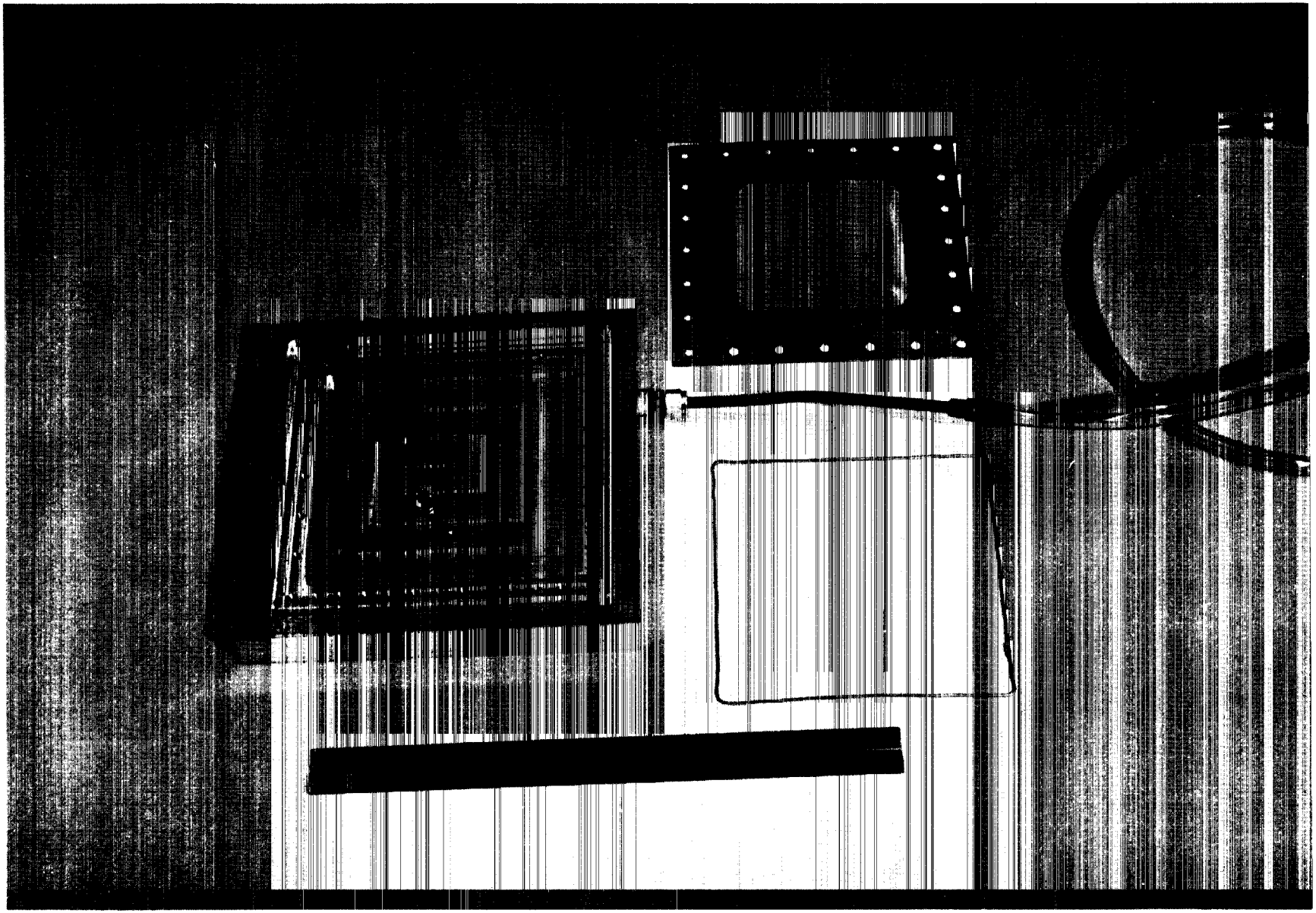

Figure 56. Attachment Evaluation Test Apparatus

3.2.9 Test IX - Film Bubble Point Feasibility Test

Bubble point testing is usually accomplished by submerging the screen in fluid and then pressurizing one side of the screen. The early channel preliminary designs were evolved to permit this type of checkout test on the channel as installed in the completed cryogen tank with no tank access requirement. This led to the solid channel design with screen on only one face which would facilitate immersion bubble point testing. However, current studies have shown that a significant design improvement can be achieved with all-screen channels. This will require a new method of bubble point testing which does not require access to or removal of the acquisition system and can be performed during the normal refurbishment of the vehicle. It was found during the bubble point testing of the interface demonstration unit (IDU) being fabricated under NAS 8-27571, that the screen could be kept completely wet with alcohol simply by pouring alcohol over the screen. The thin film of liquid formed an individual meniscus at each pore of the screen and excess liquid flowed off the screen. Since each pore was closed with its individual meniscus, there was no hydrostatic head exerted along the full height of screen and the total wetted screen height exceeded the height which could be supported if the screen devices were full of liquid. Therefore, it was practical to determine the bubble point pressure of the screen without completely submerging the device in liquid.

The problem with the procedure, when applied to large-scale vehicles without direct access to the screen, is that the entire screen surface must be wetted and evaporation controlled. One solution, which has been successfully demonstrated in a recent bench test, involves flowing saturated vapor of an appropriate bubble point test fluid (methanol, Freon 114, isopropyl alcohol, etc.) into the screen device and tank which are maintained at a temperature below that required for condensation.

Vacuum pumping the extraneous gases from the tank and/or purging the tank with the test vapor assures a one-component system; therefore, evaporation from the screen due to diffusion is alleviated. Maintaining the tank at a constant temperature assures that an equilibrium, steady-state condition is obtained in which the condensed film on the screen pores remains indefinitely. Bubble point measurements can then be taken.

The apparatus shown in Figure 57 was used to demonstrate that condensation would seal all of the pores of a screen. A cylindrical screen, 200 x 600 mesh, 3.2 cm diameter and 24 cm length was supported in the center of a 2,000 ml vacuum test flask. Isopropyl alcohol was heated to the boiling point (82°C) in a separate vapor supply flask. A vacuum pump was used to remove the air in the test flask. The vacuum pump was disconnected after closing the valve between the vacuum pump and test flask. The valve between the vapor supply flask and test flask was then opened and vapor flowed into the cooler test flask, condensing on the screen and walls. A bubble point test was then made using nitrogen gas at room temperature which demonstrated that approximately 15 cm of water column pressure was obtained, as had been observed in an earlier submerged bubble point test. Since the height of the screen device is 24 cm, whereas a column of alcohol only 15-18 cm high could be supported, this test further confirmed that a film of liquid blocking each pore in the screen could be used to test the bubble point of screens in 1-G with heights exceeding those obtainable with columns of liquid.

However, since the test flask was not insulated and was much warmer than room temperature (20°C), a steady-state condition was not reached. As the flask cooled, the alcohol on the warmer screen began to evaporate, with condensation occurring on the walls of the flasks. The test flask pressure dropped, and the resulting pressure difference between the inner region of the screen and the flask, coupled with the evaporation of the liquid sealing the screen pores, led to breakdown within 10 to 15 seconds. The test was then repeated with the flask at room temperature, and it was found that by wetting the screen by shaking the flask, the film of liquid sealed the pores indefinitely; again, a bubble point of 15 cm of water column was achieved. This second test demonstrated that a steady-state condition could be achieved with the screen pores sealed, if the flask equaled the ambient temperature, or, in general, if the test flask were approximately adiabatic.

To assure that no pores were unsealed, leading to a low leakage rate and false bubble point reading, two procedures were used. First, the absolute pressure of the test flask was monitored during the adiabatic test and was found to be constant. A more precise proof that no pores leaked was achieved

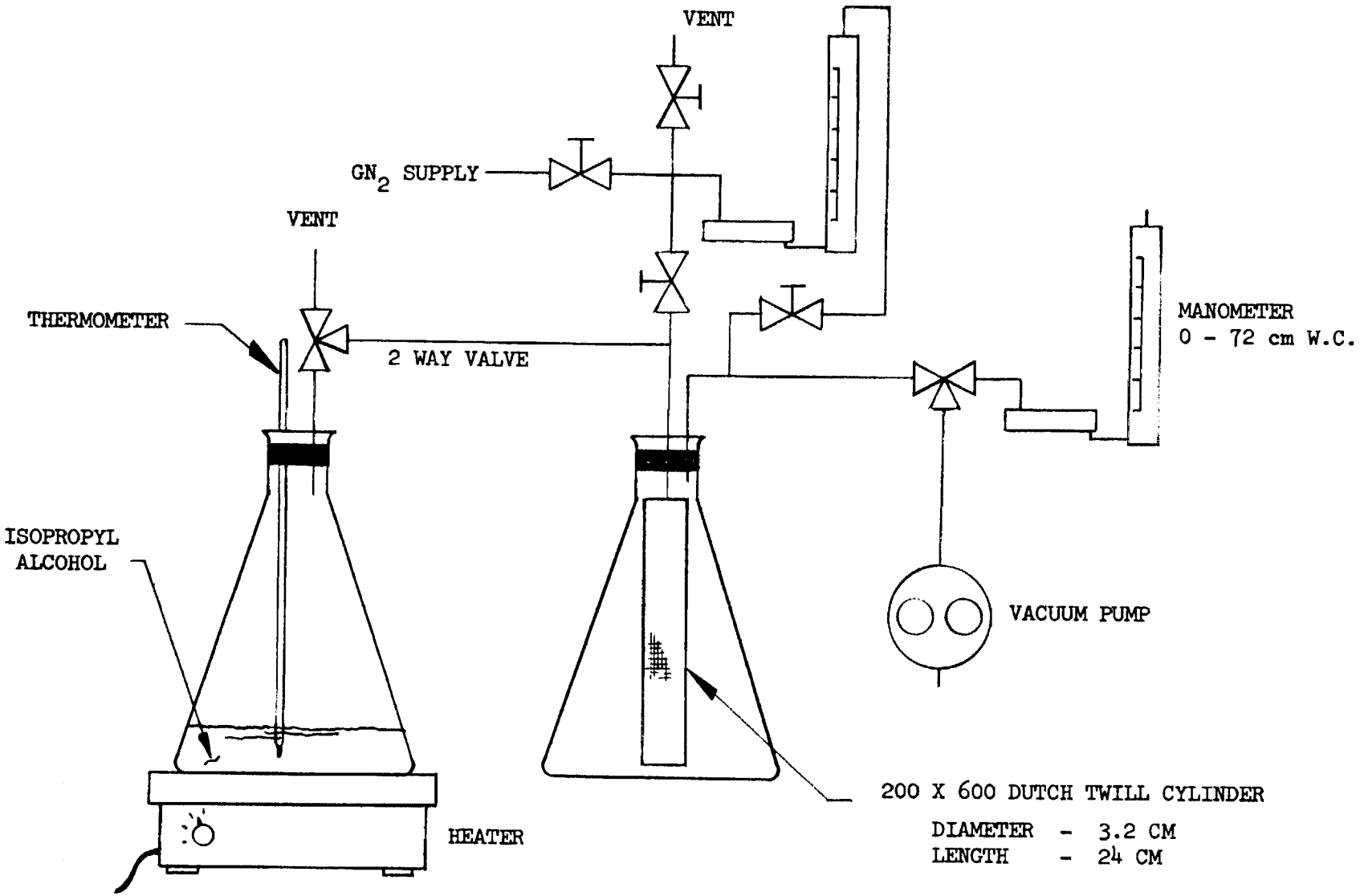

Figure 57. Film Bubble Point Evaluation Test Apparatus

inadvertently, however. Some alcohol had drained into the transparent tube leading from the needle valve (used to control the nitrogen gas flow) into the cylindrical screen. Thus, any nitrogen gas flowing into the screen device first had to bubble through the alcohol. These bubbles were more easily observed than the escaping bubbles from the standard bubble point test technique with the screen submerged in the test liquid. For the adiabatic test, it was found that a bubble point of 15 cm of water column was maintained for more than five minutes with no movement of any nitrogen bubbles through the alcohol.

The above bubble point test was a rather simple demonstration of the principle of condensation sealing of a screen, and it is felt that more extensive tests are desirable. However, the implication for screen devices is clear: All screen channels or other such localized or distributed screen devices can be tested in one-g without disassembly and removal from the propellant tanks. For localized devices, such as the start tank, it is probably more practical to forego condensing of the bubble point test vapor, and simply fill the tank with liquid, allow the liquid to drain off while replacing the liquid volume with saturated alcohol vapor, and then proceed with the bubble point test. With large tanks, the weight of the test fluid would be prohibitive and therefore the condensation technique would be used.

Based on the test results described above, as well as the bubble point test procedure used with the IDU under Contract NAS 8-27571, all screen channels can now be considered viable candidates for large, reusable vehicles without the additional costs and operational complexities of screen removal and testing prior to each flight. Only if the screens fail to meet the bubble point specification would removal and inspection be required.

3.2.10 Autogenous Pressurization Induced Screen Breakdown Experiment

It appears, on the basis of the problems discussed in the Appendix, that autogenous pressurization of exposed screen acquisition devices involves complicated low-g heat and mass transfer phenomena and unproven pressurization control techniques. In view of this need for a better understanding

of screen condensation and pressure decay induced boiling within the screen, a test with a screen device in liquid hydrogen, pressurized by hydrogen vapor, has been planned and will be performed as part of the Task B, Bench Tests.

The all-screen device will be a small and simple unit that can be directly observed. Bubble or vapor formation within the screen will be observed during controlled dewar pressure decay rates. Test apparatus and procedure details are now being finalized.

REFERENCES

1. G. W. Burge, Study and Design of a Cryogenic Propellant Acquisition System 3rd Quarterly Progress Report, McDonnell Douglas Report MDC G2940, April 15, 1972.

2. G. W. Burge, Study and Design of a Cryogenic Propellant Acquisition System 2nd Quarterly Progress Report, McDonnell Douglas Report MDC G2743, January 15, 1972.

3. D. R. Krause, Development of Lightweight Material Composites to Cryogenic Tanks for 30 Day Storage of Outer Space Final Report, McDonnell Douglas Report MDC G2742, June 1972.

4. J. N. Castle, Preliminary Evaluation in LH_2 of a Screen Surface Tension Acquisition Device, MDC G2452, August 1971.

5. J. N. Castle, Performance Testing of an Integrated Liquid Hydrogen Storage, Acquisition, and Vent System, MDC G3092, June 1972.

6. Space Shuttle Isogrid Tank Buckling Test Volume 1, Design and Analysis, NAS8-26016, February 1972 McDonnell Douglas Report MDC

7. A. L. Sherman, R. Gershman, and J. F. Osugi, Fluid Properties Handbook, McDonnell Douglas Report MDC G0814, October 1970.

8. R. F. Parmley, Handbook of Thermal Design Data for Multilayer Insulation Systems, Vol VI, Report No. LMSC A742593-VI, Lockheed Missiles and Space Co., Sunnyvale, California 11 August 1965.

9. 1972 Materials Selector, Materials Engineering, Vol 74, No. 4, September 1971.

10. D. R. Krause, Development of Lightweight Material Composites to Insulate Cryogenic Tanks for 30-Day Storage in Outer Space, Second Quarterly Report, Contract NAS8-26006, McDonnell Douglas Astronautics Report No. MDC G0775, December 1970.

11. J. N. Castle, Cryogenic Bubble Point Testing of Selected Screens. MDC G2389, August 1971.

Appendix

POTENTIAL SCREEN RETENTION BREAKDOWN PROBLEMS INDUCED BY INTERACTION BETWEEN SCREEN DEVICE AND AUTOGENOUS PRESSURIZATION GAS

As discussed in Section 3.1.1.3, autogenous pressurization, even with very low inlet temperatures, may be desirable from a weight standpoint. Interaction between autogenous pressurant gas and screen devices causes vapor condensation and ingestion into the screen device which can result in retention breakdown. The ingested liquid is warmer than that retained in the device, and pressure decay induced vaporization within the screen device can result in subsequent screen retention breakdown.

The screen device failure mode envisioned for cryogens results from the vapor pressure in the tank dropping below the saturation vapor pressure of liquid within the screen device, leading to a "boiling" (or, more precisely, vaporization) phenomenon. The rate of vaporization would be expected to increase rapidly as the tank vapor pressure drops further below the saturation vapor pressure of the liquid, because more superheat becomes available.

The existence of a stratified region of liquid would occur readily in a low-gravity environment with autogenous pressurization of propellant to a level necessary to meet practical NPSH requirements of the order of 13.8×10^3 to 69×10^3 N/m^2 (2 to 10 psi). For example, consider the autogenous pressurization of liquid hydrogen, initially at 36.5°R, to a tank pressure (i.e., hydrogen vapor pressure) of 2.07×10^5 N/m^2 (30 psia). The hydrogen vapor temperature in the ullage could vary from 41.5°R upward. Any free surface of liquid exposed to this vapor would essentially instantaneously reach a surface temperature of 41.5°R, corresponding to the vapor pressure of 2.07×10^5 N/m^2 (30 psia). Whether or not evaporation or condensation occurred at the interface would depend on the relative rates of heat transfer in the liquid and vapor regions, as

shown by the following equation for the mass flux of condensed or evaporated liquid, $\rho_L v_L(t)$:

$$\rho_L v_L(t): = \frac{q_L}{L} - \frac{q_v}{L}$$

For $\rho_L v_L(t)$ positive, condensation occurs, whereas evaporation occurs for $\rho_L v_L(t)$ negative. Figures A-1 and A-2 illustrate a qualitative comparison of the temperature profiles with condensation and evaporation. For high heat fluxes in the vapor region relative to the liquid region, as a result of high vapor temperature, convection of the vapor, or radiation, evaporation would occur. For cases of high heat fluxes in the liquid region, relative to the vapor region, condensation would occur. This case corresponds to a dual screen, or channel, with liquid flow and/or natural convection. The vapor region could be almost motionless, if confined between the screen and a cold tank wall a few inches away. It should be noted that with acceleration loads on the system, the condensed film formed at the interface will be continuously drawn into the screen so as to maintain the capillary interface within the screen mesh.

The rate of evaporation or condensation for a one component system, initially at a uniform temperature, subjected to a sudden change in pressure has been determined analytically by Knuth (References A-1 and A-2); a specific case from this analysis for liquid hydrogen with autogenous pressurization is shown in Figure A-3. The results of References A-1 and A-2 apply only to a liquid and vapor which undergo no convective motion other than the one dimensional growth or receding of the interface. Figure A-3 shows typical results from the linearized analysis, which is valid if, for each phase, the difference in specific enthalpy of the initial state and saturated state for the system pressure is small compared to the latent heat. The volume condensed (or evaporated), per square foot, or the thickness of the condensed (or evaporated) region as a function of time is obtained in the linearized case; as

$$\delta(t) = \theta_{\ell,\,i}\,(4\,\alpha_\ell\,t/\pi)^{1/2}$$

where

$$\theta_{\ell,\,i} = C_{P\ell}\,\frac{(T_\ell - T_{o\ell})}{h_{v\ell}},$$

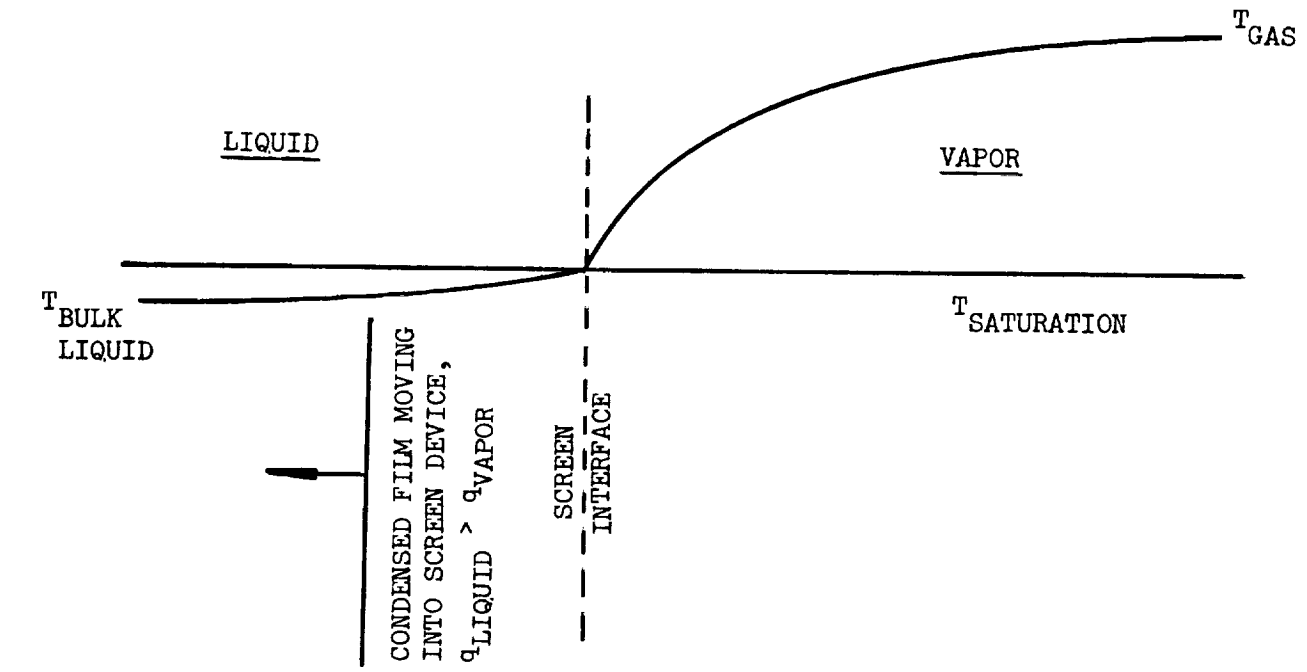

Figure A-1. Temperature Profile for Condensation

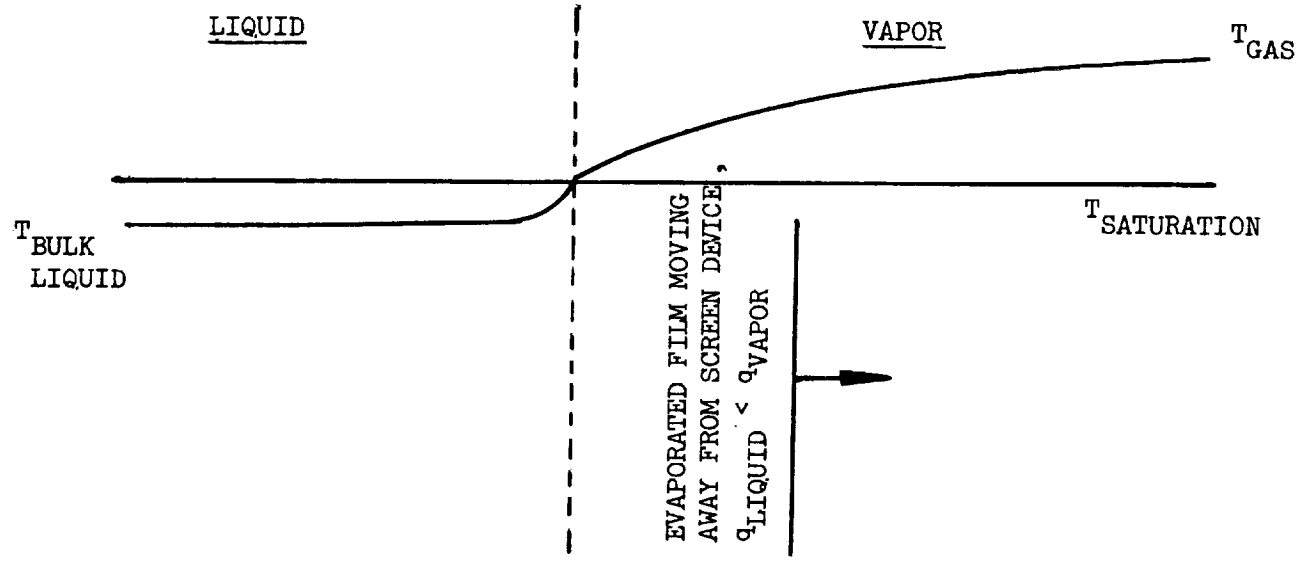

Figure A-2. Temperature Profile for Evaporation

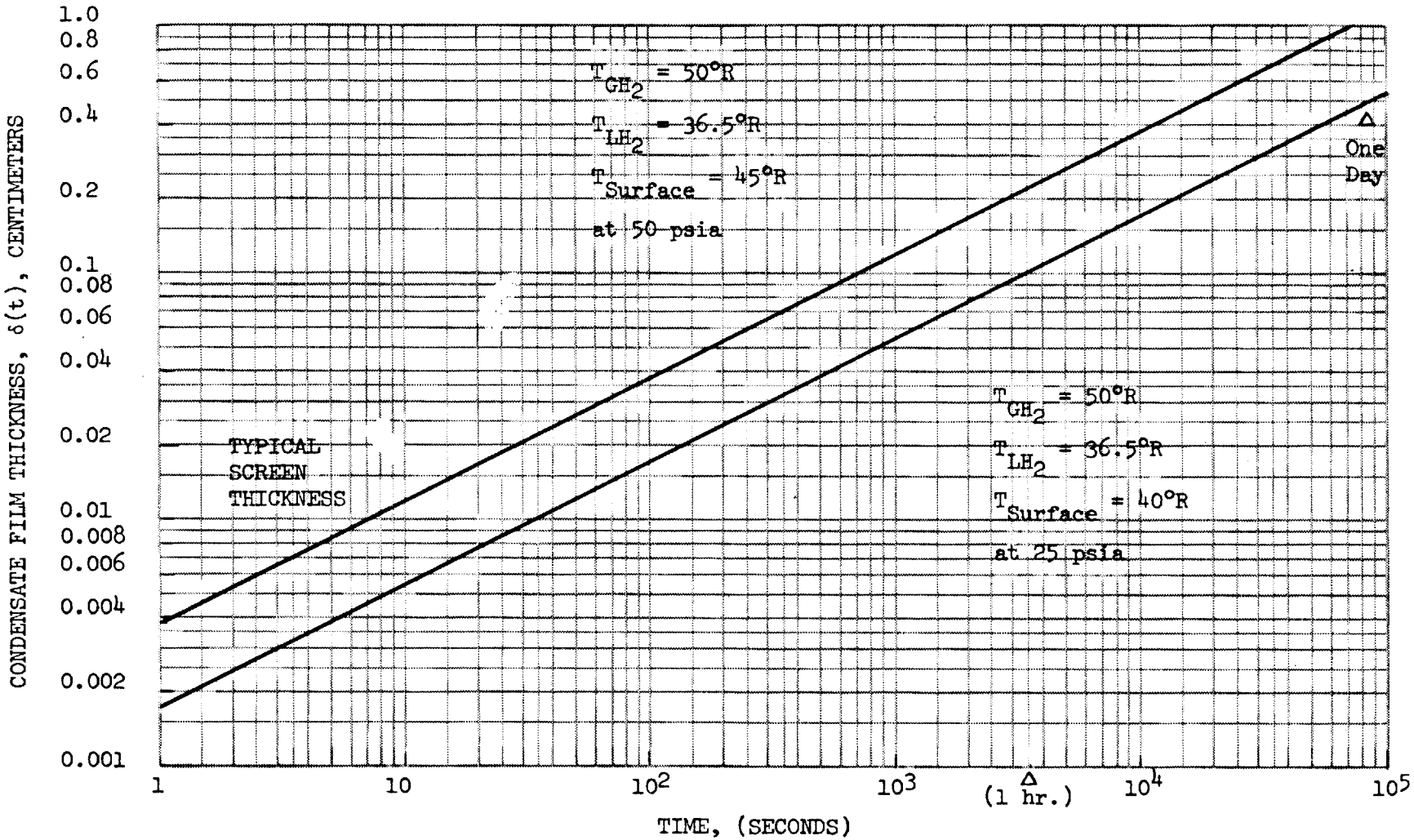

Figure A-3. Condensate Film Thickness Time Dependence -- Small Temperature Difference Approximation

α_L is the thermal diffusivity of the liquid, $C_{P\ell}$ is the specific heat of the liquid, T_ℓ is the saturation temperature for the system pressure, To_ℓ is the bulk liquid initial temperature, and Hv_ℓ is the latent heat of vaporization. Applying this result as shown in Figure A-3 for liquid hydrogen, it is seen that condensation is predicted to occur for conditions corresponding to the continuous autogenous pressurization of liquid hydrogen in orbit. Furthermore, in periods of the order of a day, significant portions of the exposed screen device will support condensed film thicknesses of the order of 1 to 3 cm. Under actual vehicle conditions, more rapid condensation rates are possible than those predicted by this idealized case. Another aspect of this envisioned screen failure mode concerns the rate of pressure decay in the tank. Slow pressure decay rates relative to the heat transfer rate in the liquid would not necessarily cause vapor bubbles to form within the screen. Consider the qualitative temperature profiles as a function of time during pressure decay shown in Figure A-4. If the difference between the maximum temperature in the liquid and the saturation temperature at the surface were always less than the superheat temperature differences required for the internal vaporization, no bubbles would form. Boiling data for liquid hydrogen shows that the superheat temperature need only be 0.1 to 0.5°R above the saturation temperature for boiling to initiate. Hence, it is expected that extremely low pressure decay rates would be required to alleviate this internal vaporization problem.

One estimate of the pressure decay rate that could occur with a Shuttle class liquid hydrogen tank with autogenous pressurization is obtained by assuming that ullage vapor condenses on a moving liquid interface induced by slosh wave amplification after engine shutdown. If condensation occurs on the exposed liquid surfaces, and the pressurization system has been shutdown, then a pressure decay will occur.[+] As the tank pressure drops below the vapor pressure corresponding to the temperature gradient within the screen device, boiling can occur within the device, leading to a possible screen drying and loss of retention capability.

[+]Continuous low-g pressurization could conceivably be used to maintain constant tank pressure, but if bulk liquid covered the pressurant inlet, as is likely in low-g, rapid cooling and condensation of the incoming vapor would occur. This procedure involves complicated low-g heat and mass transfer and has not been shown to be practical. It is therefore not considered a proven solution to the problem of low-g pressure decay induced vaporization.

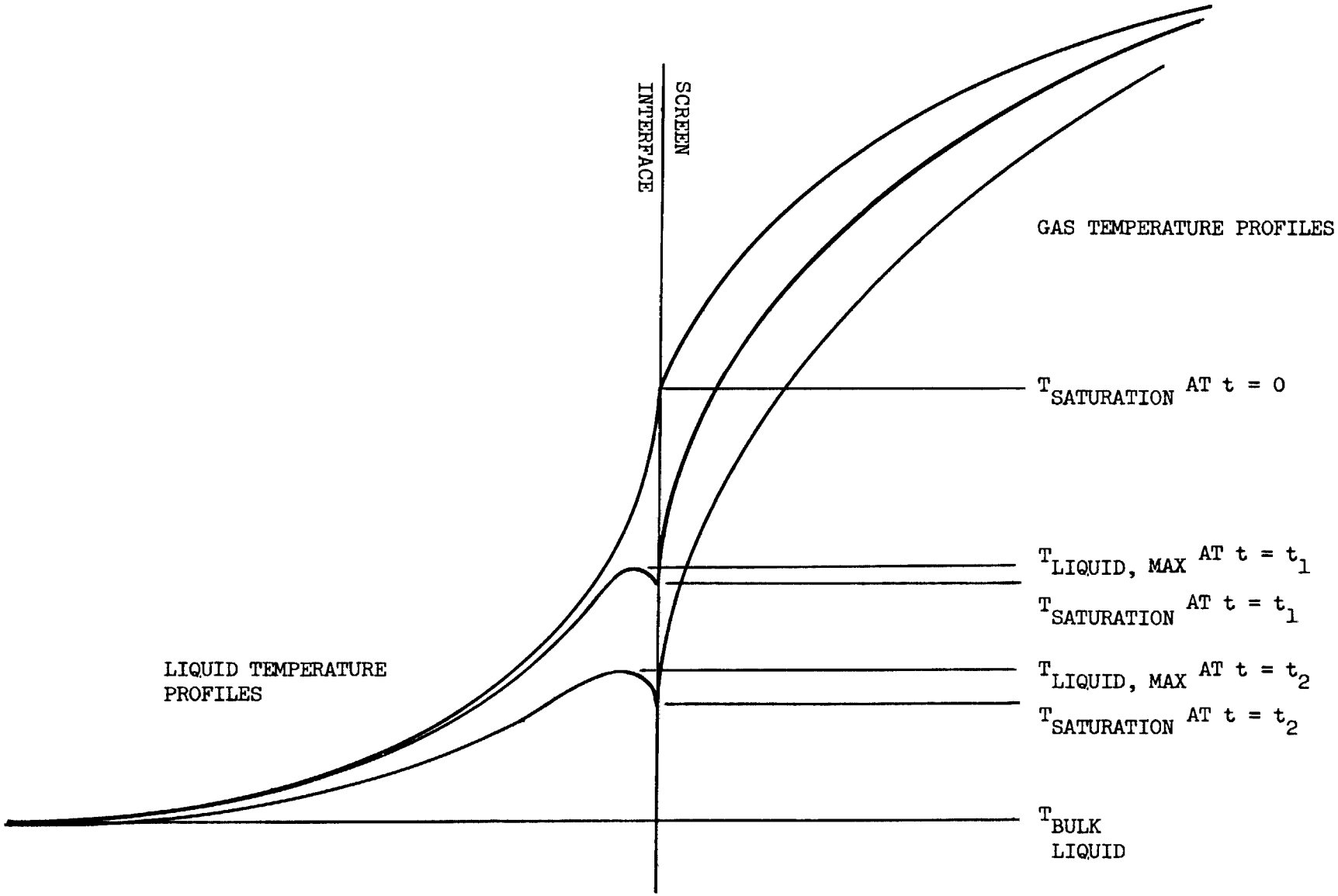

Figure A-4. Temperature Response During Pressure Decay of One-Component System

One method of analyzing the condensation process is given by Sterbentz in Reference A-3, in which a modification of Nusselt's liquid film theory is used. This method is subject to question for the case of condensation on a subcooled liquid. In Nusselt's theory, it is assumed that the thermal resistance occurs in the condensate film flowing along a solid wall. In the case of condensation on a subcooled liquid, this assumption is not strictly valid. The presence of a screen further complicates the process. During the condensation, the liquid moves through the screen pores so as to maintain an interface at the screen which supports the liquid column in the screen.

In spite of these questions, the film condensation model is a reasonable method for estimating the severity of the problem of pressure decay. According to the modified Nusselt condensation model, the condensation rate is determined by the area of liquid exposed to the warm gas, the temperature difference, and the convective velocity. After engine shutdown, the slosh wave amplification and any ACS impulses will cause relative motion between the liquid and warm vapor which will increase the pressure decay rate by increasing the heat transfer coefficient and exposed area of liquid.

An approximate analysis has been performed by Sterbentz [Reference A-3] to determine the tank pressure decay rate, given by

$$\frac{dP}{dt} = \frac{\gamma P}{Vg}\left(\frac{\rho_L}{\rho_v}\right)\left(\frac{\Delta T}{\rho_L h_{vL}}\right) A\, h_m$$

The condensation coefficient, h_m, is derived in Reference (3) for a zero-g field with a moving liquid interface in a manner analogous to Nusselt's derivation for film condensation in a gravity field. This zero gravity condensation heat transfer coefficient is derived as

$$h_m = \left[\frac{2\, k_L\, \rho_L\, h_{vL}\, u_o}{L\, \Delta T}\left(\frac{\bar{u}}{u_o}\right)\right]^{1/2}$$

The average velocity, $\bar{U}$, is 2/3 the maximum velocity, U_o, since a parabolic velocity profile is assumed. Thus, with the slight numerical error of Reference A-3 corrected, the condensation coefficient is found to be

$$h_m = 1.16 \left(\frac{k_L \rho_L h_{vL} u_o}{L \Delta T} \right)^{1/2}$$

The pressure decay rate is also determined by the ratio of exposed liquid/vapor interface area to the ullage volume. Assuming that slosh wave amplification after engine shutdown results in a circular flow of liquid around the ullage volume, the exposed area, and length, L (or perimeter), is approximated by:

$$A = \pi D_{ullage}^2$$

$$L = \pi D_{ullage}$$

The corresponding ullage volume, V_{ullage}, is approximated by $\frac{\pi D^3}{4}$. Thus, the characteristic diameter of the ullage is:

$$D_{ullage} = \frac{4V_g}{\pi}^{1/3}$$

The pressure decay rate is, therefore, determined by:

$$\frac{dP}{dt} = 2.32 \gamma P \left(\frac{\rho_L}{\rho_v} \right) \left(\frac{\Delta T}{\rho_L h_{vL}} \right) \left(\frac{k_L \rho_L h_{vL} u_o}{V_{ullage}} \right)^{1/2}$$

For small ullage volumes having large surface area to volume ratios, the decay rate increases. The decay rate is also proportional to both pressure and temperature difference, and is proportional to the square root of the liquid interface velocity, which is assumed here to be induced by slosh wave amplification.

Slosh wave amplification induced velocities occurring at engine shutdown are difficult to determine, especially in the presence of baffles and other internal hardware. However, if it is assumed, as a conservative estimate, that the

Table A-1

PARAMETERS FOR SHUTTLE TANK PRESSURE DECAY

$\gamma = C_p/C_v = 1.6$	$\Delta T = 60°R$
$P = 2.06 \times 10^5$ N/m^2 (30 psia)	$h_{vL} = 4.41 \times 10^5$ joule/kg (190 Btu/lb)
$\rho_L = 70$ kg/m^3 (4.4 lb/ft^3)	
$\rho_o = 1.6$ kg/m^3 (0.1 lb/ft^3)	$V_{TANK} = 69$ m^3 (2,450 ft^3)

$K_{liquid} = 9,050$ joule/m-sec-°K $= 1.62 \times 10^{-5} \frac{\text{Btu}}{\text{ft sec °R}}$

REFERENCES FOR APPENDIX

A-1 E. L. Knuth. Evaporations and Condensations in One Component Systems. ARS Journal. September 1962, pp 1424-1426.

A-2 E. L. Knuth. Nonstationary Phase Changes Involving a Condensed Phase and a Saturated Vapor. Physics of Fluids. Vol. 2, No. 1 Jan-Feb. 1959, pp 84-86.

A-3 W. H. Sterbentz. Liquid Propellant Thermal Conditioning System. NAS CR-72113, LMSC-A839783, pp B1-B4 and C1-C5, April 1967.